NPS ARCHIVE
1999.06
KING, R.

DUDLEY KNOX LIBRARY
NAVAL POSTGRADUATE SCHOOL
MONTEREY CA 93943-5101

DUDLEY KNOX LIBRARY
NAVAL POSTGRADUATE SCHOOL
MONTEREY CA 93943-5101

NAVAL POSTGRADUATE SCHOOL
Monterey, California

DISSERTATION

NONLINEAR DYNAMICS IN THE MODELING OF HELICOPTER ROTOR BLADE LEAD/LAG MOTION

by

Robert L. King

June 1999

Dissertation Supervisor: E. Roberts Wood

Approved for public release; distribution is unlimited.

REPORT DOCUMENTATION PAGE

Form Approved OMB No. 0704-0188

Public reporting burden for this collection of information is estimated to average 1 hour per response, including the time for reviewing instruction, searching existing data sources, gathering and maintaining the data needed, and completing and reviewing the collection of information. Send comments regarding this burden estimate or any other aspect of this collection of information, including suggestions for reducing this burden, to Washington headquarters Services, Directorate for Information Operations and Reports, 1215 Jefferson Davis Highway, Suite 1204, Arlington, VA 22202-4302, and to the Office of Management and Budget, Paperwork Reduction Project (0704-0188) Washington DC 20503.

1. AGENCY USE ONLY *(Leave blank)*	2. REPORT DATE	3. REPORT TYPE AND DATES COVERED
	June 1999	Ph.D. Dissertation

4. TITLE AND SUBTITLE
NONLINEAR DYNAMICS IN THE MODELLING OF HELICOPTER ROTOR BLADE LEAD/LAG MOTION

5. FUNDING NUMBERS
RAA80

6. AUTHOR(S)
King, Robert L.

7. PERFORMING ORGANIZATION NAME(S) AND ADDRESS(ES)
Naval Postgraduate School
Monterey, CA 93943-5000

8. PERFORMING ORGANIZATION REPORT NUMBER

9. SPONSORING / MONITORING AGENCY NAME(S) AND ADDRESS(ES)
US Army Research Office, Research Triangle Park, NC 27709-2211

10. SPONSORING / MONITORING AGENCY REPORT NUMBER
37-803

11. SUPPLEMENTARY NOTES
The views expressed in this thesis are those of the author and do not reflect the official policy or position of the Department of Defense or the U.S. Government.

12a. DISTRIBUTION / AVAILABILITY STATEMENT
Approved for public release; distribution is unlimited.

12b. DISTRIBUTION CODE

13. ABSTRACT *(maximum 200 words)*

Until recently, computer simulations of helicopter rotor dynamics have employed equations of motion that have been linearized or simplified. These modified equations of motion did not allow for the evaluation of nonlinear material properties in the rotor since higher order terms in the dynamics had been modified in the simplification process. With recent advances in both computer simulation hardware and symbolic mathematic manipulation software, the full nonlinear equations of motion may be utilized in helicopter rotor simulations. This dissertation reports on the use of the full nonlinear equations of motion in the analysis of rotor blade lead/lag motion and its effect on rotor hub and rigid body fuselage motion. Nonlinear modeling methods are implemented using Maple symbolic mathematic manipulation software and Matlab and Simulink computer simulation environments. Results are compared to the RAH-66 Comanche Froude scale wind tunnel article and new methodologies evaluated in the search for a damperless rotor system that is free of ground and air resonance mechanical instabilities.

14. SUBJECT TERMS
Air Vehicles, Modeling and Simulation, Helicopter Rotor Dynamics, Nonlinear Dynamics

15. NUMBER OF PAGES
176

16. PRICE CODE

17. SECURITY CLASSIFICATION OF REPORT	18. SECURITY CLASSIFICATION OF THIS PAGE	19. SECURITY CLASSIFI- CATION OF ABSTRACT	20. LIMITATION OF ABSTRACT
Unclassified	Unclassified	Unclassified	UL

NSN 7540-01-280-5500

Standard Form 298 (Rev. 2-89)
Prescribed by ANSI Std. 239-18

Approved for public release; distribution is unlimited

NONLINEAR DYNAMICS IN THE MODELLING OF HELICOPTER ROTOR BLADE LEAD/LAG MOTION

Robert L. King - Lecturer, Department of Aeronautics and Astronautics
M.S., Naval Postgraduate School, 1993
B.S., University of Illinois Urbana-Champaign, 1986

Submitted in partial fulfillment of the
requirements for the degree of

**DOCTOR OF PHILOSOPHY IN
AERONAUTICAL AND ASTRONAUTICAL ENGINEERING**

from the

NAVAL POSTGRADUATE SCHOOL
June 1999

ABSTRACT

Until recently, computer simulations of helicopter rotor dynamics have employed equations of motion that have been linearized or simplified. These modified equations of motion did not allow for the evaluation of nonlinear material properties in the rotor since higher order terms in the dynamics had been modified in the simplification process. With recent advances in both computer simulation hardware and symbolic mathematic manipulation software, the full nonlinear equations of motion may be utilized in helicopter rotor simulations. This dissertation reports on the use of the full nonlinear equations of motion in the analysis of rotor blade lead/lag motion and its effect on rotor hub and rigid body fuselage motion. Nonlinear modeling methods are implemented using Maple symbolic mathematic manipulation software and Matlab and Simulink computer simulation environments. Results are compared to the RAH-66 Comanche Froude scale wind tunnel article and new methodologies evaluated in the search for a damperless rotor system that is free of ground and air resonance mechanical instabilities.

TABLE OF CONTENTS

I. INTRODUCTION 1

II. REVIEW OF WORK PERFORMED BY ROBINSON 5

III. DAMPERLESS ROTOR DEVELOPMENT 11

A. BACKGROUND 11
B. GROUND RESONANCE FUNDAMENTALS 12
C. OBJECTIVES 17
D. INTRODUCTION TO DUFFING 19
1. Single Degree of Freedom Duffing Systems 19
2. Multiple Degree of Freedom Duffing Systems 26
E. DUFFING ROTOR SYSTEMS 30
1. Results of the Baseline Duffing Rotor 32
2. Baseline Case with Duffing Stiffness Added 34
3. Baseline Case with Increased Rotor Speed - Above the Region of Instability.. 38
F. GROUND RESONANCE ANALYSIS 41
1. Frequency Coalescence 41
2. Comparison with Theory - Baseline Rotor 44
3. Comparison with Theory - Duffing Rotor 46
4. The Region of Instability - Duffing Rotor 47
5. Duffing Rotor Effect on Structural Moments 50
6. Stiff-in-Plane? - Duffing Rotor 51
G. CHAOS ANALYSIS 54
1. Response to Similar Initial Conditions 54
2. Poincare Phase Plane and Phase Space Analyses 55
H. DROOPING ROTOR STABILITY 56
1. Nonlinear stiffness provides rotor stability for a wide range of physical parameters 56

IV. LINEARLY LINKED ROTOR SYSTEMS 59

A. INTRODUCTION 59
B. ROTOR WITH LINKED BLADES 60
C. LINKED BLADE PARAMETRIC STUDIES: 62
1. Linked blade & hub response varying blade interlink stiffness for baseline rotor 62
2. Linked blade & hub response varying blade interlink damping for baseline rotor 64
3. Linked blade & hub response with uneven interlink stiffness for baseline rotor 65
4. Interlink Dampers Versus Conventional Dampers 69

V. ROTOR WITH UNEVEN BLADE SPACING 71

VI. GROUND AND AIR RESONANCE ANIMATION 73

VII. DAMPERLESS ROTOR DEVELOPMENT CONCLUSIONS 77

LIST OF REFERENCES 81

APPENDIX A. COMANCHE FROUDE SCALE MODEL SIMULATION 83

APPENDIX B. MYKLESTAD BEAM MODELING METHOD 109

APPENDIX C. MYKLESTAD METHOD PROGRAM IN MATLAB 117

APPENDIX D. MAPLE WORKSHEET FOR COLEMAN MODEL..... 123

APPENDIX E. EQUATIONS OF MOTION FOR COLEMAN MODEL..... 135

APPENDIX F. SIMPLIFIED ROTOR/FUSELAGE EQUATIONS OF MOTION..... 137

APPENDIX G. 5 BLADED EQUATIONS OF MOTION WITH POLYNOMIAL SNUBBER FUNCTIONS 139

APPENDIX H. 5 BLADED POLYNOMIAL S-FUNCTION INPUT FILE..... 147

APPENDIX I. 5 BLADED POLYNOMIAL S-FUNCTION 151

INITIAL DISTRIBUTION LIST..... 159

LIST OF FIGURES

Figure 1 - Simplified Rotor Model [After Ref. 1] 6
Figure 2 - Validation of simple model with solution of Coleman's linearized model 7
Figure 3 - Quantitative validation of simple model against Deutsch Criteria 9
Figure 4 - Ground resonance flowchart 15
Figure 5 - Ground resonance hub motion 16
Figure 6 - Simple Duffing system 20
Figure 7 - Duffing time history 21
Figure 8 - Duffing system resonance 23
Figure 9 - Duffing resonance frequencies [After Ref. 18] . 25
Figure 10 - Three DOF Duffing system 27
Figure 11 - Three DOF Duffing system time histories 28
Figure 12 - Effect of increasing Duffing stiffness in three DOF system 29
Figure 13 - Rotor with Duffing stiffness in the lead/lag dynamics 31
Figure 14 - Baseline case, blade lead angles without Duffing stiffness 33
Figure 15 - Baseline case, hub lateral displacement without Duffing stiffness 34
Figure 16 - Baseline case, blade lead angles with Duffing stiffness 35
Figure 17 - Baseline case, hub lateral displacement with Duffing stiffness 36
Figure 18 - Hub lateral vibration, baseline case with Duffing stiffness 37
Figure 19 - Blade lead angles, increased rotor speed with Duffing stiffness 39
Figure 20 - Hub lateral displacement, increased rotor speed with Duffing stiffness 40
Figure 21 - Hub lateral vibration comparison 41
Figure 22 - Coleman plot of baseline rotor with Duffing stiffness 43
Figure 23 - Coleman plot for baseline rotor 44
Figure 24 - Baseline rotor region of instability 45
Figure 25 - Coleman plot for Duffing rotor 47
Figure 26 - Change in region of instability with Duffing stiffness included 48
Figure 27 - Example Hub Time Histories 49
Figure 28 - Lead/lag restoring moments 50
Figure 29 - Soft in-plane frequencies at 239 RPM 52
Figure 30 - Soft in-plane frequencies at 310 RPM 53
Figure 31 - Poincare section of hub lateral motion 55
Figure 32 - Phase space of blade lead motion 56
Figure 33 - Reduced rotor speed comparison 58
Figure 34 - Four bladed interlink baseline 62
Figure 35 - Blade elastic interlink results 63

Figure 36 - Blade damper interlink results 65
Figure 37 - Blades #1 and #2 linked 67
Figure 38 - Blades #4&1 and #2&3 linked 68
Figure 39 - Conventional dampers versus interlink dampers 69
Figure 40 - Baseline rotor with 60-120-60-120 blade spread72
Figure 41 - Rotor animation 75

ACKNOWLEDGEMENTS

The Comanche Froude-scale modeling work performed for this dissertation was sponsored by the National Rotorcraft Technology Center (NRTC) and the Rotorcraft Industry Technology Association (RITA) under the supervision of Sikorsky Aircraft, project number 99-01-2.2(4). Research supervisors for Sikorsky were Mr. Bob Blackwell, Mr. Bob Sopher, Dr. Jerry Miao, Mr. Tom Lawrence and Dr. Raj Shenoy. Their support is greatly appreciated.

The damperless rotor development was sponsored by the US Army Research Office, Triangle Park, NC, under contract number 37-803. Research supervisors for the Army are Dr. Gary L. Anderson (ARO) and Dr. Jeffrey D. Singleton (ARL Langley). Their support is also greatly appreciated.

The doctoral dissertation advisor for this work is Dr. E. Roberts Wood, Department of Aeronautics and Astronautics, Naval Postgraduate School. His help in the completion of this dissertation was indespensible. I would also like to thank the members of my committee, Dr. Bob Ormiston, Professors Don Danielson, Russ Duren, and Hal Titus, for taking the time out of their already busy schedules to guide me through to completion.

Most importantly, I would like to thank my wife, Margaret, who was both Mother and Father for our three daughters while I completed this research. This degree was truly a family effort.

I. INTRODUCTION

One of the goals of this research was to develop a flexible computational tool to analyze the dynamic and aeromechanical behavior of advanced technology coupled rotor/fuselage systems. Initially, a series of programs were developed utilizing the symbolic processing software, Maple®, the computational software, Matlab®, and the simulation software, Simulink®, by LT Christopher Robinson [Ref. 1]. It was desired that the computational tool be simple to understand and lend itself to easy reprogramming by any user knowledgeable in the field of dynamics and in the use of the software programs mentioned. It was also desired that the developed programs allow for a sufficient capability so that the effects of introducing advanced technologies into rotor system designs could be accurately modeled. This dissertation reports on further advances in this computational tool development, and analysis based on these new tools. The nonlinear rotor simulation that was developed as part of this research is a very powerful tool for analyzing rotors that do not have multiple load paths to the hub.

Historically, rotor analysis was performed using approximate equations of motion. In order to reduce the complexity of the computer code involved and to reduce

computation times, these equations were simplified by eliminating higher order terms [Refs. 2,3]. Subsequently, either linearized equations were used or select nonlinear terms were retained using a ranking system or ordering scheme, such as that used by Friedmann, [Ref. 4].

As hingeless helicopter main rotors became more commonplace, a need arose for a rotor simulation tool that would accurately model nonlinear mechanical properties so that these nonlinearities could be exploited. It was desired to develop an analysis tool that would be able to reliably model the effects of nonlinearities in the rotor and hub mechanical and geometric parameters. For this reason, Robinson and Wood developed a utility for creating the full nonlinear, coupled equations of motion. Robinson utilized the symbolic manipulation software Maple® for this purpose.

Current trends in helicopter technology and manufacturing have favored the use of bearingless rotor designs that make use of advanced composite materials. These designs offer many advantages over more conventional articulated rotors in reliability and maintainability. A potential payoff from the successful use of the technologies mentioned above is the damperless rotor; a design that offers major returns in the form of decreased rotor system weight, reduced parts count, and reduced maintenance requirements.

Composites and other advanced materials that can be applied for a damperless rotor make modeling rotor behavior more difficult, however. These materials have the potential for exhibiting nonlinear behavior that cannot be accurately modeled without utilizing the full nonlinear equations of motion for the system.

The goal of this dissertation is to examine alternative designs for a damperless helicopter rotor. This effort met with success by taking advantage of nonlinear stiffness in the blade root end to avoid divergent motion in the rotor blade lead/lag degrees of freedom. This oscillatory instability is better known as ground and air resonance instability.

II. REVIEW OF WORK PERFORMED BY ROBINSON

For background on progress reported in this dissertation, it is important to first review LT Robinson's thesis work. This work preceded that of the author. Tasks performed by Robinson included the formulation of a Maple® based symbolic processing worksheet that formulated nonlinear equations of motion given energy expressions for helicopter rotor model degrees of freedom. Simulink® based computer simulations were developed from the equations of motion derived by the symbolic processor for a simple three bladed rotor based on that used by Coleman [Refs. 5,6].

Robinson, Wood, and King reported on a new method for formulating the full non-linear equations of motion for ground/air resonance stability analysis of helicopter rotor systems [Ref. 7]. The full set of non-linear equations was developed by Lagrangian approach using symbolic processing software for expanding the equations. The symbolic software was further utilized to automatically convert the equations of motion into C or Fortran source code formatted for numerical integration. Simulink® then applied a Runga-Kutta integration scheme to generate time history plots of blade and fuselage motion. Damping levels were determined from the time history simulations by a Matlab® program, which used

the Moving Block Technique for establishing damping levels from the coupled rotor-body response.

Robinson's model, based on that of Coleman, is shown in Figure 1, [Ref. 1].

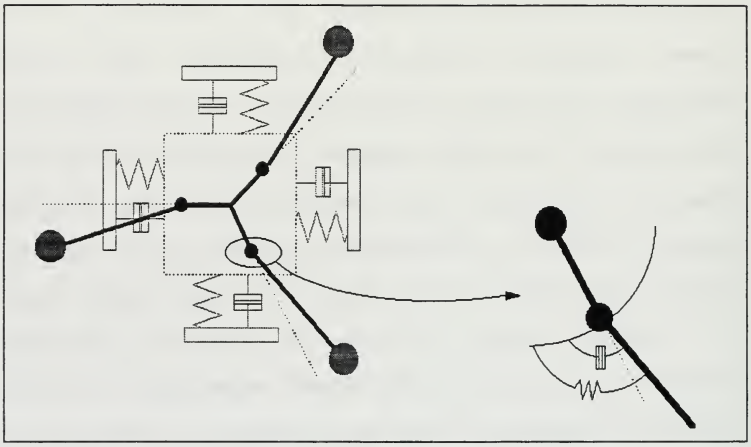

Figure 1 - Simplified Rotor Model [After Ref. 1]

Robinson verified his symbolic Lagrangian derivation by comparing his results to Coleman's. Figure 2 shows results of a comparison of the two methods for an unstable case where a moderate amount of damping has been added to both rotor blades and fuselage.

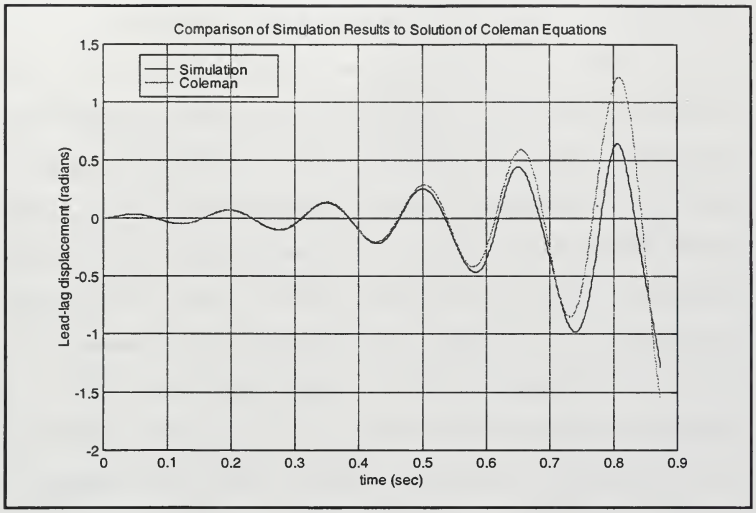

Figure 2 - Validation of simple model with solution of Coleman's linearized model

In Figure 2, Robinson shows excellent agreement between the two solutions with departure occurring only when displacements are very large. This is to be expected since the simulation model of this paper does not assume small angle theory whereas the Coleman-Feingold-Bramwell model does.

For a more quantitative proof of the validity of the new method, it was tested against Deutsch's Criteria [Ref. 8]. Based on Coleman's analysis, Deutsch showed that the product of the hub (landing gear) damping and the blade lead/lag damping must be greater than a prescribed value to

collapse the band of unstable blade frequencies: λ_p λ_ϕ > λ_3 (p-1). The following Figure shows results of successive sweeping across the unstable band using the new nonlinear analysis. The respective cases represent those where Deutsch's prescribed damping is applied (D=1.0), and other cases where the damping is greater than that required by Deutsch (D=1.1) or less (D=0.8, 0.9). For each case considered, the center of instability is seen to be the point of minimum value on the given line. With the new nonlinear analysis, Deutsch's criteria applied at the center of instability provides nearly a neutrally stable result with a near zero damping ratio. Deutsch's criteria is conservative in that the critical point for his criteria, or bucket of each curve, still shows positive damping when analyzed with the NPS simulation. Three years after Robinson, Rafanello verified the conservative nature of Deutsch's criteria by matching simulation results to Wood's HSS-2 ground resonance analysis, [Refs. 9, 10].

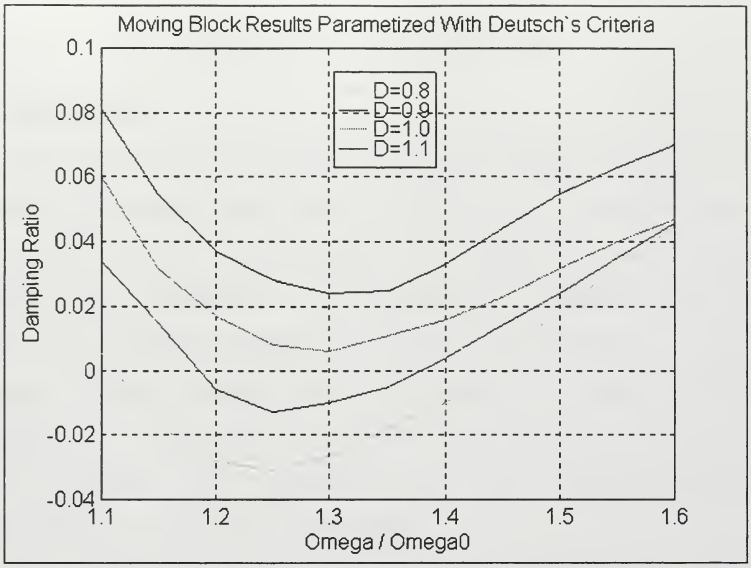

Figure 3 - Quantitative validation of simple model against Deutsch Criteria

III. DAMPERLESS ROTOR DEVELOPMENT

A. BACKGROUND

Ground and air resonance are particularly destructive mechanical instabilities that can occur in helicopters with fully articulated, bearingless, or hingeless main rotor designs. The phenomenon of ground/air resonance is the result of coupling between rigid body motions of the fuselage on its landing gear, or in the air, and lead-lag oscillations of the rotor blades in their plane of rotation. When it occurs, the instability can build to destructive proportions in a matter of seconds.

The equations of motion describing the dynamics of the coupled rotor-fuselage system are nonlinear and generally quite complex even for simplified models. The fundamental theory of air and ground resonance is credited to the classic work of an NACA engineer, Robert Coleman, who first published his theory in the early 1940's [Ref. 5]. As computational power improved with the evolution of digital computers, more general techniques for analyzing rotor system stability were developed.

As stated earlier, due to the complexity of the equations of motion, ground and air resonance analysis was historically restricted to linear analysis until very recently. This frequently restricted the scope of many

studies and potential solutions. With a few noteworthy exceptions, nonlinearities in ground and air resonance research programs have not typically investigated beyond traditional damping methods, such as hydraulic damping.

This chapter entitled "Damperless Rotor Development" investigates various options for damperless rotors that maintain some margin of stability, or avoidance of ground and air resonance without the employment of auxiliary lead/lag dampers.

In general, rotorcraft lag dampers are heavy, expensive items that can require extensive maintenance. By developing rotors that do not require these dampers, payoffs in 1) reduced maintenance time and cost, 2) reduced hub complexity and parts count, 3) reduced rotor drag, and 4) reduced rotor signature could potentially be reaped.

An effort in the elimination of these dampers applies directly to a famous quote from the father of the business jet, Bill Lear, "Strive for design simplicity: you never have to fix anything you leave out."

B. GROUND RESONANCE FUNDAMENTALS

Ground and air resonance instability is centered around blade/hub interactions at one of the fuselage rigid body modes. The rotor acts as a forcing function, producing undesired responses or even resonance in the fuselage

dynamics. The rotor changes the frequency of mechanical vibrations as they transfer from the rotating frame down into the non-rotating frame. If the blades have a primary mode in lead/lag at some frequency ω_{lag}, and Ω is the frequency of rotation of the rotor system, shears are transmitted through the mast and into the non-rotating hub at frequencies $(\Omega \pm \omega_{lag})$. The progressing mode $(\Omega + \omega_{lag})$ is heavily damped and normally plays no role in ground resonance. The regressing mode $(\Omega - \omega_{lag})$ provides the potential for destruction, however. If one of the fuselage rigid body modes is near in frequency to the regressing mode and there is insufficient damping, blade lead/lag and fuselage displacement amplitudes can build to destructive proportions. While the helicopter is still in contact with the ground, the fuselage roll mode is often close in frequency to the regressing lag mode, normally in the 2-5 Hz range.

In general, the spectrum of classical ground resonance to air resonance could be referred to as "aeromechanical stability." Since articulated rotors normally do not experience air resonance, aerodynamics and flap degrees of freedom play little roll in ground resonance. Therefore, articulated rotors may be modeled using Coleman's methods. Hingeless and bearingless rotors experience more coupling in the blade degrees of freedom. In addition, body pitch and

roll coupling through flap moments of cantilever blades can result in air resonance. Bearingless and hingeless rotors, where Coleman's equations are not sufficient to model the problem, require more sophisticated models. Flap degrees of freedom and aerodynamics were not used to model the Coleman-like rotor models in this report.

In the typical rotor, there are, in fact, significant nonlinearities. Especially noteworthy are friction in dampers and oleos that sometimes result in the appearance of instability following a moderately large external force excitation. Thus, the typical scenario for ground resonance is initiated by the fuselage being perturbed by some external force such as a gust, a rolling ship deck, uneven terrain while ground taxing, or combat damage. The fuselage motion, typically in roll, induces asymmetrical lag motion in the rotor blades. This asymmetrical response shifts the combined CG of the rotating components away from the center of rotation, resulting in an unbalance in the centrifugal force seen by the rotor mast. The unbalanced centrifugal force results in increased fuselage motion, compounding the problem. This cycle is depicted in flowchart form in Figure 4.

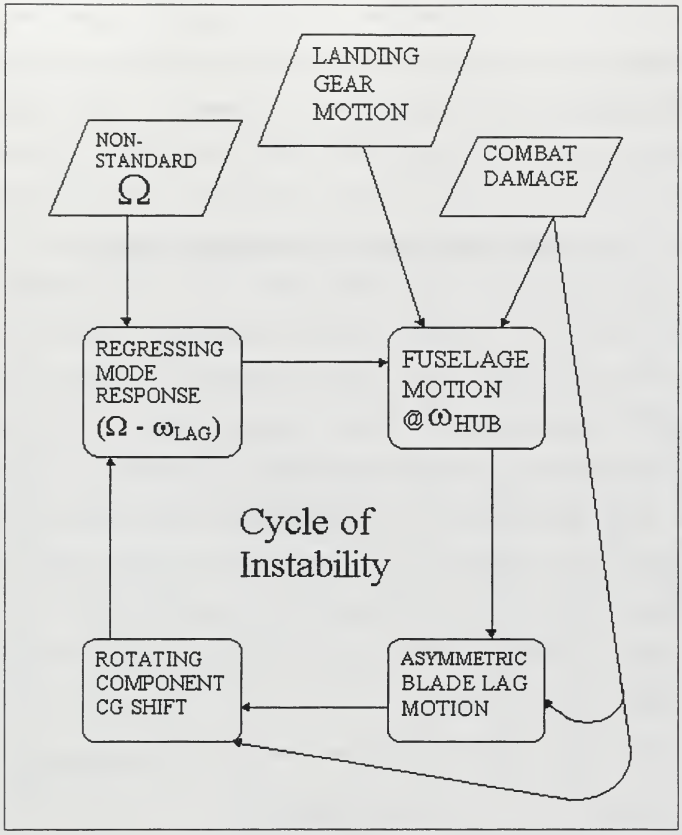

Figure 4 - Ground resonance flowchart

A typical fuselage on its landing gear has a roll mode frequency in the proximity of the regressing mode frequency of the rotor system. If these modes are sufficiently near to each other and there is insufficient system damping, ground resonance can occur.

A plot of hub motion for a typical case of ground resonance can be found in Figure 5. Note the spiraling divergence of the hub center of mass in the horizontal plane.

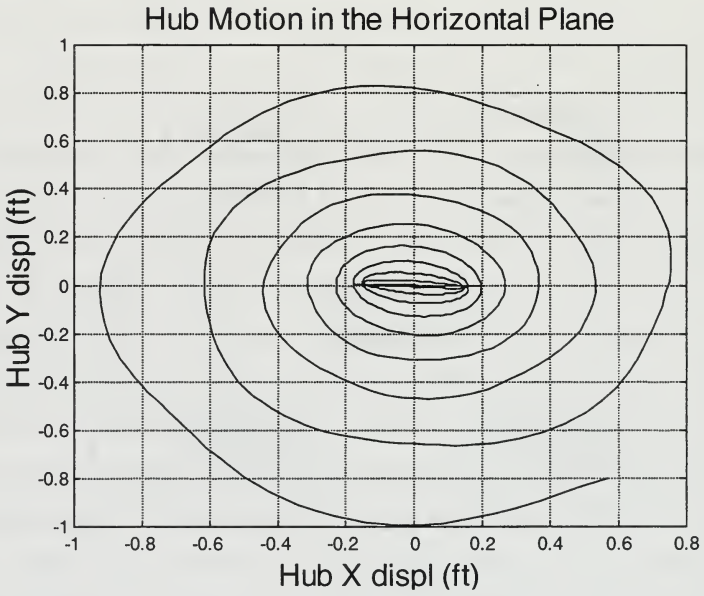

Figure 5 - Ground resonance hub motion

Following the work of Robert Coleman, a more complete work, based on his analysis, was collected and published by Coleman and Feingold [Ref. 6]. Deutsch supplemented Coleman's work by establishing a criterion for system damping necessary to eliminate ground resonance [Ref. 8].

Numerous other researchers have contributed to understanding the ground resonance problem since Coleman, Deutsch, and Feingold. The papers following Coleman essentially completed the investigation of the linearized system for ground resonance. Hammond applied Floquet theory, but to consider the case of unequal lead/lag damping among the blades [Ref. 11]. (The NPS rotor simulation can also apply unequal lead/lag damping values at each blade.) Tongue, Flowers, Jankowski, Tang, Dowell, and most recently, Gandhi and Chopra [Refs. 12-14] investigated nonlinear effects in blade and fuselage damping. Ormiston explored linear aeromechanical stability of rigid blades with spring restrained hinges, and later, investigated rotor modeling with a sophisticated finite element analysis code and various nonlinear damping models [Refs. 15, 16].

C. OBJECTIVES

The objective of the present work is to explore the potential of eliminating the snubber-damper or damper on hingeless rotor designs and replace it with a flexbeam that has been modified to possess nonlinear properties. Thus, the purpose is to employ the nonlinear properties of the flexbeam to introduce nonlinear dynamic characteristics that will replace unbounded instability with small amplitude limit cycle oscillations, and prevent catastrophic

destruction of the helicopter. This work is well suited to the new NPS rotor simulation analysis that can accurately model nonlinear mechanical properties.

The significance of this new research is that allowance of nonlinearities at the blade root may result in an acceptable bounded response in the parameter region where linear theory would predict instability, or may introduce new regions of unacceptable response in the parameter region where linear theory would predict stability. Evidence of the latter may be found in the numerous aircraft lost in the documented cases of ground resonance. Modern soft-inplane rotors, such as that first introduced on the BO-105, have the additional possibility of encountering this lead lag instability in flight [Ref. 17].

The work reported here attempts to abandon the use of auxiliary damping methods in the rotating system as a means of eliminating ground and air resonance. Only the damping inherent to the typical landing gear system and the built-in structural damping of the flexbeam in bending are utilized in the cases shown. The ground/air resonance cycle is detuned by shifting the blade natural frequency in lead/lag to avoid the coalescence of the regressing mode with the fuselage rigid body modes. A nonlinear flexbeam is characterized by change in stiffness properties with change in amplitude. Therefore, as blade lead/lag amplitude

changes, there is a corresponding change in its lead/lag frequency. This method differs from some previous methods of preventing ground resonance in that coalescence is avoided through natural frequency shift instead of dominating the dynamics of the system through damping. In the case of this thesis, this is accomplished by introducing a classic nonlinear stiffness known as Duffing-type nonlinear stiffness at the blade root.

D. INTRODUCTION TO DUFFING

1. Single Degree of Freedom Duffing Systems

For the first part of the investigation, an exploration of the one degree of freedom Duffing system is considered to understand the effects of cubic stiffness for a simple harmonic oscillator. With damping excluded, Duffing's equation can be expressed as:

$$\ddot{x} + \omega_0^2 x + hx^3 = G\cos(\omega_1 t)$$

where the driving function is $G\cos(\omega_1 t)$. The coefficient, G, is the ratio between the amplitude of the force and the mass of the moving system. Coefficients ω_0^2 and h depend on the parameters of the system, with the Duffing coefficient, h, being positive for a "hardening spring" and negative for a "softening spring."

One of the interesting phenomena appearing in systems governed by Duffing's equation is that, in addition to generating harmonics of the driving frequency, discontinuous jumps in amplitude occur as the frequency of the exciting force is either increased of decreased at a constant rate.

A simple one degree of freedom Duffing spring mass system is shown in Figure 6.

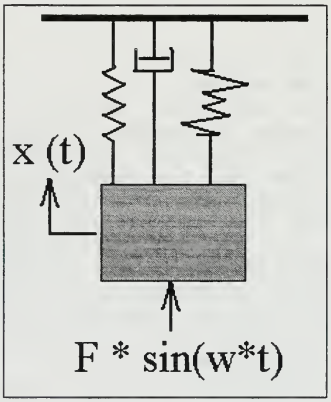

Figure 6 - Simple Duffing system

A simple simulation was written to obtain time histories for this system with user supplied mass, linear damping, linear stiffness, forcing amplitude, forcing frequency, and Duffing stiffness terms. The Simulink® 5th order Runge-Kutta integration scheme is used here.

An example time history that illustrates the effect of exciting frequency (both increase and decrease) is presented in Figure 7.

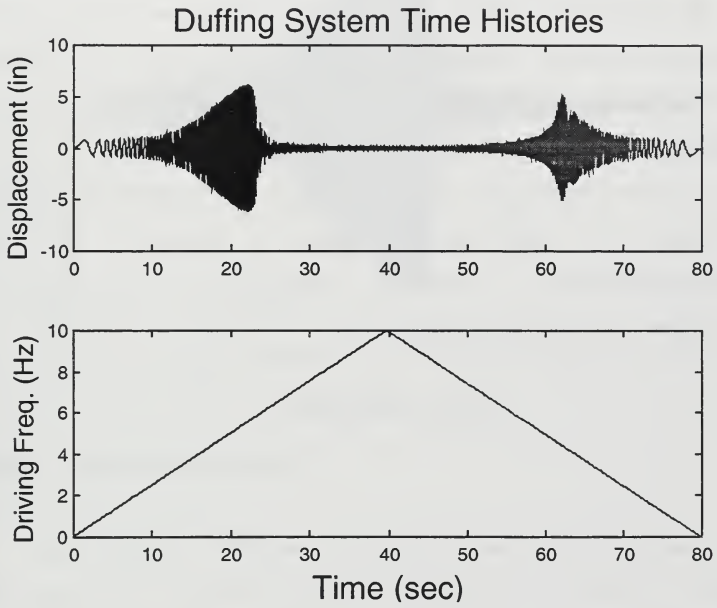

Figure 7 - Duffing time history

The inputs for this time history are contained in the following table:

Table 1 - Table caption

Linear stiffness = 4000 lb/in	Mass = 6 slugs
Duffing stiffness = 100 lb/in^3	Damping = 14 lb*s/in

Driving Force 1/2 amplitude = 500 lb

The top subplot in Figure 7 is the time history of the mass displacement with a stiffening Duffing spring included in the dynamics. The second subplot in this figure is the driving frequency used in the top plot as a function of time. The system goes through resonance both as the driving frequency is increased and again as it decreases.

If one takes this time history and transforms it as a function of driving frequency, instead of time, dissimilarities in the two resonances can easily be discerned, as shown in Figure 8.

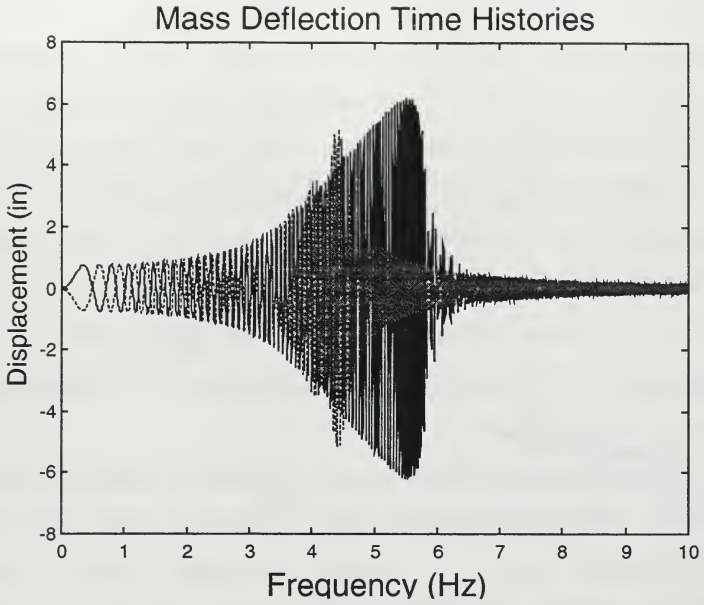

Figure 8 - Duffing system resonance

The system reaches resonance as the frequency is increased, but unlike a linear system that gradually reduces the displacement amplitude, in this case, the Duffing system experiences a sudden drop-off in displacement amplitude. Then, as the driving frequency is decreased from a value above resonance, the system does not follow the same path in resonance amplitude, but reaches a relative maximum in displacement at a frequency less than the case for

increasing driving frequency. These sudden changes in displacement amplitude are referred to as "Duffing jumps."

Shown in Figure 9 is a nonlinear resonance curve for a hardening Duffing spring system, reproduced from Cunningham [Ref. 18]. A typical linear resonance curve has been superimposed on Cunningham's original figure. The resonant frequency for the linear system would not change, but remain fixed at ω_0. The physical reason for these jumps can be visualized in this plot of the resonance of the nonlinear Duffing system.

As the driving frequency is increased from the left on the plot, the system displacement amplitude grows until the system reaches point A. Further increase in the driving frequency drops the displacement amplitude down to B, a Duffing jump.

As the driving frequency is decreased from the right, the system drives right through point B to point C, where the solution becomes unstable. As the driving frequency is decreased lower than that found at point C, the only stable displacement amplitude becomes point D, another Duffing jump.

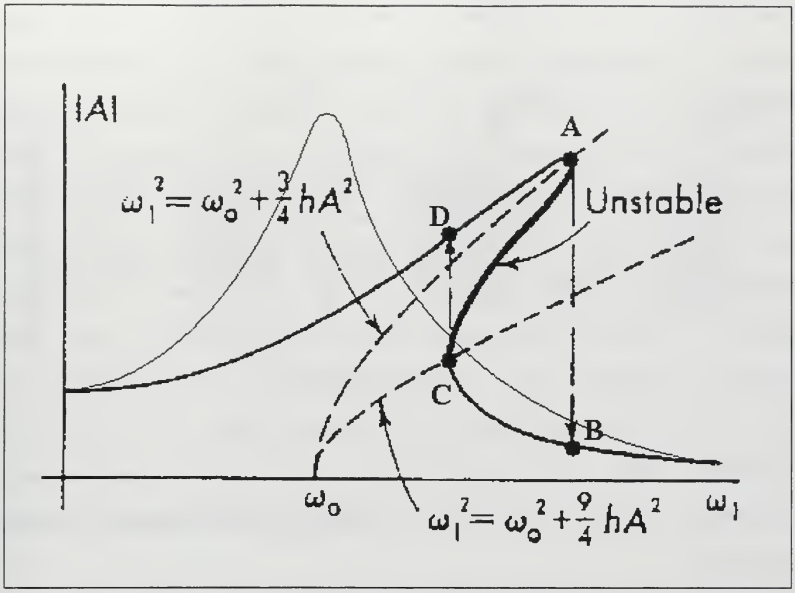

Figure 9 - Duffing resonance frequencies [After Ref. 18]

Unlike the linear system, the Duffing system increases the natural frequency as a function of displacement amplitude. For larger displacements, the resonance frequency increases due to this stiffening. The relation for this frequency shift is derived by Cunningham as:

$$\omega_r = \sqrt{\frac{K}{M} + \frac{3K_d A^2}{4}}$$

It should be noted that if the sign of h is allowed to reverse, h<1, (softening spring), the same kind of phenomena exists. The primary difference is that now the nonlinear

resonance curve is skewed towards the lower, rather than higher frequencies. Since ground and air resonance are determined by coupling of the rotor blades with lead/lag motion in the plane of rotation, it was hoped to take advantage of these sudden decreases in displacement amplitude. This decrease in blade lead/lag motion would subsequently reduce the severity of the offset centrifugal force on the hub. The employment of Duffing in the rotor lead/lag dynamics did, in fact, reduce the susceptability of the rotor to ground and air resonance, but not due to the Duffing jumps as hypothesized. The shift in natural frequency detuned the ground resonance sequence of events, instead.

2. Multiple Degree of Freedom Duffing Systems

Since the rotor system to be simulated was a three bladed design, investigations in a three degree of freedom Duffing system were also performed. A depiction of this system may be found in Figure 10. The possibility existed in this multiple DOF nonlinear system that reductions in resonant displacement amplitude could be achieved through coupling between the three degrees of freedom in the helicopter rotating frame.

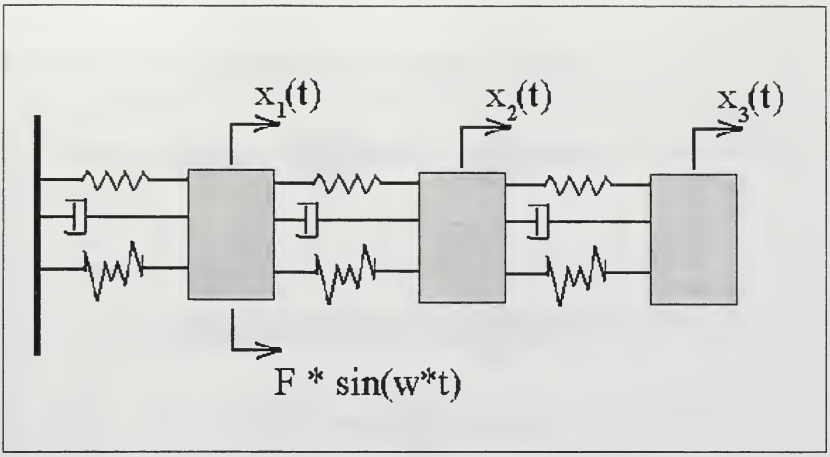

Figure 10 - Three DOF Duffing system

As shown, the Duffing spring/mass system described earlier was expanded into a three mass system. Each mass was linked by adjacent linear springs, linear dampers, and Duffing springs. An example time history of this three DOF system follows. The input parameters are the same as the one DOF case shown previously. The three resonant peaks are clearly visible.

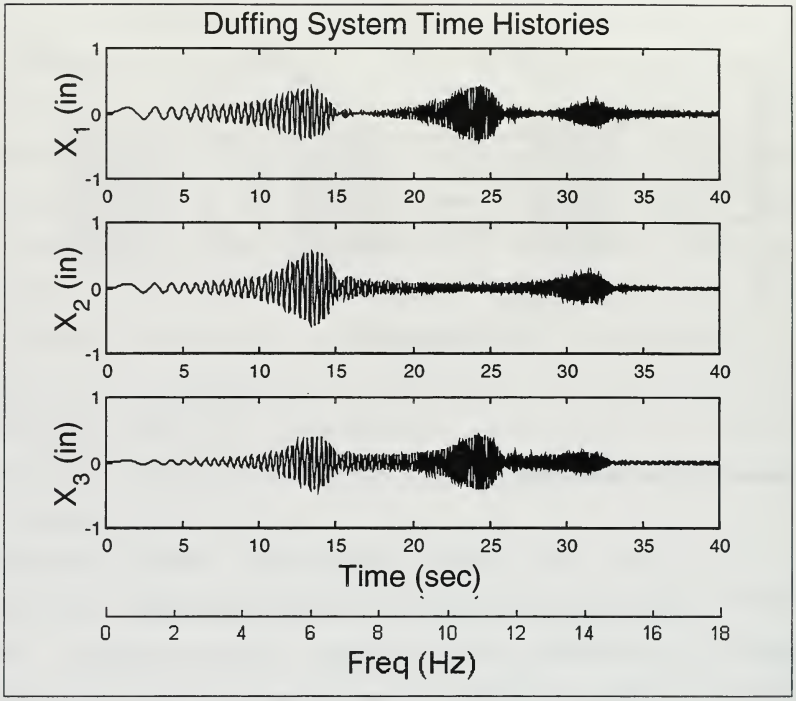

Figure 11 - Three DOF Duffing system time histories

In general, no substantial changes in the dynamics in the neighborhood of the first resonant frequency of this system were noted over the one DOF system. The second and third modes were most effected by variation in the Duffing terms of the system. By increasing the Duffing terms, the higher order modes tended to flatten out, showing resonant

behavior over larger ranges of the driving frequency. Three plots showing this trend are shown in Figure 12, first the linear system with no Duffing stiffness, with an intermediate Duffing coefficient, then with a large Duffing coefficient.

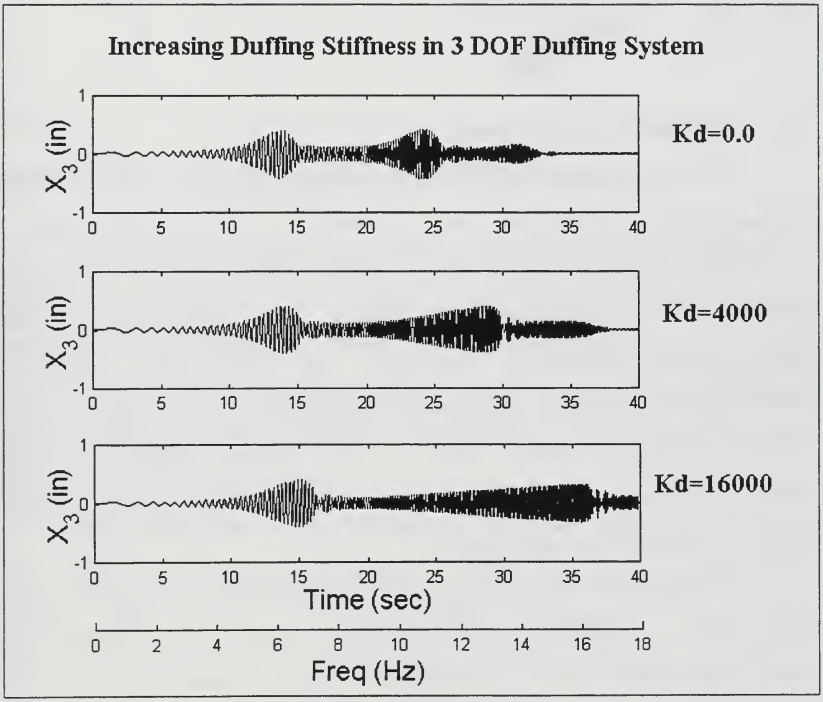

Figure 12 - Effect of increasing Duffing stiffness in three DOF system

Since the ground and air resonance problem is more closely associated with the lower resonant frequencies of the rotor, no advantage in the ground/air resonance problem was gleaned from these higher order Duffing system analyses. The shift in resonance frequencies, however, still showed promise in rotor applications, as discussed in the following section.

E. DUFFING ROTOR SYSTEMS

As discussed previously, ground and air resonance are effectively driven by two phenomena: 1) the proximity of rotor and hub vibratory modes, and 2) the ability of system damping to maintain reasonable DOF amplitudes when approaching resonance. Damping, the traditional means of solving the ground resonance problem, can dominate the system dynamics through the velocity terms. Except for high damping ratios, this approach does little to shift system modal frequencies, however.

The method of passive rotor stability presented here utilizes a nonlinear Duffing type spring to address the coalescence part of the problem, while attempting to settle for whatever damping is inherent to the system. This approach eliminates the need for auxiliary damping devices for the blade lag degrees of freedom.

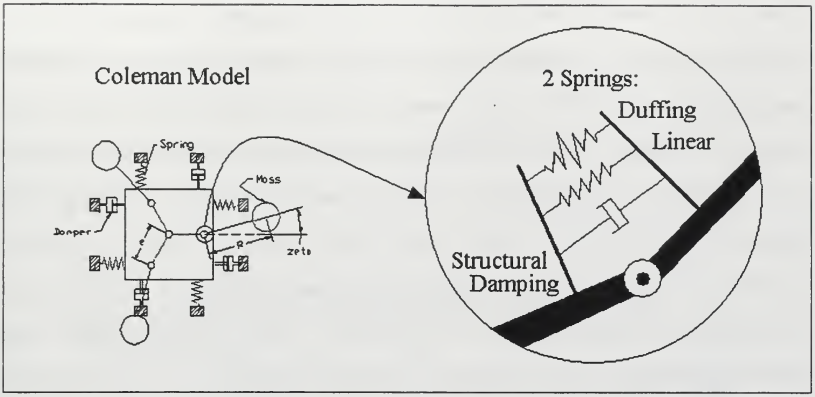

Figure 13 - Rotor with Duffing stiffness in the lead/lag dynamics

Duffing stiffness is added into the Coleman model as depicted in Figure 13. Both linear and nonlinear rotary springs plus structural damping are incorporated across the blade lag hinge. Stiffness and damping values can be defined separately for each blade to allow for asymmetric blade property investigations.

The addition of a hardening Duffing spring increases the lead/lag natural frequency of the blade as a function of blade lead angle, detuning the resonance. As blade amplitudes increase in a typical ground resonance sequence of events, the regressing mode is driven to a lower frequency as the blade natural frequency in lag is increased due to stiffening. This effectively breaks the sequence of events previously depicted in flowchart form. This shift in

the rotor's regressing mode puts the blade lag motion in a limit cycle instead of letting displacements increase without bound. For the case of soft in-plane rotors that drive through the ground resonance region of instability upon rotor engagement, upon leaving this region, the dynamics return to what one would expect from a soft in-plane rotor at rotor speeds above the region of instability. Outside the region of instability, the linear terms once again dominate the dynamics, with little or no ill effects of the Duffing stiffness seen in the dynamics.

1. Results of the Baseline Duffing Rotor

The NPS nonlinear rotor simulation was utilized in the following investigation. To provide the most robust application of Duffing springs to the ground resonance problem, simulations are performed at the center of the region of instability unless otherwise stated. This baseline case is of a rotor with the following values:

Table 2 - Table caption

Ω = 25.0 rad/s (239 RPM)	M_{hub} = 180.0 sl (5800 lbs)	M_{blade} = 6.0 sl (193 lbs)
e = 0.5 ft	$R_{blade\ CG}$ = 10.5 ft	ω_{lag} / Ω = 0.6
Structural Damping in Lag = 2.0%		
Viscous Damping in Hub = 2.0%		

Time histories of blade and hub displacements for this rotor with no Duffing stiffness employed are illustrated in Figure 14 and Figure 15. The first plot shows the blade lag angles clearly diverging from their initial zero displacement angles.

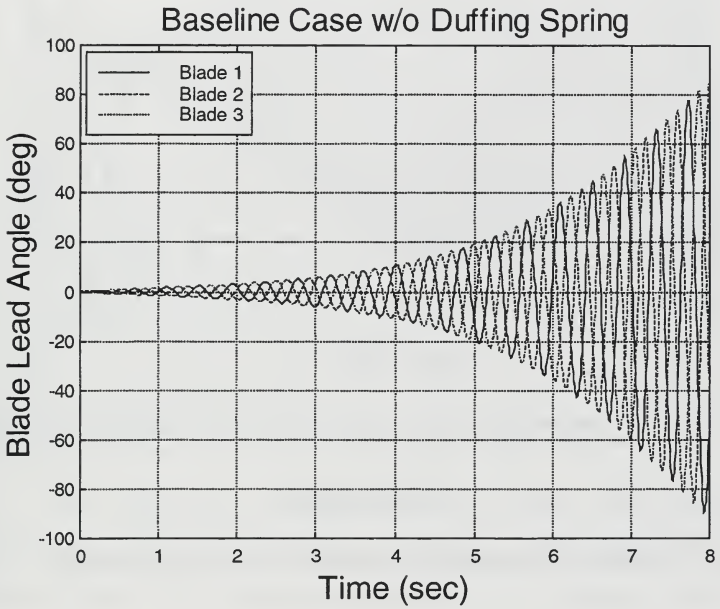

Figure 14 - Baseline case, blade lead angles without Duffing stiffness

The X direction of the isotropic hub motion is plotted in Figure 15. The hub has an initial lateral displacement of 0.2 feet to initiate the ground resonance behavior of the

system. Like the blade plot above, the hub motion clearly is subject to an oscillatory divergence.

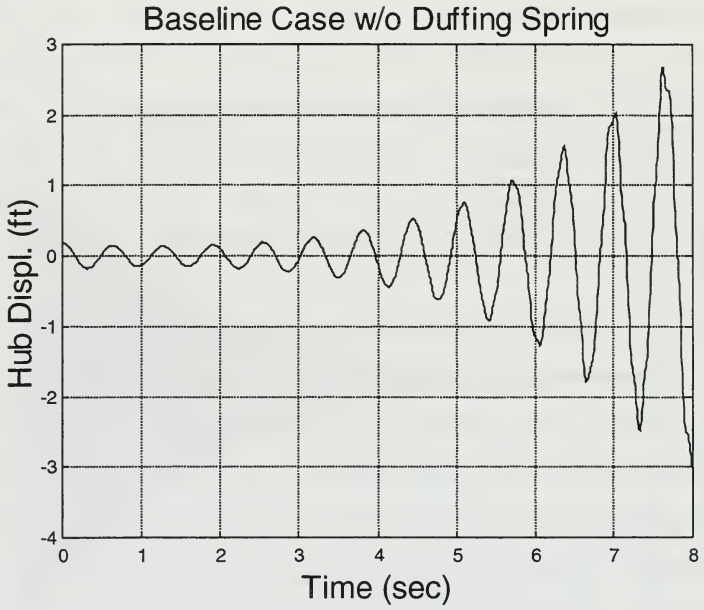

Figure 15 - Baseline case, hub lateral displacement without Duffing stiffness

2. Baseline Case with Duffing Stiffness Added

The next set of time histories gives results for the same rotor, but with Duffing spring terms added. The ratio of the Duffing stiffness coefficient to the linear stiffness coefficient is 20.0 for Figure 16 and Figure 17.

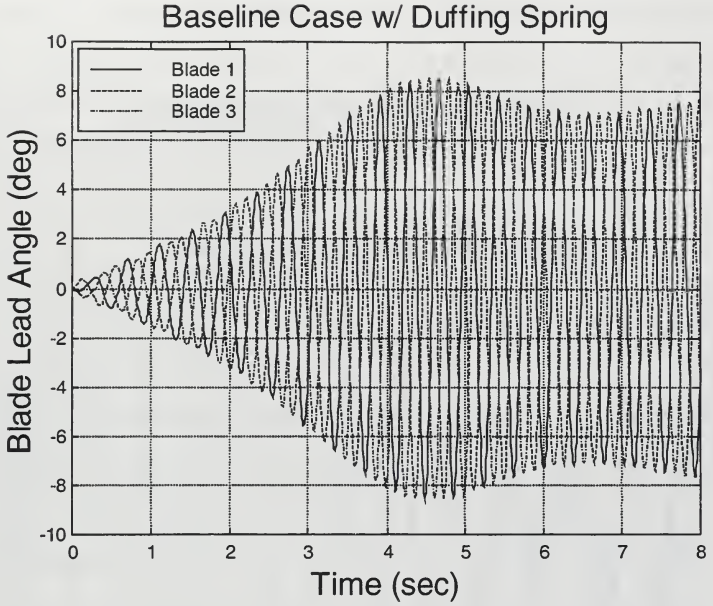

Figure 16 - Baseline case, blade lead angles with Duffing stiffness

The nonlinear stiffness clearly keeps the previously unstable blade lag response in check. Since the rotor for this case is linearly unstable, a limit cycle of approximately 8 degrees in the blade lag motion is produced.

A plot of the hub motion follows. Limit cycle motion, in general, is not considered desirable because it results in additional structural vibration in the non-rotating aircraft components. The amplitude of the lateral motion

depicted in this plot is sufficiently large that concerns over hub vibration levels were raised.

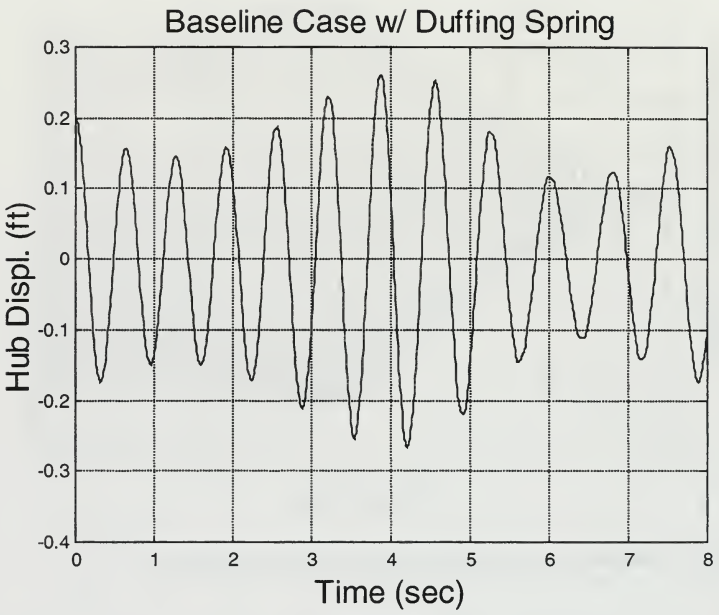

Figure 17 - Baseline case, hub lateral displacement with Duffing stiffness

The lateral vibrations experienced by the hub are plotted in Figure 18. The derivative of the hub velocity was taken numerically to obtain the hub lateral vibration data plotted. Since numerical derivation of a sampled signal tends to increase the effect of noise in the data, this plot is provided as a means of discerning the overall vibration

levels, not as an explicit means of calculating the vibration time history. The final vibratory levels are on the order of one-half the acceleration of gravity. Vibrations of this magnitude might be larger than desired, even for transient ground operations.

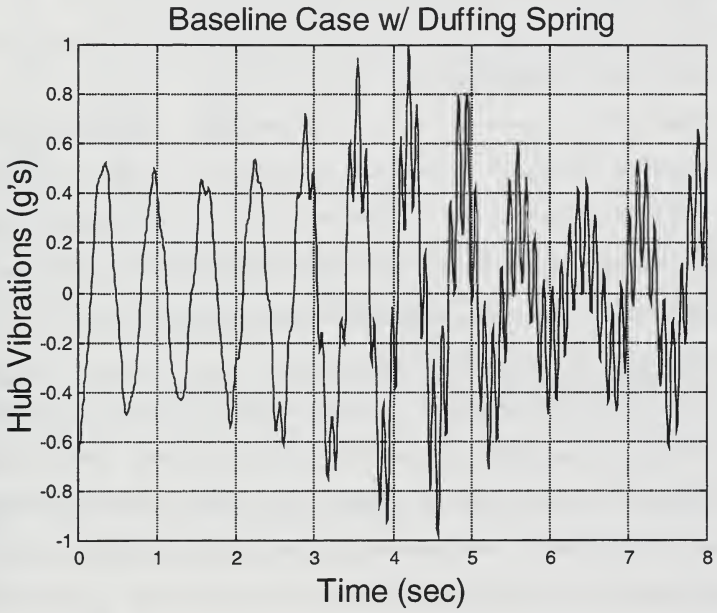

Figure 18 - Hub lateral vibration, baseline case with Duffing stiffness

3. Baseline Case with Increased Rotor Speed - Above the Region of Instability

The case that produced the unacceptable vibration levels presented above is one that was originally unstable and represents a worst-case operating regime for the rotor: the center of the region of instability. Even if the nonlinear stiffness was included in the rotor design, it is doubtful a production rotor would be designed to operate at its center of instability.

Most soft in-plane rotors are designed to operate with rotor speeds slightly above the region of instability. The rotor drives through the unstable region on engagement and disengagement. It is also possible to encounter these low Ω regimes during extreme maneuver, maintenance checks or as the result of a system failure.

For the baseline rotor presented here, the blade center of mass is at a radial location of 10.5 feet; it roughly represents a 20-ft radius rotor. For this size blade, 25 rad/sec (239 RPM) is an unusually low operating speed. If Ω is increased to approximate a 650 ft/sec tip speed in a hover, Ω would increase to 32.5 rad/sec (310 RPM).

To examine the effects of the inclusion of nonlinear stiffness at the higher rotor speed, plots of the blade and hub motion are provided in Figure 19 and Figure 20 for comparison with the linear rotor shown previously.

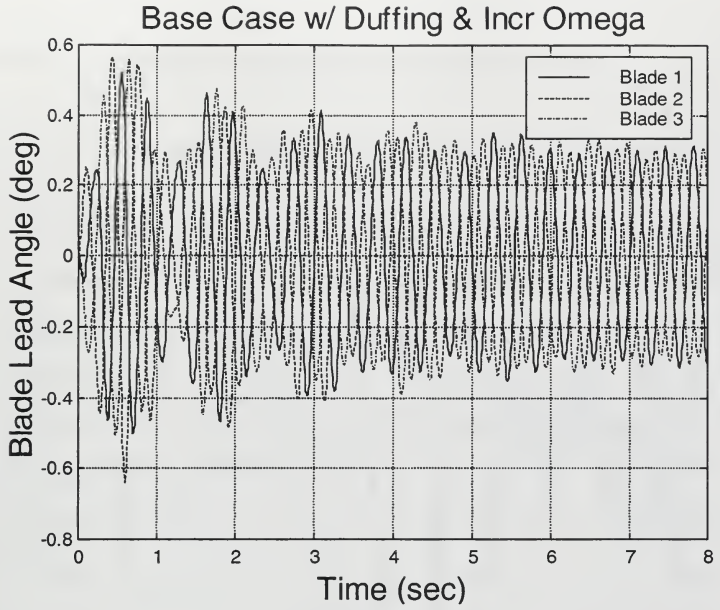

Figure 19 - Blade lead angles, increased rotor speed with Duffing stiffness

Since the rotor is now being operated with a rotor speed slightly above the region of instability, the hub and blade displacements are less for the same initial conditions. The lag limit cycle amplitude is reduced from 8 degrees all the way to 0.3 degrees.

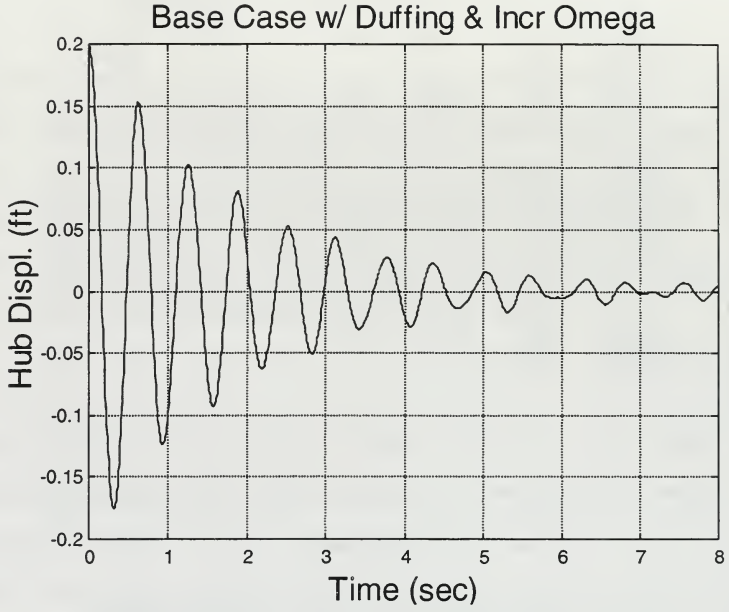

Figure 20 - Hub lateral displacement, increased rotor speed with Duffing stiffness

The hub lateral displacement saw a substantial decrease, as well. The hub limit cycle amplitude for the Duffing rotor drops 80% from the value it had at the lower rotor speed.

For comparison, the hub lateral vibrations for the Duffing rotor at both rotor speeds are plotted in Figure 21. The vibration amplitude drops almost an order of magnitude

to less than 0.05 g's, a level that is certainly in the window of today's production rotorcraft.

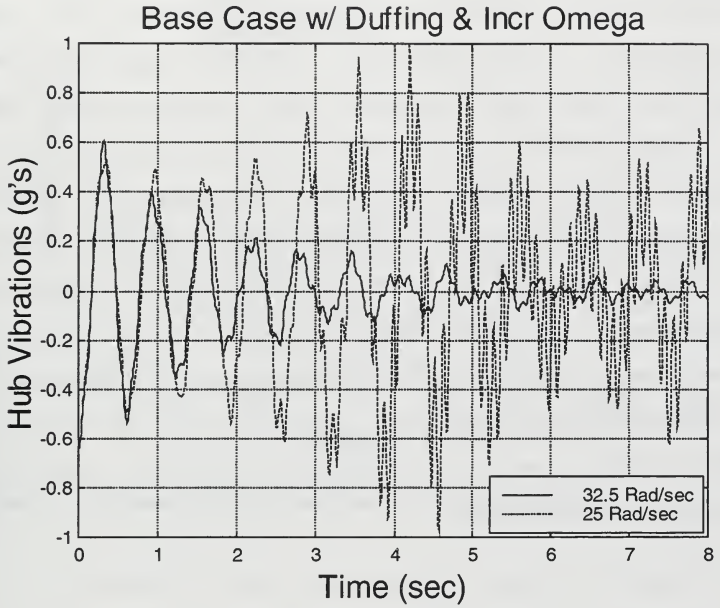

Figure 21 - Hub lateral vibration comparison

F. GROUND RESONANCE ANALYSIS

1. Frequency Coalescence

In the use of nonlinear stiffness to avoid ground and air resonance, fundamental questions arise: 1) In what way does the stiffness effect the coalescence of the regressing

lag mode to the rigid body mode? and 2) Are the restoring moments produced of reasonable magnitude?

Figure 22 is the Coleman Plot of the baseline rotor with and without Duffing stiffness included at the blade root end. It can be seen from the plot that the linear spring only case has coalescence with the hub lateral mode at a rotor operating RPM of 239, as depicted earlier in the divergent time histories, Figure 14 and Figure 15. With the inclusion of the stiffening Duffing spring, the non-rotating lag natural frequency is increased due to the increased lag displacement. This blade stiffening shifts the regressing lag mode away from the hub modal frequency at any operating RPM where resonance may occur. The action of the hardening Duffing spring keeps the frequency coelesence above the instantaneous rotor RPM.

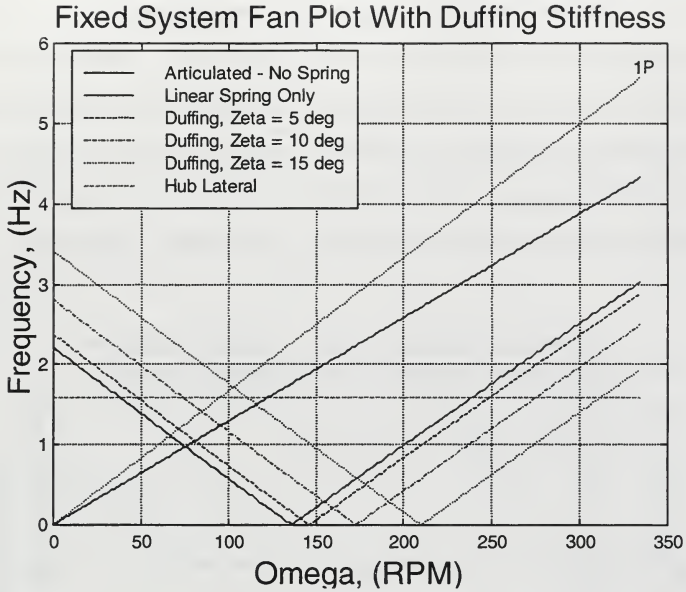

Figure 22 - Coleman plot of baseline rotor with Duffing stiffness

It should be noted that Duffing springs of sufficiently low magnitude do not stabilize the rotor, in fact, the rotor RPM that results in ground resonance is increased slightly over the rotor RPM where the linear rotor would experience ground resonance. For this reason, the Duffing replacement of auxilary lag damping produces less hub motion for rotors with a lag frequency in the upper range, 0.6 or 0.7 per rev, vice the lower 0.3 per rev range, which produces unacceptable hub and blade motion.

2. Comparison with Theory - Baseline Rotor

A Coleman stability plot for the baseline rotor follows. This plot was produced from Matlab® code that was modified from Rafanello [Ref. 9]. One can see the region of instability between 225 RPM and 266 RPM. This plot is for the baseline rotor with no Duffing stiffness employed.

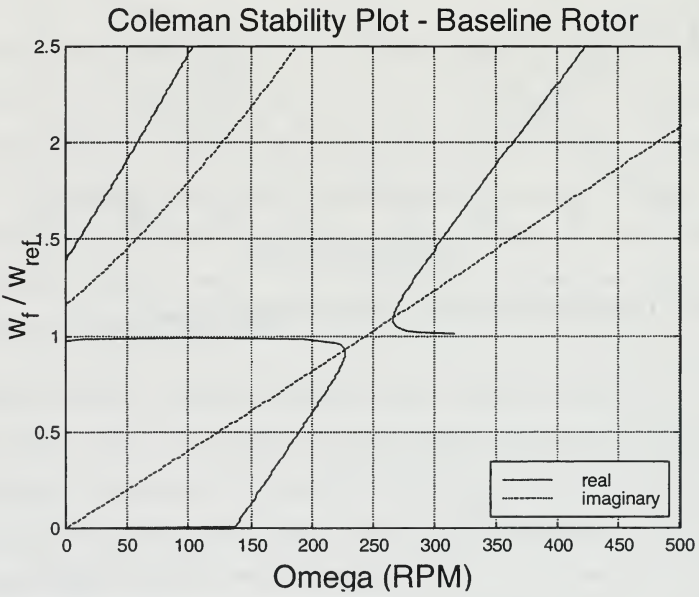

Figure 23 - Coleman plot for baseline rotor

One can see the duplication of this region of instability in the simulation results, Figure 24. This stability plot matches the plot from Coleman quite well. The

region of instability begins at 225 RPM in similar fashion to the theory. The NPS simulation becomes stable at 261 RPM where the theory does not predict stability until 266 RPM. This difference matches the results found by both Robinson and Rafanello in that Coleman's linear analysis, as applied by Deutsch, produces slightly conservative stability criteria for ground resonance [Refs. 1, 9].

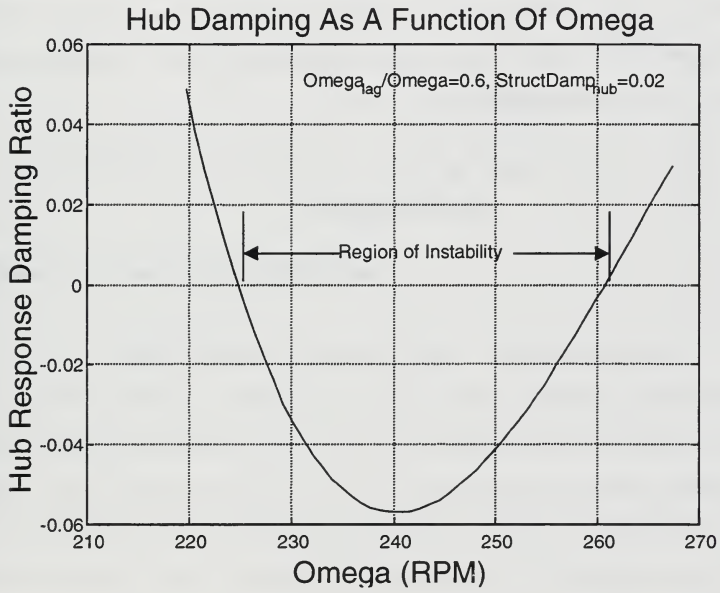

Figure 24 - Baseline rotor region of instability

3. Comparison with Theory - Duffing Rotor

The following Coleman stability plot is for the baseline rotor with 8 degrees lag amplitude with a Duffing coefficient 20 times the linear stiffness. One might note that Coleman's is a linear analysis. This linear analysis is applied to the nonlinear Duffing rotor at a single instance in time with a specific lead angle, and is not valid at any other blade lead angle. One can immediately see that the nominal rotor speed of 239 RPM is now stable. The Duffing stiffness in the rotor continuously drives the unstable region above the RPM of the rotor.

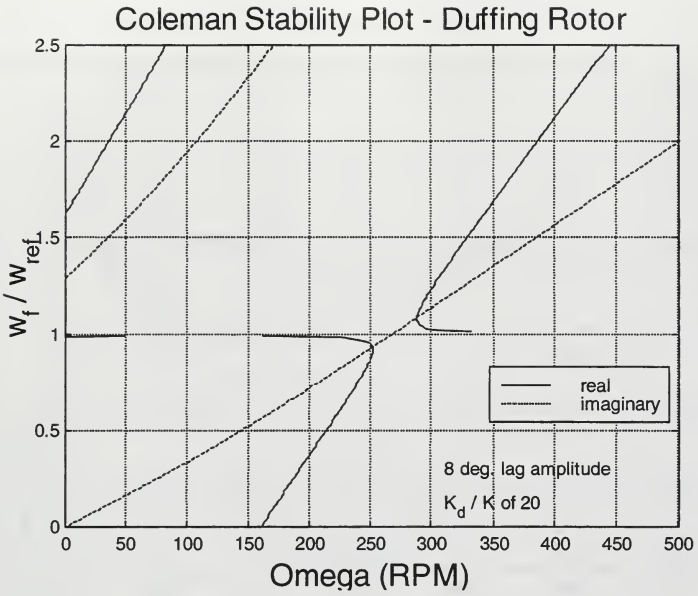

Figure 25 - Coleman plot for Duffing rotor

4. The Region of Instability - Duffing Rotor

The overall effects of including Duffing stiffness in the lead/lag dynamics can be more easily discerned in Figure 26. Hub lateral stability at a variety of rotor speeds is plotted for four different Duffing blade stiffnesses. The introduction of Duffing stiffness at 10 times the linear stiffness greatly increases overall hub motion stability, but does not stabilize the rotor. A Duffing stiffness just over 30 times the linear stiffness would provide a stable baseline rotor for all rotor speeds.

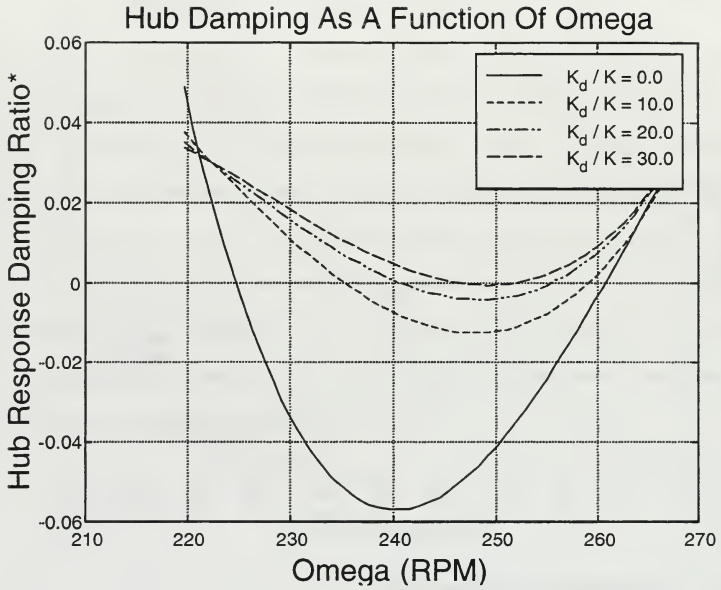

Figure 26 - Change in region of instability with Duffing stiffness included

It should be noted that in Figure 26 that the damping values plotted on the Y-axis are linear approximations for damping obtained from a nonlinear system time history (for all but the $K_d/K=0.0$ line). The Hilbert transform method was used to determine damping from the hub lateral time history for each point on the lines depicted. The last 8 seconds of a 9 second simulation were used as inputs to the damping analysis. Example time histories for the Kd/K=20.0 rotor

follow in Figure 27. These plots were taken at the three separate rotor speeds labeled.

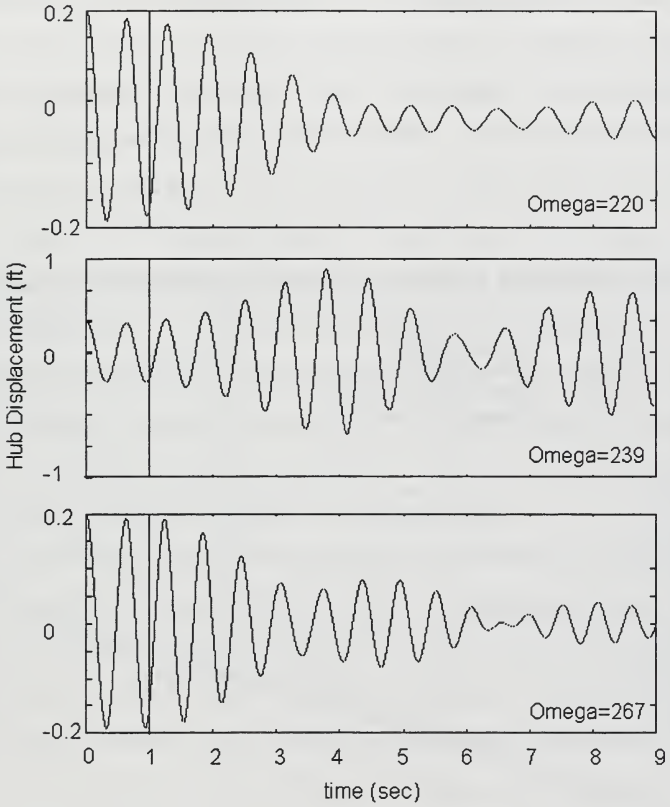

Figure 27 - Example Hub Time Histories

5. Duffing Rotor Effect on Structural Moments

Figure 28 depicts the blade restoring moment due to the combination of linear and nonlinear stiffness as a function of blade lag displacement. For the baseline rotor operated at the center of instability, the lag amplitude was approximately 8 degrees. This condition increases the restoring moment less than 50% from the linear spring only case.

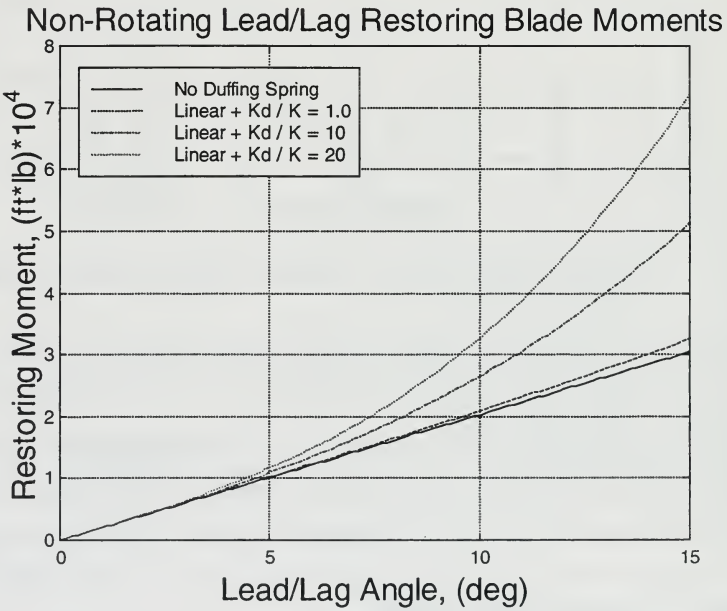

Figure 28 - Lead/lag restoring moments

Keep in mind, however, that a blade experiencing these increased loads due to root end stiffness encounters no lag moments from the now removed auxiliary lag damper. Also, the 8-degree lead angles seen in the baseline case with Duffing stiffness (Figure 16) was for a "worst case" at the center of the region of instability. The center of instability is an unlikely nominal design RPM for a rotor, even one with nonlinear stiffness. For the cases shown with increased Ω, the blade lead angles were on the order of a degree, which shows virtually no additional restoring moment on this plot. The addition of Duffing stiffness at reasonable rotor speeds, therefore, is not producing blade bending moments that current rotor designs do not already handle.

6. Stiff-in-Plane? - Duffing Rotor

In ground resonance analysis, one additional question arises: Since a stiffening term is being employed, is the rotor becoming stiff-in-plane? A stiff-in-plane rotor is one that has a lead/lag natural frequency greater than the rotating frequency of the rotor head. For the baseline rotor with a rotary spring Duffing stiffness coefficient 20 times the linear stiffness coefficient, the rotor only goes stiff-in-plane when the blade lag amplitude exceeds 6 degrees at 239 RPM. For the baseline rotor with Duffing stiffness employed, the rotor can go stiff-in-plane. If the rotor is

operated off the center of instability, however, it does not go stiff-in-plane.

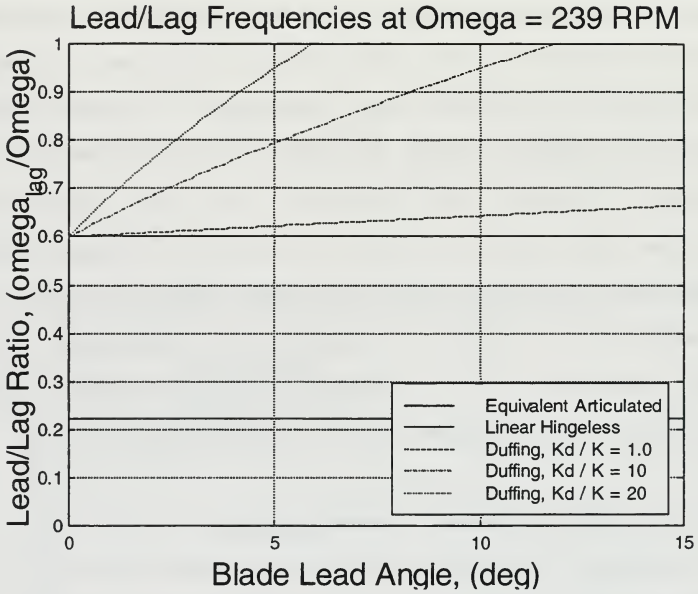

Figure 29 - Soft in-plane frequencies at 239 RPM

As depicted in Figure 30, in this case, the rotor goes stiff-in-plane when the blade lag amplitude exceeds 12 degrees for this baseline rotor with Duffing stiffness employed at 310 RPM.

At the increased rotor operating speed of 310 RPM, the limit cycle lag amplitude was less than a degree. For lead angles of this small amplitude, the rotor sees very little

migration towards stiff-in-plane from its initial lag frequency. Since the exact same baseline rotor is modeled, note that the lag natural frequency is changed due to the increase in rotor RPM. What was a 0.6 per rev lag frequency rotor is now a 0.6*(239/310)Ω = 0.46 per rev lag frequency rotor.

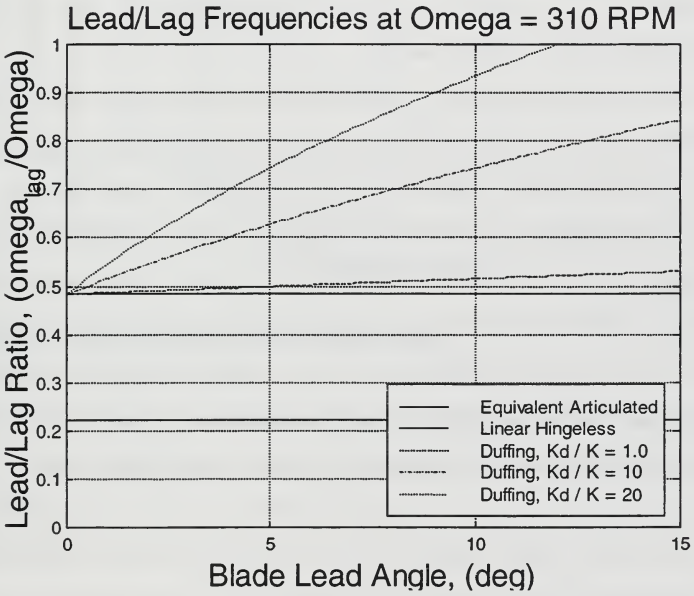

Figure 30 - Soft in-plane frequencies at 310 RPM

G. CHAOS ANALYSIS

1. Response to Similar Initial Conditions

Duffing's equation is well documented in the literature. In Ueda [Ref. 19], parameter combinations that produce chaotic response from Duffing's equation are summarized. Since chaotic response in the blade lag motion is undesired, a check of the simulation time histories must be completed to rule out chaotic response for the Duffing rotor presented in this paper.

One characteristic of chaotic systems is vastly differing time histories resulting from nearly identical initial conditions. Figure 31 is a Poincare section of the lateral response for the baseline hub with Duffing stiffness. Three initial conditions of hub displacement are plotted. The hub response depicted in this plot is not chaotic; the sampled points on the phase plane are nearly identical for the three cases. The sample frequency for this Poincare section is the regressing lag frequency, $(\Omega-\omega_{lag})$.

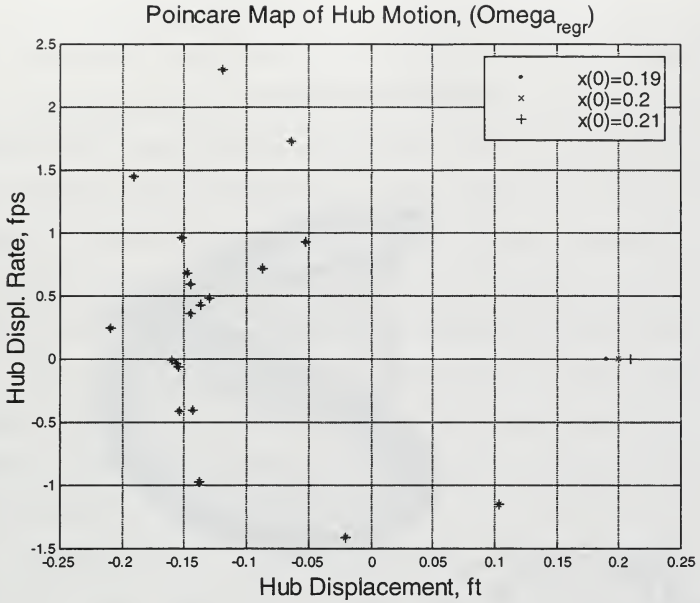

Figure 31 - Poincare section of hub lateral motion

2. Poincare Phase Plane and Phase Space Analyses

In addition, chaotic motion would not follow a prescribed form in phase space. Figure 32 is the blade lead/lag motion plotted in 3-D phase space with the blade lead angle rate on the vertical axis, the lead angle on the radial axis, and the phase plane rotated at the lead/lag natural frequency. The initial conditions of zero lead angle and rate quickly begin to track a predictable path in the phase space, showing no tendency towards chaos.

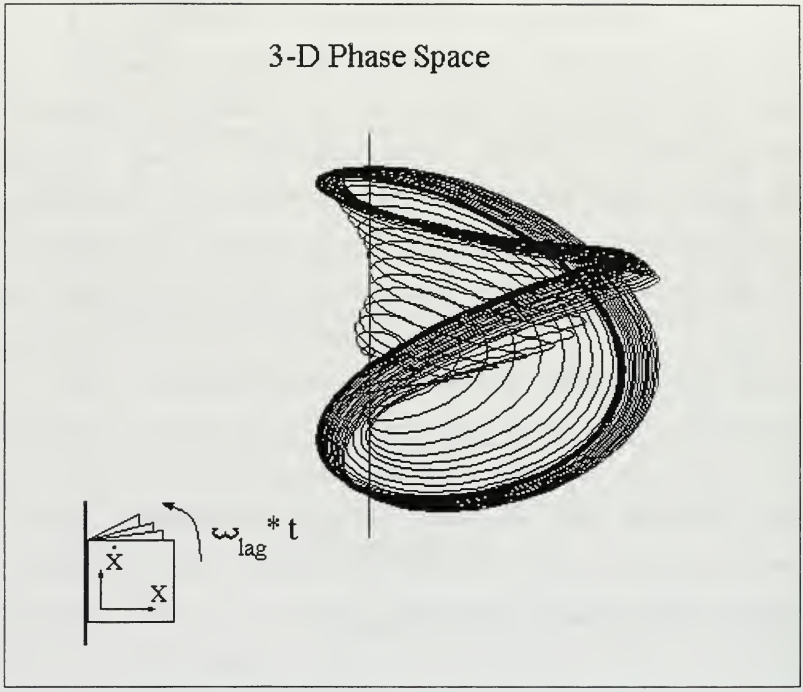

Figure 32 - Phase space of blade lead motion

H. DROOPING ROTOR STABILITY

1. Nonlinear stiffness provides rotor stability for a wide range of physical parameters

Rotor design engineers must insure rotor stability for a wide range of operating parameters. The fuselage rigid body natural frequency in roll is a strong function of the

fuselage inertial properties. Different fuel loads, cargo and passenger configurations effect fuselage rigid body natural frequencies. Landing gear properties, such as strut cleanliness, strut oleo servicing, and tire inflation can also effect these frequencies. The engineer must work to obtain a stable rotor under all these conditions. In addition to fuselage characteristics changing, rotor blade properties can change. Helicopter operators can change trim tab and pitch link settings, effecting the way the blade tracks. They can also change blade tip weights in the dynamic balancing process, which has a strong effect on blade inertias.

Historically, larger lead/lag dampers than were necessary were employed in final designs in an attempt to maintain rotor stability over all possible operating conditions. The dampers were used as an engineering "safety net." In Figure 33, the Duffing stiffness in the rotor is used as a similar safety net for rotor speed reduction. Reduced rotor speeds could be experienced as a result of system failure or during maintenance checks, in addition to rotor engagement and disengagement. This figure compares a rotor with Duffing stiffness to a rotor with linear stiffness only. As rotor RPM is reduced, both rotors enter the region of instability and experience resonance. The linear rotor quickly reaches hub displacement amplitudes

that could cause catastrophic failure. The Duffing rotor encounters smaller hub displacements, avoiding loss of the helicopter. In this case, the Duffing stiffness is used as a rotor safety feature, avoiding the large hub displacements that result in failure as the rotor speed is reduced.

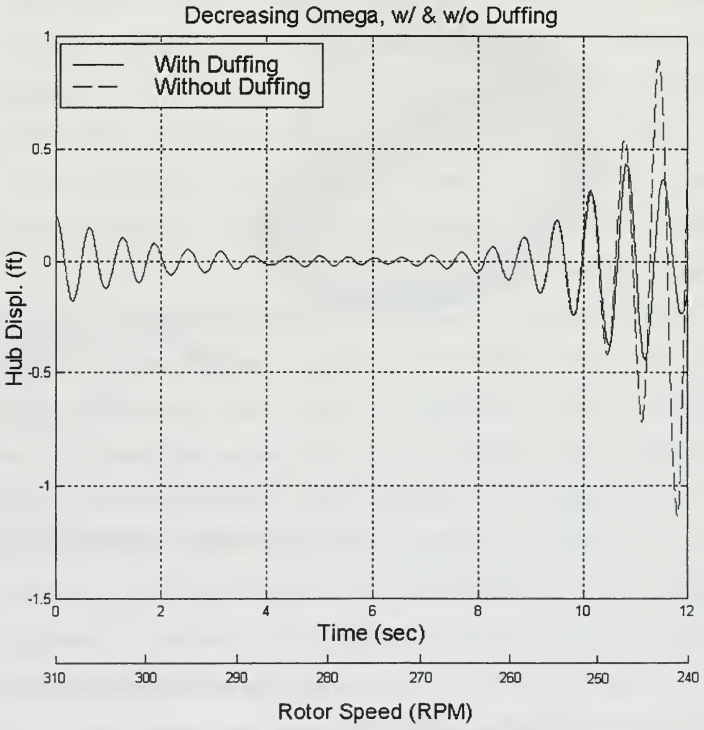

Figure 33 - Reduced rotor speed comparison

IV. LINEARLY LINKED ROTOR SYSTEMS

A. INTRODUCTION

The helicopter in ground resonance could be compared to a simple harmonic oscillator. The rotor acts as the exciting force, and the rigid body motion of the helicopter is the response. If one desires to avoid resonance, one could take one of two approaches to the problem. Frequencies of the system could be modified, which would avoid coalescence. Either the exciting force frequency (the rotor regressing mode) or the oscillator natural frequency (the fuselage rigid body natural frequencies) could be changed to avoid driving the system into resonance.

The other approach that could be used is the modification of the resonant mode shape. Changing the mode shape naturally changes the mode's resonant frequency. By linking the blades together, the mode shapes of the blades' lead/lag motion are changed. Modifying the mode shape, in turn, alters the blade natural frequency in lead/lag and the regressing mode of the rotor. Therefore, by linking the blades, the potential exists to avoid ground/air resonance by detuning the rotor-body dynamics, thus avoiding ground and air resonance in a similar manner to the nonlinear stiffness approach already discussed.

B. ROTOR WITH LINKED BLADES

A four bladed rotor simulation was developed similarly to the Coleman-like three bladed rotor used in the damperless rotor investigations and the Comanche five bladed rotor used in the second chapter. This baseline rotor was intentionally chosen to be unstable. The equations of motion for this new four bladed simulation were also derived using Lagrange's method in a Maple® worksheet. Unlike the other rotor simulations, this new four bladed rotor had the additional capability of linking the blades, either elastically or rigidly. In addition to linear stiffness as a function of the angle made between the blade and its nominal position with respect to the hub, in this case, rotary stiffness terms were added as functions of the lead/lag angles made between adjacent blades. All linked stiffness and damping values were linear.

If traditional linear root-end stiffness were described as $M_n=k_\zeta*\zeta_n$ for the n^{th} blade, then this new interlink stiffness could be described as:

$$M_n=k_{inter(n+1)}(\zeta_{n+1}-\zeta_n)+k_{inter(n)}(\zeta_{n-1}-\zeta_n)$$

Where K_{inter} is the interlink stiffness (moment/angle), and $(\zeta_{n+1}-\zeta_n)$ and $(\zeta_{n-1}-\zeta_n)$ are the instantaneous lag angle differences between the nth blade and its two adjacent neighboring blades, (n+1) and (n-1). The simulation was also

given the capability of linking the blades with viscous dampers which were functions of blade lead angle rate differences:

$$M_n = c_{inter(n+1)}(\dot{\zeta}_{n+1} - \dot{\zeta}_n) + c_{inter(n)}(\dot{\zeta}_{n-1} - \dot{\zeta}_n)$$

Investigations in the potential payoffs of inter-blade linking follow in the next three sections. The baseline case properties for the four bladed interlink rotor may be found in the following table:

Table 3

Ω = 25.0 rad/s (239 RPM)	M_{hub} = 160.0 sl (5150 lbs)	M_{blade} = 4.0 sl (129 lbs)
e = 0.5 ft	R = 10.5 ft	ω_{lag} / Ω = 0.6
Linear Damping in Lag = 1.0%		
Linear damping in Hub Lateral Motion = 2%		

Time histories for the baseline case blade lead angles may be found in Figure 34. This case also has been purposely set inside the region of instability, and clearly diverges.

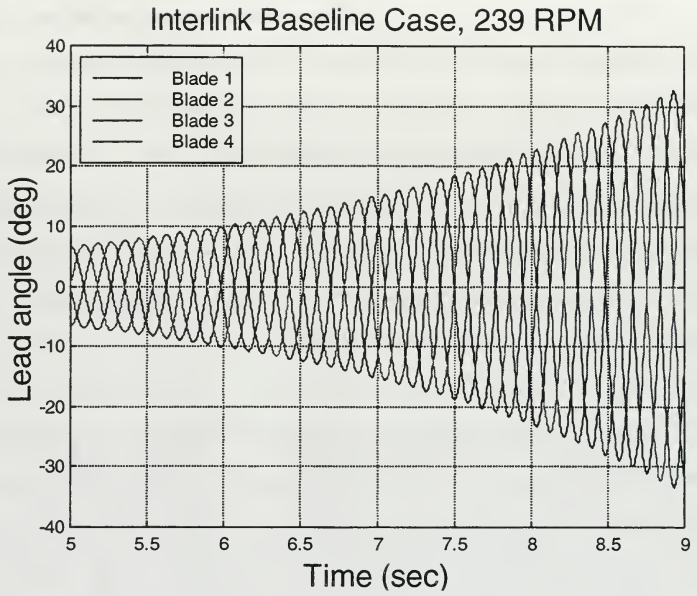

Figure 34 - Four bladed interlink baseline

C. LINKED BLADE PARAMETRIC STUDIES:

1. Linked blade & hub response varying blade interlink stiffness for baseline rotor

The effects of varying blade interlink stiffness for four different hub damping values can be seen in Figure 35. For the cases presented, each blade is elastically linked to each of the two neighboring blades in series. For very low interlink stiffness, K_{link}/K_{blade} is low, the simulations are unstable, similar to the baseline case, as would be expected. As the interlink stiffness is increased, however,

a sharp increase in rotor stability occurs in the region where the blade interlink stiffness is of the same order of magnitude as the flexbeam chord-wise stiffness, K_{blade}. For these cases, previously unstable rotors were stabilized for all but the lowest hub damping of 1%.

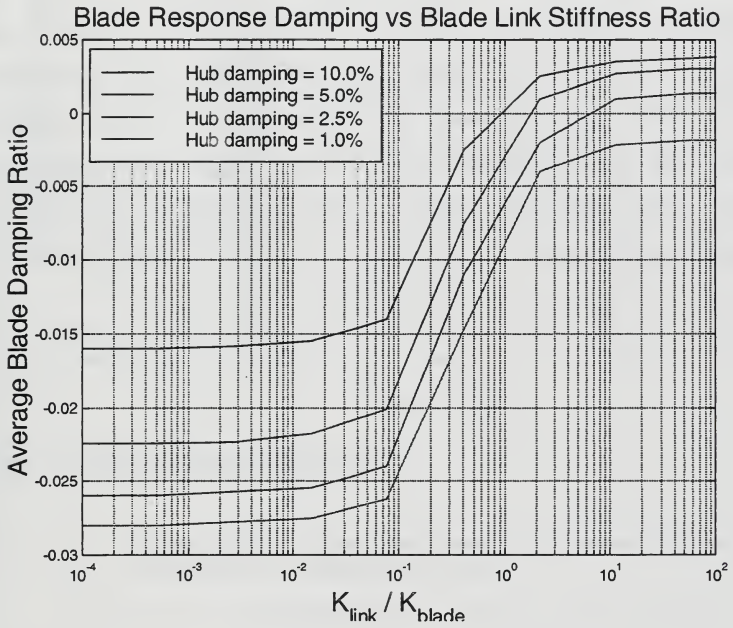

Figure 35 - Blade elastic interlink results

2. Linked blade & hub response varying blade interlink damping for baseline rotor

Interlinking dampers was also attempted. All four blades were interconnected by similar dampers, thus putting the interlink dampers in series. Recall for the baseline four bladed rotor that linear blade damping was only 1.0%. For inter-blade damping, the same four hub values are plotted in Figure 36. The interlinking of blade dampers also proves effective. Unlike the case of the interlinked stiffness, this increase in stability is to be expected since the overall system damping has been increased, even though the additional dampers are implemented in less than traditional means.

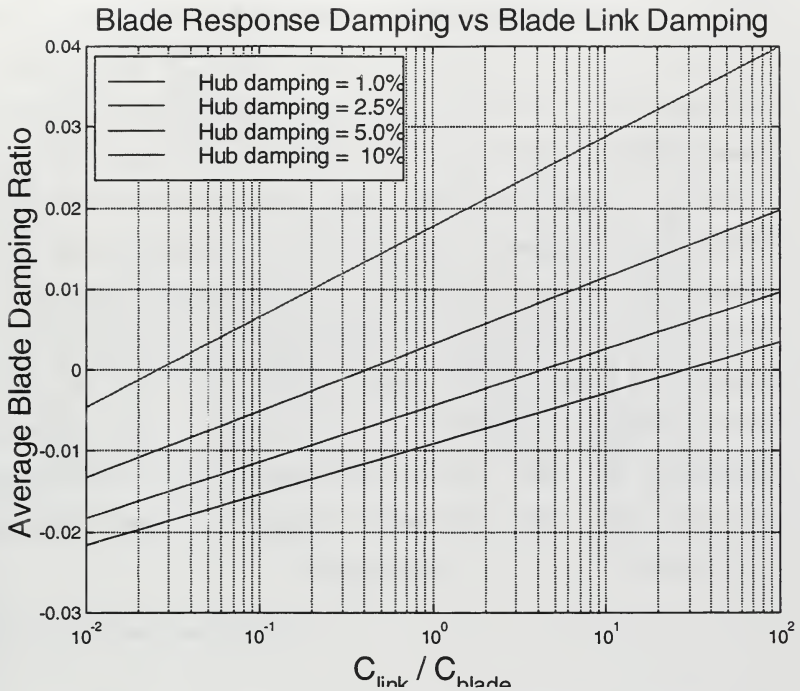

Figure 36 - Blade damper interlink results

3. Linked blade & hub response with uneven interlink stiffness for baseline rotor

Looking at unsymmetrical blade interlinking was accomplished so as to change the relative phasing of the blades in ground resonance. Note that for the divergent baseline case (no linking), each blade moves 90 degrees out of phase with its neighbor in the case of a four-bladed rotor. In general for an n-bladed rotor, Coleman showed that

during divergence the blades moved at a phase angle of $2\pi/n$ (radians) or 360/n (degrees) with respect to each other. It was expected that disrupting this phasing would change the magnitude of the rotor CG offset from the center of rotation, in turn reducing the coupling into the fuselage degrees of freedom. This is due to the fact that we can change the natural frequency of a system by altering its eigenvalue (changing the spring rate) or by altering its eigenvalue (changing the mode shape). In Figure 37, the #1 and #2 blades alone are linked. This action does reduce the amplitude of the blade lead angles over the baseline unstable case, but all cases using this method diverged, nonetheless.

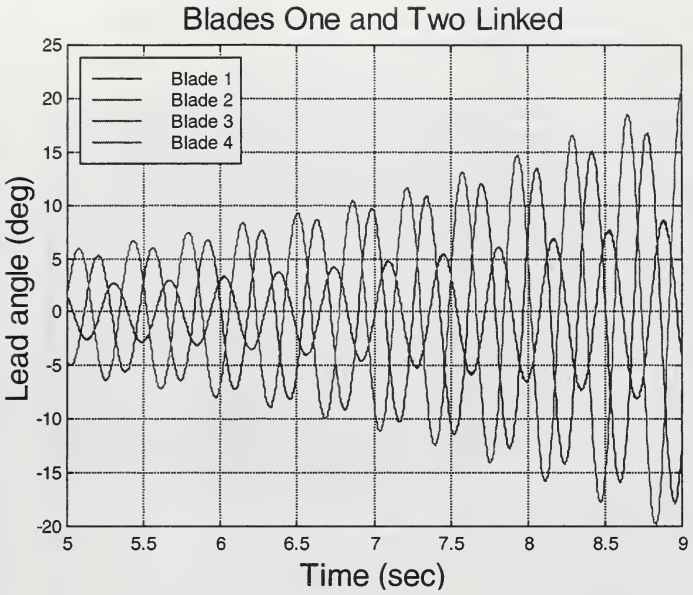

Figure 37 - Blades #1 and #2 linked

Linking the blades in pairs, however, showed far different results. In Figure 38, the #1 and #4 blades are linked, and the #2 and #3 blades are linked. This interlinking in pairs stabilizes the rotor. For a linearly unstable rotor, blade limit cycle amplitude is only 2 degrees.

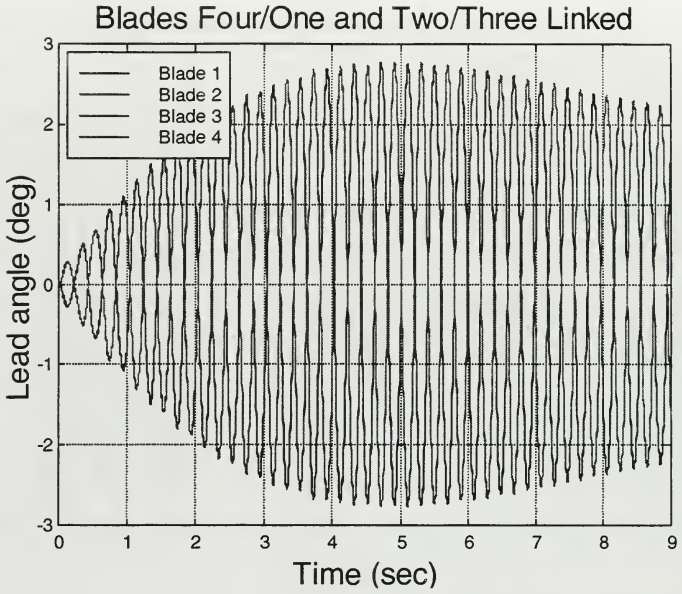

Figure 38 - Blades #4&1 and #2&3 linked

By linking the blades in adjacent pairs, the four bladed rotor acts more like a two bladed rotor, unable to enter ground resonance. This method of stabilizing the rotor shows promise in that the aerodynamic and handling response characteristics of a multi-blade rotor can be maintained, but the rotor exhibits the mechanical stability normally found in two bladed rotors.

4. Interlink Dampers Versus Conventional Dampers

In Figure 39, traditional blade dampers are compared to interlink dampers. Essentially, the four lead/lag dampers that might be found on a rotor have been detached from the hub and remounted between the four blade roots. Identical damping values were used for the two lines plotted.

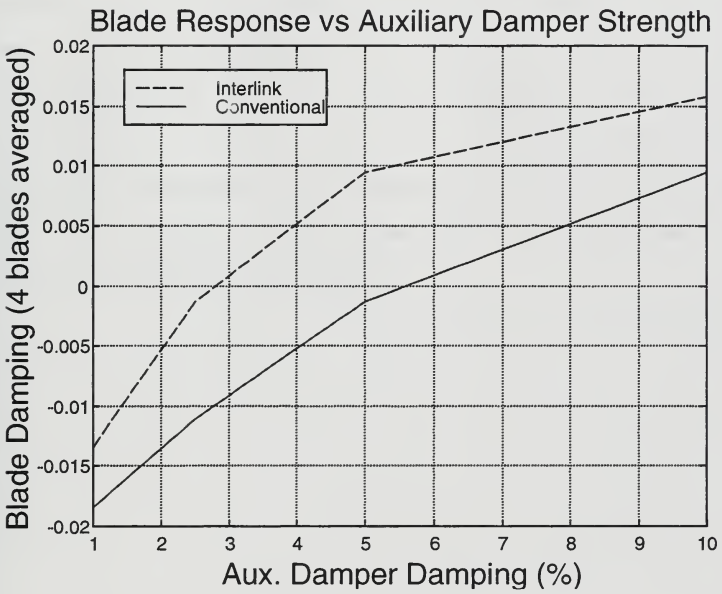

Figure 39 - Conventional dampers versus interlink dampers

The interlink damping proves more effective for a given damping value. Instead of the dampers acting independently for each blade, the new system takes advantage of the fact

that the blades are 90 degrees out of phase with each other, essentially amplifying the input to the dampers. Since weight is always a driving issue in aircraft design, if the dampers were mounted between the blades, instead of from the blade to the hub, smaller dampers could be installed and still maintain the desired damping in the blade chord-wise dynamics.

V. ROTOR WITH UNEVEN BLADE SPACING

As long as unsymmetrical rotors are being investigated, the effect of modifying blade spacing was also attempted. Blade motion time histories from a 60-120-60-120 degree spread rotor can be found in Figure 40. This rotor layout is similar to the AH-64 Apache tail rotor, where the four blades are not positioned 90 degrees apart, but instead arranged in an X pattern, not a perfect cross. The Apache-like rotor also exhibited blade divergence. The blade pairs diverged at different rates, but the same overall response was noted: mechanical instability was not avoided for any of the rotor speeds investigated for the case where uneven blade spacing was introduced.

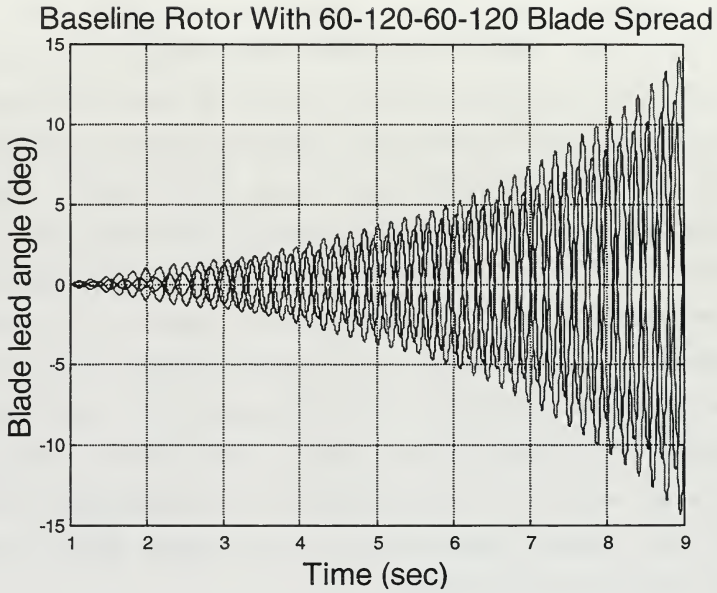

Figure 40 - Baseline rotor with 60-120-60-120 blade spread

VI. GROUND AND AIR RESONANCE ANIMATION

Obviously, numerous cases and configurations were simulated in the course of this research. All these simulations were performed on a PC running Simulink®. Utilizing the numerical analysis capabilities of Matlab® including the Hilbert damping analysis, numerous quantitative parameters were generated.

In an attempt to provide a better qualitative picture for what the rotor was doing, an animation routine was written that would show the engineer visually what the blades and hub were doing in the horizontal plane. The animation routine written as part of this research plots the rotor blades as simple lines at the computed lead angle from the simulation at every time step. The depicted rotor does not rotate, so that blade action can be observed. The center of rotation is also changed. The animated blade center is plotted at the hub X and Y position with respect to the inertial frame, also obtained from the simulation at every time step. In this way, the outward spiral of the hub is also depicted as part of the animation.

Though no numerical results are obtained, the animation routine was found very useful in providing an overview of rotor states. Four example frames of this simulation are shown in Figure 41. These frames show the progression of

blade movement in a typical ground resonance scenario. Notice how the animation illustrates the spiral motion of the CG of the rotor around the center of rotation. The 90 degree blade phasing is also easily discernible.

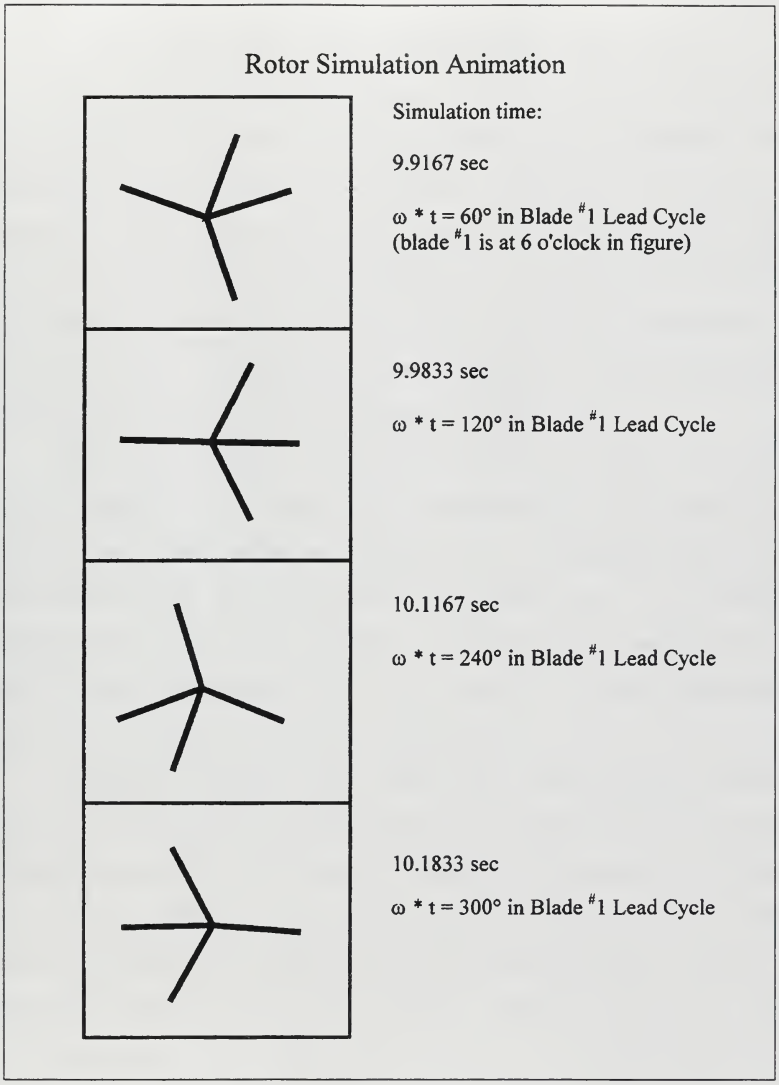
Rotor Simulation Animation
Simulation time:
9.9167 sec
ω * t = 60° in Blade #1 Lead Cycle
(blade #1 is at 6 o'clock in figure)
9.9833 sec
ω * t = 120° in Blade #1 Lead Cycle
10.1167 sec
ω * t = 240° in Blade #1 Lead Cycle
10.1833 sec
ω * t = 300° in Blade #1 Lead Cycle

Figure 41 - Rotor animation

VII. DAMPERLESS ROTOR DEVELOPMENT CONCLUSIONS

With the advent of hingeless and bearingless main rotor helicopters, interest in nonlinear rotor dynamics has increased significantly in recent years as an area to research for improved rotor stability. With the rapid evolution of high-speed processors and recent developments in software technology, we now have the tools available to explore rotor system nonlinear dynamics and potentially achieve helicopter rotor mechanical stability.

This dissertation furthered the development of a nonlinear analysis tool that has the capability of modeling a rotor's nonlinear material properties. Most importantly, the simulation did not incorporate assumptions or ordering schemes that limit the number of terms in the equations of motion and subsequently skew the output. In the simulation used, not a single term was eliminated.

Potential methods for passively controlling lead/lag motion of helicopter blades have been developed. One of the methods presented utilizes Duffing-type nonlinear stiffness in the root end of the rotor blade in addition to linear spring and damping properties. The Duffing spring provides a restoring force that is a cubic function of the blade lead/lag deflection. This nonlinearity shifts the first in-plane natural frequency of the blade as a function of the blade lag angle. This shift in blade natural frequency

effectively varies the regressing mode frequency. The resulting shift in the regressing mode prevents coalescence with hub resonant frequencies. For a linearly unstable rotor-fuselage system, inclusion of the Duffing spring results in limit cycle behavior in the blade lead/lag degrees of freedom and in hub translational motion.

An analysis of the limit cycle motion effect on hub vibrations was also completed. The replacement of blade auxiliary lag dampers with nonlinear springs results in increased hub vibration levels if the resulting system is highly unstable in the linear analysis. Rotors that are marginally stable, or stable, in the linear analysis produce vibration levels that are not uncommon in production rotorcraft.

The primary conclusions of this research on damperless rotors are:

- Application of nonlinear stiffness properties to the blade lead/lag degrees of freedom can effectively improve helicopter ground/air resonance stability characteristics.
- Stability characteristics are improved through frequency mismatch, not by dominating system dynamics with high damping.
- Blades with low lead/lag natural frequencies have greater potential for producing unacceptable vibration levels in

both dynamic and non-rotating components if Duffing stiffness is employed.

- Interblade rigid and elastic coupling has the potential to eliminate helicopter unbounded blade motion.
- In this case, the interblade coupling achieves stability by altering the phase of relative blade response. That is, the response eigenvector has been altered.
- Interblade viscous damping, selectively applied, can be a more efficient use of blade auxiliary dampers than the conventional blade-to-hub arrangement.
- Uneven blade spacing, for the case examined (60-120-60-120), did not prove effective in avoiding helicopter ground and air resonance.

LIST OF REFERENCES

1. Robinson, C. S., "Modeling and Analysis of Helicopter Ground Resonance Utilizing Symbolic Processing and Dynamic Simulation Software," Aeronautical Engineer's Thesis, Naval Postgraduate School, March 1997.

2. Tongue, B. H. and Flowers, G., "Nonlinear Rotorcraft Analysis," International Journal of Nonlinear Mechanics, Vol. 23, No 3, September 1987, pp. 189-203.

3. Tongue, B. H. and Flowers, G., "Nonlinear Rotorcraft Analysis Using Symbolic Manipulation," Applied Mathematical Modeling, Vol. 12, April 1988, pp. 154-160.

4. Warmbrodt, W. and Friedmann P., "Formulation of Coupled Rotor/Fuselage Equations of Motion," Vertica, Vol. 3, 1979, pp. 245-271.

5. Coleman, R. P., "Theory of Self-Excited Mechanical Oscillations of Hinged Rotor Blades," NACA Advance Restricted Report 3G29, 1943.

6. Coleman, R. P. and Feingold, A. M., "Theory of Self Excited Mechanical Oscillations of Helicopter Rotors with Hinged Blades," NASA Report 1351, 1958.

7. Robinson, C. S.; Wood, E. R.; and King, R. L., "Full Nonlinear Simulation of Coupled Rotor-Fuselage Response Using Symbolically Derived Equations of Motion, American Helicopter Society 54th Annual Forum and Technology Display, Washington DC, May 20-22, 1998.

8. Deutsch, M. L., "Ground Vibrations of Helicopters," Journal of the Aeronautical Sciences, Vol. 15, No. 5, May 1946.

9. Rafanello, S. P., "Modeling the Coupled Rotor/Fuselage Response of the H-3 Sea King Utilizing the NPS Full Nonlinear Response Simulation," MS Thesis (Aeronautics), Naval Postgraduate School, March 1999.

10. Wood, E. R., "Preliminary Report on Mechanical Instability of HSS-2 Helicopters," Sikorsky Engineering Report No. 61163, 14 November 1958.

11. Hammond, C. E., "An Application of Floquet Theory to Prediction of Mechanical Instability," Journal of the American Helicopter Society, October 1974, pp. 14-23.

12. Tongue, B. H. and Jankowski, M. D., "Construction and Analysis of a Simplified Nonlinear Ground Resonance Model," Journal of Sound and Vibration, 1988, 122, pp. 233-241.

13. Tang, D. M. and Dowell, E. H., "Influence of Nonlinear Blade Damping on Helicopter Ground Resonance Instability," Journal of Aircraft, Vol. 23, No 2, February 1986, pp. 104-110.

14. Gandhi, F., and Chopra, I., "An Analytical Model for a Nonlinear Elastomeric Lag Damper and Its Effect on Aeromechanical Stability in Hover," Journal of the American Helicopter Society, October 1994, Vol 39, pp. 59-69.

15. Ormiston, R. A., "Rotor-Fuselage Dynamics of Helicopter Air and Ground Resonance," Journal of the American Helicopter Society, April 1991, pp. 3-20.

16. Ormiston, R. A., "Application of 2GCHAS to the Investigation of Aeromechanical Stability of Hingeless and Bearingless Rotor Helicopters," American Helicopter Society 51st Annual Forum and Technology Display, Fort Worth, TX, May 9-11, 1995.

17. Reichert, G., Weiland, E.,"Long Term Experience with a Hingeless/Composite Rotor," AGARD Conference Proceedings, May 1977.

18. Cunningham, W. J., Introduction to Nonlinear Dynamics, McGraw-Hill, 1958.

19. Ueda, Y., "Steady Motions Exhibited by Duffing's Equation: A Picture Book of Regular and Chaotic Motions," New Approaches to Nonlinear Problems in Dynamics, Holmes (ed.), SIAM, 1980.

APPENDIX A. COMANCHE FROUDE SCALE MODEL SIMULATION

Comanche Rotor Design Overview

Engineering data on the Boeing/Sikorsky RAH-66 Comanche Froude scale wind tunnel model was obtained from Sikorsky Aircraft as part of a research program initiated through the National Rotorcraft Technology Center (NRTC) [Refs. A1, A2]. Additional material on the Comanche rotor is provided by Tarzanin and Panda [Ref. A3].

The Boeing/Sikorsky report obtained by NPS outlines testing procedures, results, and basic rotor design geometry of the Comanche model rotor. The Comanche rotor design utilizes a bearingless main rotor (BMR) flexbeam arrangement for blade lead/lag, flap, and feathering degrees of freedom. A cuff, which is stiff in torsion and bending, encases the flexbeam and provides input torques in the feathering axis to the blade at the outboard end of the flexbeam, at the cuff/blade joint. A damping device called the snubber-damper is mounted between the inboard end of the cuff and the hub to provide additional damping and stiffness in the blade lead/lag degrees of freedom. A depiction of this rotor is given in Figure A1, reproduced from Panda.

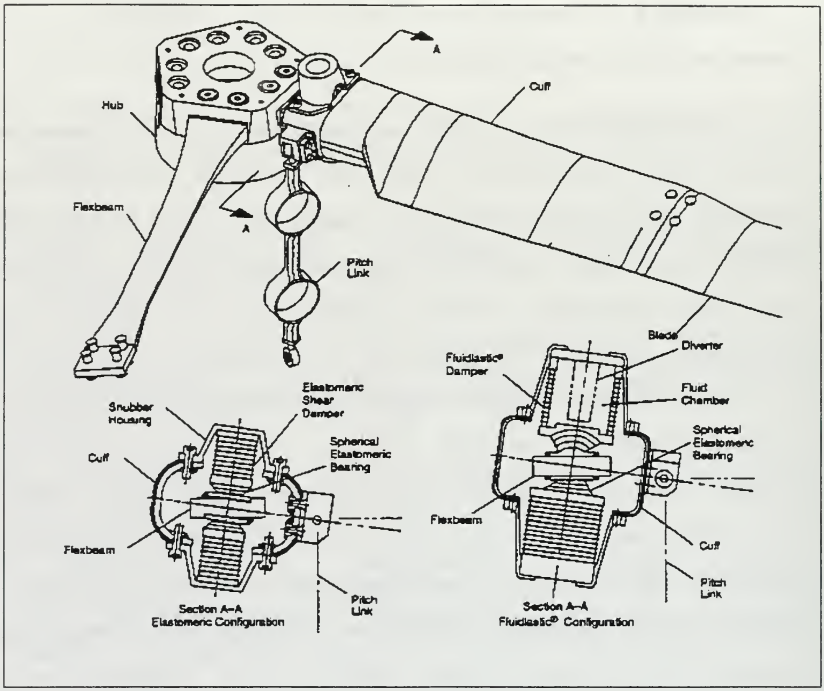

Figure A1 - Froude scale Comanche rotor design [From Ref. A3]

Description of Nonlinear Snubber-Damper

The snubber-damper is made up of alternating layers of metal and elastomer, which provides damping when the layers are put in shear. Unfortunately, the damping and stiffness values for the snubber-damper are not constant; they are a strong function of the snubber-damper displacement amplitude. The initial snubber-damper designs provided very little damping for small deflections.

In addition to the low damping values, snubber-damper stiffness tended to rise sharply for very small amplitudes. Plots of the snubber-damper stiffness and loss factor were published by Panda and follow as Figure A2, [Ref. A3]. The "Elastomeric Damper" depicted is the device used in the 1992-1993 wind tunnel tests and the "Fluidlastic®" damper was the result of a redesign, tested in 1995.

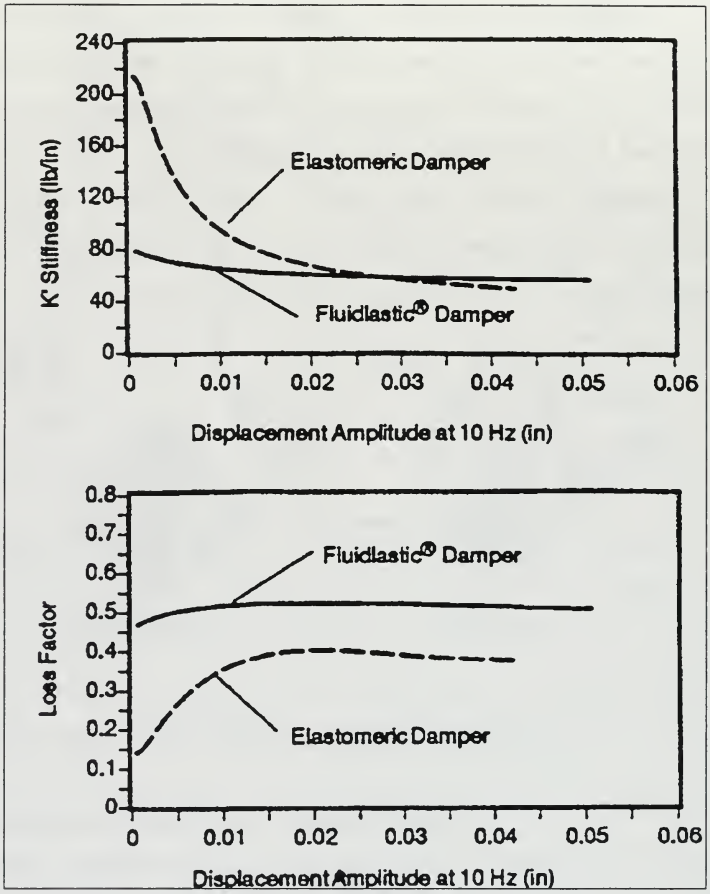

Figure A2 - Snubber-damper stiffness and loss factor [From Ref. A3]

Inherent in the design of these devices, the snubber-dampers exhibit hysteresis in their blade restoring force as a function of displacement. Panda reported the Comanche

elastomeric snubber-damper as having sufficiently low damping at small displacements that this device caused limit cycle oscillations in the blade chord-wise motion. This limit cycle motion produced undesired vibrations in the coupled rotor-fuselage system. The Fluidlastic® snubber-damper alleviated the severity of the limit cycle motion problem. One can see less reduction in the Fluidlastic® damper loss factor at small displacement amplitudes in the lower plot of the previous Figure.

Flexbeam and Cuff Modeling

In order to accurately model the 1/6 scale Comanche wind tunnel test rotor, flexibility in the blade and flexbeam had to be accurately modeled. Initially, a linear beam approximation was used. This was done primarily as a first iteration in the model design process. The linear theory also provided data for verification of a Myklestad method that was coded in Matlab® as an additional task in this research.

Comanche Model Assembly

The Comanche 1/6 scale flexbeam and blade were modeled using the Myklestad program. Example output of a 1-inch blade tip deflection in lag follows as Figure A3.

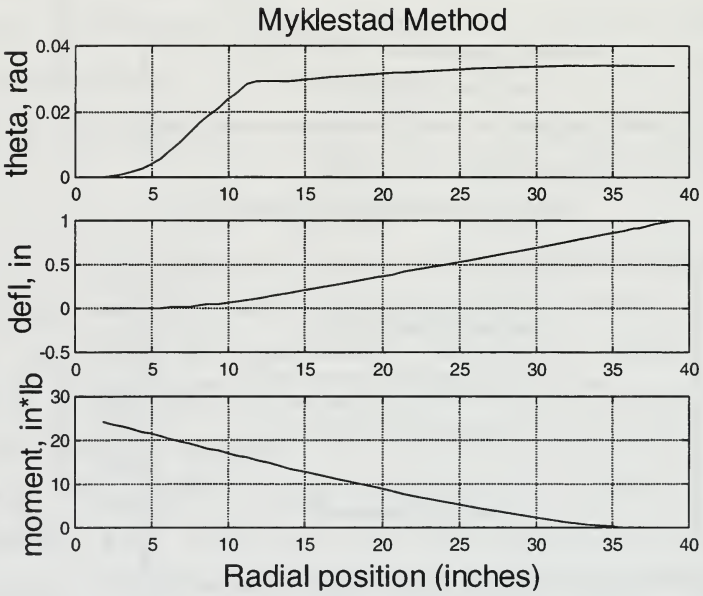

Figure A3 - Combined flexbeam/blade analysis

Using the Myklestad program, the equivalent offset was found to be a constant value of 8.52 inches from the center of rotation, with the snubber-damper not installed. This equivalent offset is highlighted in Figure A4 by a small circle.

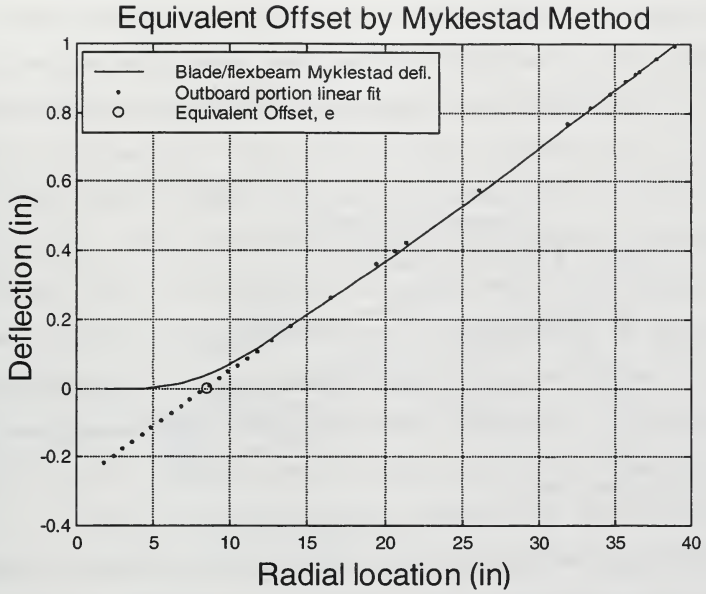

Figure A4 - Flexbeam/blade deflection

From Figure A4, it can be easily seen that the outboard aerodynamic portion of the blade moves as a rigid body for in-plane bending at the frequencies of interest. Therefore, the portion of the blade outboard of the equivalent offset was modeled as a single degree of freedom. Since the slope change in the combined model is at the root end in the soft region of the flexbeam, an articulated type attachment could be used for mathematical modeling of the hingeless rotor in the Simulink® simulation.

Using the blade mass distribution data provided, a blade mass and moment arm were computed. A blade moment of inertia was calculated from this data about the equivalent offset. This inertia was then broken down into an equivalent mass, m_b, and moment arm, l. The blade was modeled as a point mass at a distance l from the offset, such that the total mass of the actual blade matched the point mass value in the model. For accurate modeling of the lead/lag dynamics, it was desired that e*S/I for the actual blade match e/l for the point mass model, where S is the first mass moment of the blade and I equals the second mass moment of the blade. The blade model was determined to be a 0.0129 slug point mass at a radial location of 30.06 inches.

Model parameters for the portion of the blade outboard of the effective offset are compared to the actual blade in the following table:

Table A1

	Froude Model	NPS Model
Blade/cuff moment of inertia, I	4.5212 sl*in^2	
Blade/cuff mass moment, S	0.2099 sl*in	
Blade/cuff mass, m_b	0.0129 sl	
I/S	21.5407 in	
Blade lag offset		8.5435 in
Point mass radial location		30.0642 in

The cuff is far stiffer than the flexbeam, providing an essentially rigid sleeve around the flexbeam. For lead/lag motion, the flexbeam simply bends inside the interior dimensions of the cuff. Since the snubber-damper attaches at

the inboard end of the cuff, the snubber-damper displacements were considered to be a function of an extension of the cuff/blade joint angular displacement and off-axis deflection, as seen below in Figure A5:

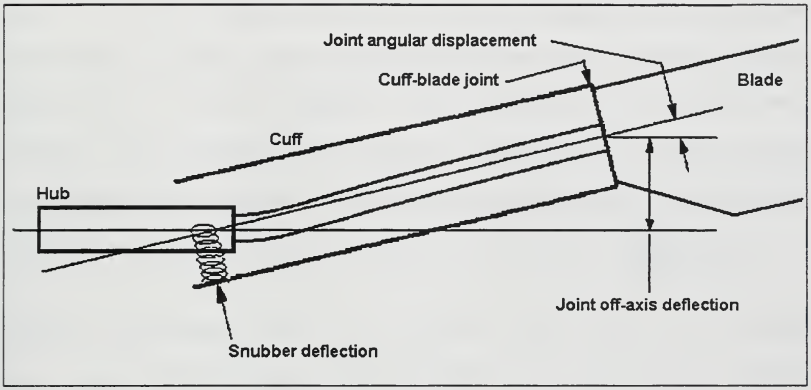

Figure A5 - Snubber-damper motion as a function of cuff/blade joint motion

Assuming a constant equivalent offset for blade lead/lag motion, a geometric gain was computed for snubber-damper displacement as a function of blade lead/lag angle. Using the physical properties of the blade root end, the geometric gain was computed to be 5.937 inches of snubber-damper deflection in shear for every radian of blade lead, assuming small lead/lag angles.

Snubber-Damper Model

The NPS nonlinear rotor simulation was modified to incorporate nonlinear snubber-damper coefficients in both stiffness and damping. The loss factors made available in the Boeing/Sikorsky report were first converted to dimensional damping coefficients. The loss factor is defined as the out-of-phase force divided by the in-phase force. Since the experimental loss factor data in the report was recorded at a fixed driving frequency of 10 Hz, the loss factor data could be converted to dimensional damping values. The dimensional damping value may be expressed as:

$$c(x) = \frac{\eta k(x)}{\omega}$$

where η is the loss factor, k is the nonlinear snubber-damper stiffness, ω is the forcing function frequency, and x is the snubber-damper displacement.

Traditional hydraulic and viscous damping methods were attempted in the nonlinear snubber-damper mathematical model, in addition to higher order curve fits. A fourth order fit, $c(x) = c_4x^4 + c_3x^3 + c_2x^2 + c_1x + c_0$, in displacement was decided upon as the best trade-off between accuracy and model order reduction. A linear relationship was used for snubber-damper displacements greater than 0.6 inches.

The polynomials formulated for both the snubber-damper damping and stiffness formulations follow:

Table A2

1992 Elastomeric snubber-damper:
$c=-842875x^4+87576.8x^3-2847.07x^2+25.01x+0.47$
$k=336241084x^4-38666827x^3+1547897x^2-26483.84x+233.32$
1995 Fluidlastic® snubber-damper:
$c=116695.68x^4-14022.78x^3+609.0x^2-12.05x+0.59$
$k=38512436.84x^4-4491019.58x^3+183336.70x^2-3147.25x+79.71$

where c is in lbs/in/s, k in lbs/in, and x in inches. The stiffness and damping results are compared to the snubber-damper laboratory data provided in the plots that follow:

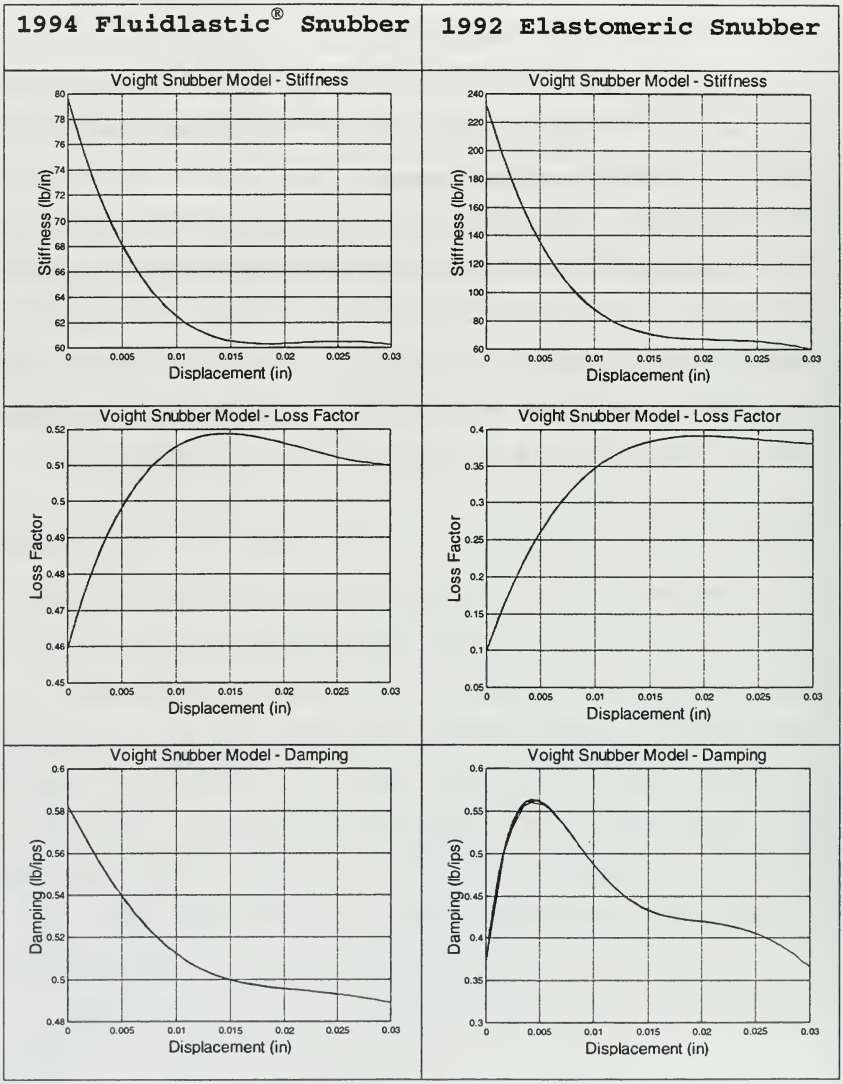

Figure A6 - Snubber-damper stiffness and damping properties

NPS Simulation Results for the 1/6 Scale Comanche

Example results of the NPS rotor simulation follow. The inputs for these plots may be found in the following table:

Table A3 - Helicopter physical and aerodynamic parameters

Helo Physical and Aerodynamic Parameters	
% Rotor speed, rad/sec	Omega=870*(pi/30)
% Equivalent lag offset, inches	e1=8.5235
% Equivalent blade length, inches	l=21.5407
% Snubber radial location, inches	Rs=2.5984
% Lead/lag stop position, rads	No lag stops modeled
% Mass of rotor blades, slugs	mb=0.0129
% Effective mass of fuselage, slugs	Mx= 0.6452 My= 1.3802
% Blade azimuth phase angles, rads	Phi(1:5)=[0 2 4 6 8]*pi/5
% geometric gain of snubber movement from lag, in/rad	gg=5.1121
% Spring stiffness polynomial for lead-lag, in*lbs/radian) (1995 snubber)	Kbeam=[0,0,0,0,660.9141] Ksnub=[38512436.84*gg^4, -4491019.58*gg^3,183336.70*gg^2, -3147.25*gg,79.71] *(e1-Rs)^2 Kpoly=Kbeam+Ksnub
% Lead-lag stop spring constants, in*lbs/radian	Ks=0 No lag stops modeled
% Damping polynomial in lead-lag (in*lb/(rad/sec)) (1995 snubber)	Cpoly=[116695.68*gg^4, -14022.78*gg^3,609.0*gg^2, -12.05*gg,0.59] *(e1-Rs)^2
Linear springs in translation, lbs/in	K(1)=297.38 K(2)=217.93
Linear damping in translation, (lbs/(in/sec))	c(1)=1.29 c(2)=1.88
Non-linear damping in translation, lbs/(in/sec)^2)	v=0
Fuselage initial displacements, in (all other IC's = 0.0)	xXi=0.1 xYi=0.1

The fourth order snubber-damper model is employed in the simulation depicted in the following time histories. All blades are given initial conditions of zero lead angle displacement and zero velocity. All rotor and hub dynamics are initiated by a 0.1 foot displacement in both the x and y

dimensions of hub motion. Hub response from these initial conditions is shown in Figure A7. This initial condition is equivalent to a lateral restraining force on the hub of 36.87 lbs. being released at time t=0.0 in the simulations. This comparatively large impulse was set to insure coupling of the rotor/body dynamics.

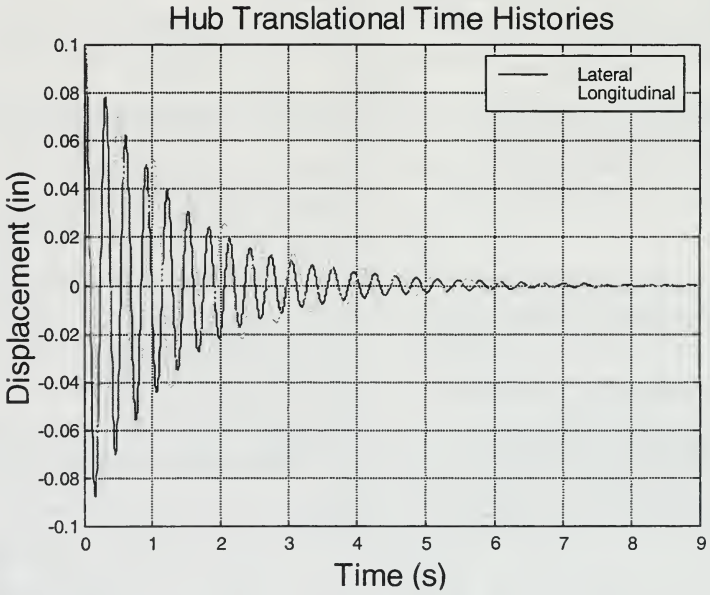

Figure A7 - Hub translational time histories

The Comanche wind tunnel tests utilized a shaker in the fuselage to initiate rotor/body coupling prior to recording time histories for analysis. Since the initial conditions

varied for each test in the tunnel, duplication of the exact initial conditions was impossible with the simulation, and the fixed initial conditions on the hub displacement were used. The Boeing/Sikorsky report describes this process as follows:

> "The blade lead-lag mode was excited by the swashplate cyclic shaker operating at the fixed system lead-lag regressing frequency. When required, a fine adjustment was made to maximize the lead-lag response of the model. The amplitude was monitored (on line) by a spectrum analyzer. When the forced response was judged to be maximum, the shaking was stopped, marking the beginning of the transient decay. The following 10 seconds of chord bending and fuselage roll-pitch data was collected and analyzed by a moving-block method to determine the frequency and damping ratio of the mode being investigated." [Ref. A2]

Response to the relativey stiff rotor blades is shown in Figure A8. The Comanche lead/lag frequency was reported to be $0.71\Omega_0$ for the 1995 system, $0.692\Omega_0$ for the 1992 system.

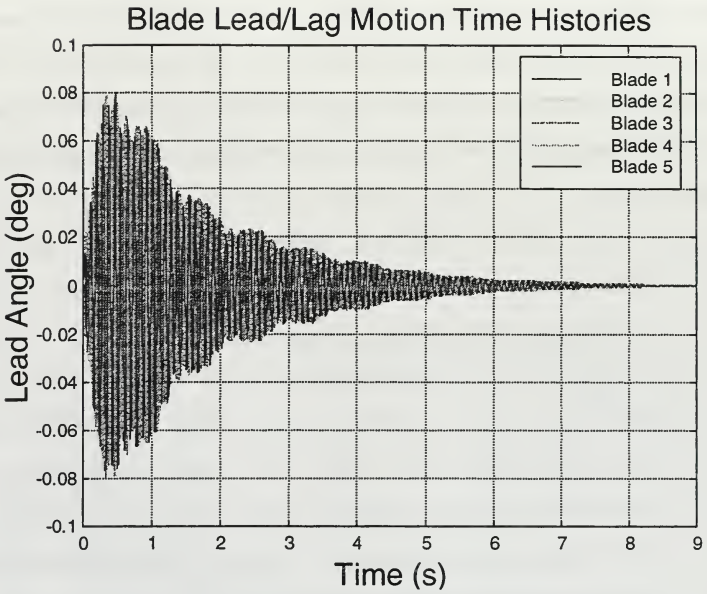

Figure A8 - Blade lead angle time histories

Damping for each of the five blades was determined using a Hilbert transform method [Ref. A5]. The damping value for the blades was then averaged for the final 8 seconds of the 9 second time history. This average was then converted to a fixed system damping value replicating the method used in the Comanche test:

> "The rotating system damping ratio is converted to a fixed-system damping ratio by multiplying by the ratio of the rotating-system lead-lag mode frequency

(ω_ζ) to the fixed-system lead-lag regressing mode frequency (Ω-ω_ζ)." [Ref. A2]

An example output of the Hilbert damping analysis for the #5 blade follows:

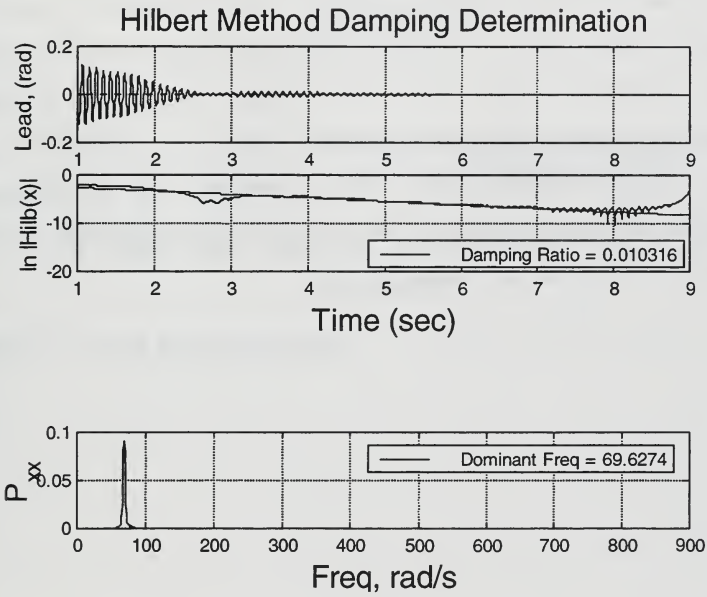

Figure A9 - Blade motion damping analysis

The top subplot is the time history of blade lead angle that was analyzed. The second subplot is the natural logarthm of the absloute value of the Hilbert transform of

the signal. A first order fit to this plot is also shown. The damping of the signal was then computed by dividing the negative of the slope by the time history frequency. The primary frequency of the time history is determined by power spectral density using Matlab®'s discrete fourier transform function, "fft.m." The results of the power spectral density are shown in the third subplot. This Hilbert transform method works well for signals dominated by a single mode. Smith obtained more accurate results with the Hilbert transform method than with Moving Block for signals with a single mode present [Ref. A5]. Results of the Hilbert transform damping analysis of the two hub degrees of freedom follow in Figures A10 and A11.

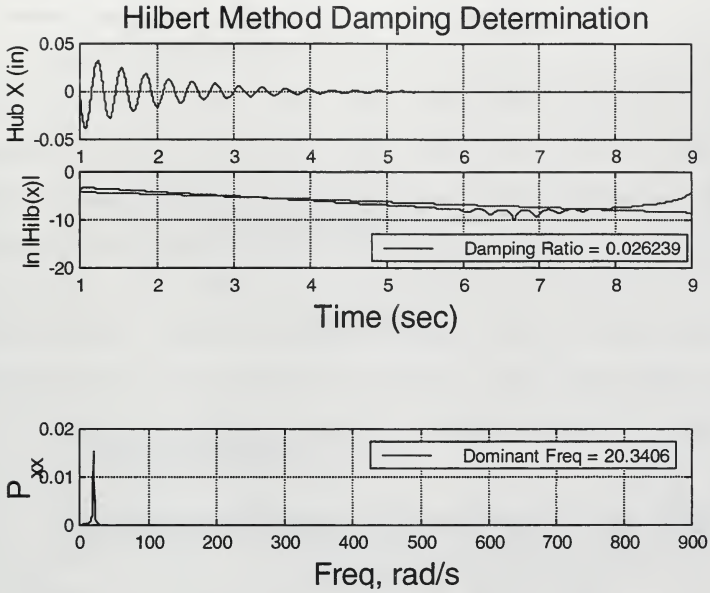

Figure A10 - Hub X direction damping

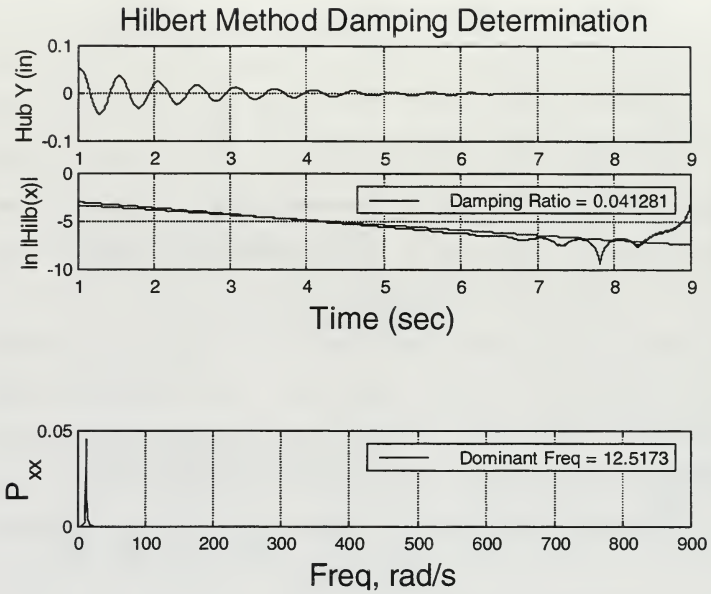

Figure A11 - Hub Y direction damping

The frequencies obtained from the NPS simulation are summarized in the following table:

Table A4

	NPS Simulation	Boeing/Sikorsky report
Hub X	3.23 Hz	3.20 Hz
Hub Y	1.99 Hz	2.00 Hz
Lead/Lag	0.76Ω	$0.692\Omega_0$

Comparison with Test Data

The goal of the application of the NPS simulation to the Comanche scale rotor data was the matching of fixed system damping values to the test data and to UMARC. The plot that follows reproduces the Boeing/Sikorsky report's Figure 50b, from the 1992 test results [Ref. A1]. The 1992 test data was chosen as a more rigorous test of the NPS simulation, since the snubber-damper used in the 1992 tests exhibited greater nonlinear behavior. The first plot, Figure A12, shows the NPS simulation's initial results:

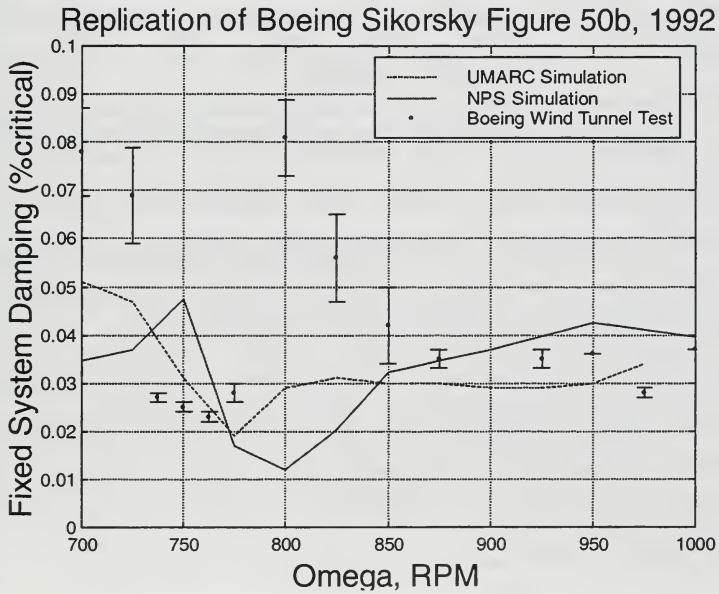

Figure A12 - Initial NPS simulation results

The geometric gain, the snubber-damper shear to blade lead angle ratio, was considered a soft parameter and varied in an atttempt to obtain more accurate matching with the existing data.

As the geometric gain was increased, slightly better results were obtained. The following plot shows the results of increasing the geometric gain by a factor of 1.5. From these results, the wind tunnel model, it is assumed, was seeing more snubber-damper movement than the modeling method assumptions had called for. This soft parameter, the geometric gain, is related to the multiple load path problem alluded to earlier. In brief, the basic assumptions underestimated the amount of snubber-damper motion with lead angle changes. Recall only lead/lag motion is modeled, and the bearingless Comanch rotor model experienced coupling in the lead/lag dynamics from other model degrees of freedom.

With the advantage of having the test data results a priori, the model was tuned to best replicate the wind tunnel data using the geometric gain as a tunable parameter. With the higher geometric gain mentioned, the NPS simulation appeared to replicate the model data slightly better than UMARC at the lower RPM's tested. At higher rotor speeds, the difference between the two simulations is negligible.

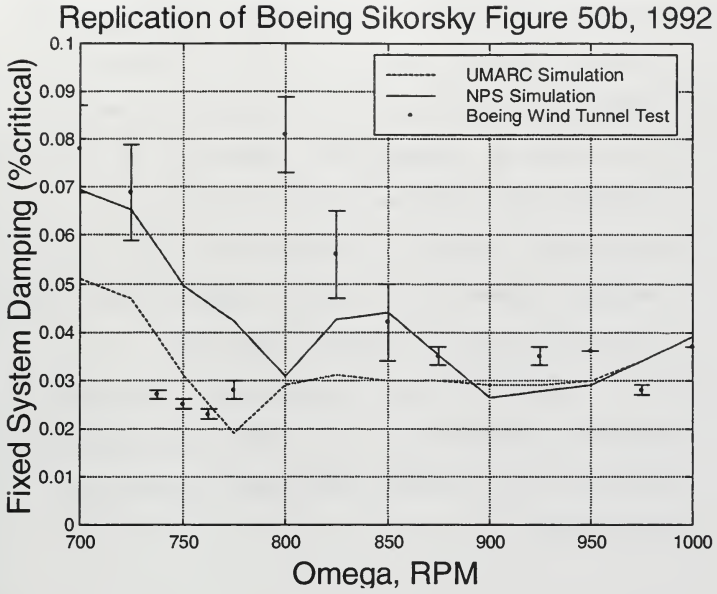

Figure A13 - Final NPS simulation results with increased geometric gain

Comanche Modeling Conclusions

- If the physical rotor exhibits migration of the effective offset with varying lead angles and velocities, forcing a hingeless rotor into an articulated model contaminates the results.
- The inclusion of aerodynamics, coupling in the rotor lead/lag, flap, and torsion should be included in the modeling of a bearingless rotor.

- Modeling the blade portion that is outboard of the effective offset with only two parameters, blade length and tip mass, is incapable of matching all the inertial properties required to accurately simulate both lead/lag and hub motion.
- Additional degrees of freedom are required in the lead/lag dynamics to better approximate multiple load paths from the blade to the hub.
- For a fledgling code, the NPS simulation shows potential in modeling rotors with nonlinear physical parameters and further development should be considered.

LIST OF REFERENCES

A1. Mychalowycz, E.; Panda, B.; Zientek, T.; Gabel, R.; "Interim Report - Aeromechanical Stability Wind Tunnel Test of the RAH-66 Helicopter," 1993.

A2. Mychalowycz, E.; Panda, B.; Sheffler, M.; O'Brien, T.; "Final Report - Aeromechanical Stability Wind Tunnel Test of the RAH-66 Helicopter," 1995.

A3. Tarzanin F. J., and Panda, B., "Development and Application of nonlinear Elastomeric and Hydraulic Lag Damper Models," 36th AIAA SDM Conf., New Orleans, LA, April 1995.

A4. Den Hartog, J. P., Mechanical Vibrations, McGraw-Hill, 1956.

A5. Smith, C. B., and Wereley, N. M., "Transient Analysis for Damping Identification in Rotating Composite Beams

with Integral Damping Layers," Journal of Smart Materials and Structures, No. 5, 1996.

APPENDIX B. MYKLESTAD BEAM MODELING METHOD

In 1944, Myklestad published a method for finite element analysis of beams in bending for vibrations applications in his book, "Vibration Analysis" [Ref B1]. His method breaks a beam into segments that have essentially linear behavior over the segment length. Equations of motion of each of the separate elements are then tied together as separate degrees of freedom. In Myklestad's method, each beam element is defined as a point mass and a massless elastic element in bending, as depicted in Figure B1, modified from Gerstenberger and Wood [Ref. B2].

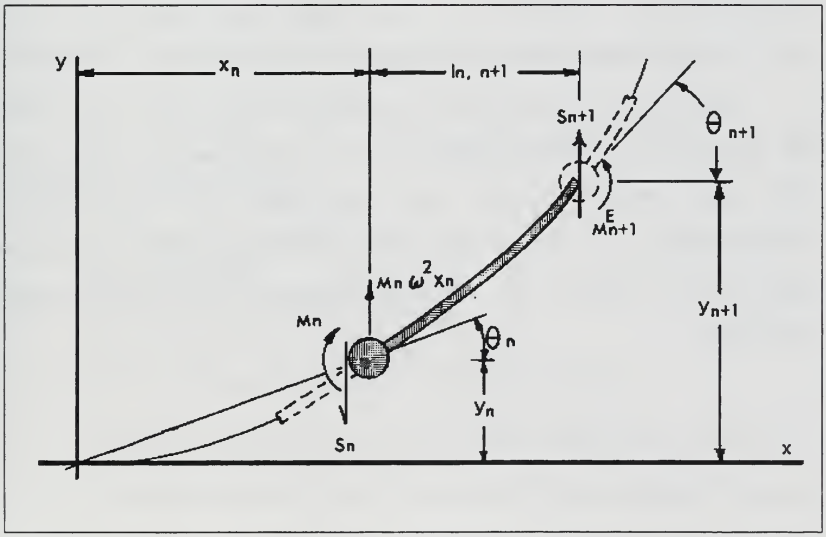

Figure B1 - Typical Myklestad beam element [After Ref. B2]

By defining element members in this way, a beam with inertial and mass properties that change as a function of beam longitudinal position may be well approximated. Shear, moment, angular displacement and beam deflection may be described for each element as follows:

$$S_{n+1} = S_n + m_n y_n \omega^2$$

$$M_{n+1} = M_n + l_{n,n+1} S_{n+1}$$

$$\Theta_{n+1} = \Theta_n + \frac{l_{n,n+1}}{E_n I_n} M_{n+1} - \frac{l_{n,n+1}^2}{2E_n I_n} S_{n+1}$$

$$y_{n+1} = y_n + l_{n,n+1}\Theta_n + \frac{l_{n,n+1}^2}{2E_n I_n} M_{n+1} - \frac{l_{n,n+1}^3}{3E_n I_n} S_{n+1}$$

where ω is the first beam natural frequency in bending, $l_{n,n+1}$ is the segment length, E_n is the element stiffness, and I_n is the element second area moment.

Myklestad's method may be modified from the simple beam in bending to rotating beams by the inclusion of centrifugal and blade tension terms. For this case, the x-y plane is transformed to a radial and off-axis displacement frame, as depicted in Figure B2, also reproduced from Gerstenberger and Wood.

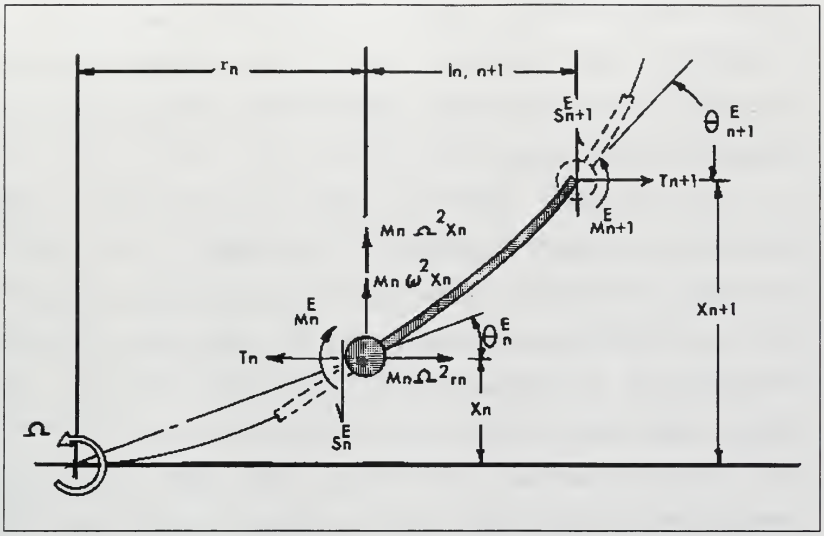

Figure B2 - Typical rotating Myklestad beam element [From Ref. B2]

The equations for a Myklestad beam element in the rotating frame follow:

$$S_n = S_{n+1} + m_n(\omega^2 + \Omega^2)x_n$$
$$T_n = T_{n+1} + m_n\Omega^2 r_n$$
$$M_n = M_{n+1} + S_{n+1}l_{n,n+1} - T_{n+1}(x_{n+1} - x_n)$$
$$\Theta_n = \Theta_{n+1}(1 - T_{n+1}U_{n,n+1}) + M_{n+1}V_{n,n+1} - S_{n+1}U_{n,n+1}$$
$$x_n = x_{n+1} + \Theta_n l_{n,n+1} + T_{n+1}\Theta_{n+1}G_{n,n+1} - M_{n+1}U_{n,n+1} - S_{n+1}G_{n,n+1}$$

where $V_{n,n+1} = l_{n,n+1}/E_n I_n$, $U_{n,n+1} = l_{n,n+1}{}^2/2E_n I_n$, *and* $G_{n,n+1} = l_{n,n+1}{}^3/3E_n I_n$.

A program written in the Matlab® application language that analyzes a beam using Myklestad's method may be found elsewhere in the Appendicies. This program analyzes beam or

rotor blade inertial, geometric, and stiffness data for any number of beam segments, up to the limitations of the Matlab® host program used. Both rotating and non-rotating beams can be analyzed.

The program also has the capability of applying different boundary conditions at the ends of the beam. An articulated blade requires zero moment and displacement at the lag hinge where a hingeless rotor requires zero angular displacement and deflection at the root end. In both cases, shear and moment must be zero at the blade tip.

Linear beam theory was utilized as a means of verifying output of the Myklestad bending program. In the case of the flexbeam, where clamped end restoring moments were needed, the rotary spring constant of $\frac{M}{\Theta}=\frac{EI}{l}$ was used to check the Myklestad output. This rotary spring constant for the blade, namely the flexbeam root-end moment per unit tip angular deflection, was a required input for the NPS rotor simulation.

Frequencies of oscillation were checked against Den Hartog's text "Mechanical Vibrations" [Ref. B1]. For example, the first lag frequency of the hingeless blade determined by the Myklestad program was checked with the cantilevered beam frequency from Den Hartog, $\omega=3.52\sqrt{\frac{EI}{\mu l^4}}$.

The plots in Figure B3 shows typical output of the Myklestad program. The third subplot, the moment as a function of beam longitudinal position, shows a comparison to linear theory. The example beam used in this comparison has a length of 10 inches, a weight distribution of 0.1 lb/in, and a constant EI of 10000 $lb*in^2$. It can be seen that the Myklestad program correctly applies the four boundary conditions of zero slope and deflection at the root, and zero shear and moment at the tip. It should be noted that a small correction is made to the shear at the tip of the beam. This is done due to the final Myklestad element having a net shear at the tip one beam element away from the final mass element. This tip correction to shear is common practice in applications of Myklestad's method.

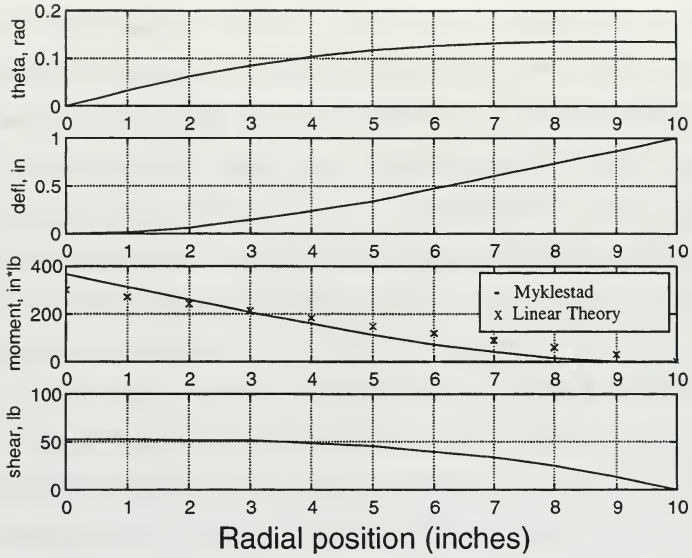

Figure B3 - Myklestad analysis output

The following table compares a non-rotating cantilevered beam to Den Hartog's closed form equations, verifying the frequencies obtained from the Myklestad program:

Table B1

	Linear theory	Myklestad
Non-rotating cantilevered beam	69.6484 Hz	69.2986 Hz

The Myklestad computer code follows in the appendices.

LIST OF REFERENCES

B1. Den Hartog, J. P., Mechanical Vibrations, McGraw-Hill, 1956.

B2. Gerstenberger, W. and Wood, E. R., "Analysis of Helicopter Aeroelastic Characteristics in High-Speed Flight," AIAA Journal, Vol. 1, No. 10, Oct., 1963.

APPENDIX C - MYKLESTAD METHOD PROGRAM IN MATLAB

```
function myklestad

clear
format compact

% Required inputs:
Ohm=0;                          % Rotor rad/sec
tolb=0.1;                % tolerance in acceptable assumed frequency
(rad/sec)

load h66blade.mat -ascii
el=2.5984;
      % snubber radial location, in
radius=38.976;
      % blade radius, in
rb=fliplr(h66blade(:,1)'*radius);                % in
wb=fliplr(h66blade(:,2)');                                  % lb in^2
EIb=fliplr(h66blade(:,3)');                           % lb/in
rf=rb(1:17);
wf=wb(1:17);
EIf=EIb(1:17);
figure(4),plot(rf,EIf/1000),grid
xlabel('Radius (in)','FontSize',16)
ylabel('EI, in^2Klb','FontSize',16)
title('EI vs Radial Location for Flexbeam','FontSize',16)
muf=(wf/32.2);
nfe=length(rf);

doutbd=[diff(rf),0];
dinbd=[0,diff(rf)];
mEIf=sum((dinbd+doutbd)/2.*EIf)/(rf(nfe)-rf(1));
disp([' The flexbeam length is: ',num2str(rf(nfe)-rf(1)),' in'])
disp([' The mean EI for the flexbeam is: ',num2str(mEIf),' lb*in^2'])

% obtain beam natural frequency and root-end transfer matrix
% Finds natural frequency and dynamics matrix using
% Myklestad method for beam bending

k=0;

if nfe~=length(EIf)
   error('The EI vector is not the same size as the r vector.')
elseif nfe~=length(muf)
   error('The mass/length vector is not the same size as the r
vector.')
end

omega_1=3.52*sqrt(mean(EIf)/(mean(muf)*(rf(length(rf))-rf(1))^4));
      % rad/sec
omega=[0.9 1.1]*omega_1;
```

```
%*****************WHILE LOOP*********************
while (abs(omega(1)-omega(2))>tolb)
   k=k+1;

      %  Th_tip = 1, all others zero
   tip=[1; 0; 0; 0];
      state=mykloop(tip,omega(1),rf,muf,EIf,Ohm);

      % compute b components of dynamics matrix
   bTh=state(1,1); bX=state(2,1); bM=state(3,1); bS=state(4,1);
      %b=[bTh, bX, bM]
                        % debug
   %plotstate(2,r,state,omega(1)),pause
      % debug

      % X_tip = 1, all others zero
      tip=[0; 1; 0; 0];
      state=mykloop(tip,omega(1),rf,muf,EIf,Ohm);

      % compute a components of dynamics matrix
   aTh=state(1,1); aX=state(2,1); aM=state(3,1); aS=state(4,1);
      %a=[aTh, aX, aM]
                        % debug
   %plotstate(3,r,state,omega(1)),pause
      % debug

      % compute determinant
   dynam=[bTh,aTh;bX,aX];           % cantilevered blade


      if k==1
      omega=fliplr(omega);
      err=det(dynam);
   else
      err=[det(dynam),err];
      % use linear interpolation for next guess at omega
            omega=[max(0,omega(1)-err(1)*((omega(2)-omega(1))/(err(2)-
err(1)))), omega];
      %[spline(err,omega,0), omega];            % optional spline
method
   end


end   % while loop
%*****************WHILE LOOP*********************


% debugging
disp([' ',num2str(k),' iterations in obtaining root transfer matrix'])
figure(3),plot(omega(2:k+1),err,omega(2:k+1),err,'o')
xlabel('omega'),ylabel('determinant'),grid,title('Convergence Plot')

Mj=-bM;
```

```
Kj=aM/rf(nfe);
disp(' ')
disp(' For Simulation Inputs, the Flexbeam Produces')
disp(['   the following values for Omega = ',num2str(Ohm*30/pi),'
RPM'])
disp([' Mj = ',num2str(Mj),' in*lb/rad deflection at the joint'])
disp([' aS = ',num2str(aS),' So/Xt for root transfer matrix'])
disp([' Kj = ',num2str(Kj),' lb/in deflection at the joint'])

plotstat(2,rf,state,omega(1))
tip=[1; 0; 0; 0];
state=mykloop(tip,omega(1),rf,muf,EIf,Ohm);
bTh=state(1,1); bX=state(2,1); bM=state(3,1);
plotstat(3,rf,state,omega(1))

%%%%%%%%%%%%%%%%%%%%%%%%%%%%%%%%%%%%%%%%%%%%%%%%%%%%%%%%%%%%%%%%%%%

load h66cuff.mat -ascii

nel=length(h66blade(:,1));
rc=fliplr(h66cuff(:,1)'*radius);                    % in
wc=fliplr(h66cuff(:,2)');                                % lb in^2
ra=rb(17:length(rb));
wa=wb(17:length(wb));

rca=[rc,ra];
      % in
wca=[wc,wa];
      % lb in^2

S=0;I=0;M=0;
for n=2:length(rca)
   dr=rca(n)-rca(n-1);
   wdr=mean(wca(n-1:n));
   rcent=mean(rca(n-1:n));
   S=S+rcent*dr*wdr;
   I=I+rcent^2*dr*wdr;
   M=M+dr*wdr;
end

Mb=-(e1^2*M^2-2*e1*M*S+S^2)/(-e1^2*M+2*e1*S-I);
Ms=(S^2-I*M)/(-e1^2*M+2*e1*S-I);
R=-(e1*S-I)/(-e1*M+S);

disp([' Mb = ',num2str(Mb),' slugs for blade mass at position R'])
disp([' Ms = ',num2str(Ms),' slugs for mass at snubber position'])
disp([' R  = ',num2str(R),' inches radial location for mass Mb'])
disp(' ')


%%%%%%%%%%%%%%%%%%%%%%%%%%%%%%%%%%%

function state=mykloop(tip,omega,r,mu,EI,Ohm)
% next step subfunction in Myklestad method
```

```
nbe=length(r);
l=[diff(r)];l=[l l(length(l))];                          % delta-r in
V=l./EI;
      % 1/(in*lb)
U=(l.^2)./(2*EI);                                                    %
1/lb
G=(l.^3)./(3*EI);                                                    %
in/lb
T=fliplr(cumsum(fliplr(mu.*r)))*Ohm^2;          % lb

% tip correction to shear:
tip(4)=tip(4)+(mu(nbe-1)*l(nbe-1)*(omega^2+Ohm^2)*tip(2))*.47;

state=[zeros(4,nbe-1),tip];               % initialize state

for n=(nbe-1):-1:1

   Th=state(1,n+1);                  % theta
      X=state(2,n+1);                % deflection
      M=state(3,n+1);                % moment
      S=state(4,n+1);                % shear

      Thn = Th*(1+T(n)*U(n))-M*V(n)-S*U(n);
      Xn = X-Thn*l(n)+T(n)*Th*G(n)-M*U(n)-S*G(n);
   Mn = M+S*l(n)-T(n)*(X-Xn);
   Sn = S+mu(n)*l(n)*(omega^2+Ohm^2)*Xn;

   %[Thn;Xn;Mn;Sn]                                                    %
debug

   state(:,n)=[Thn;Xn;Mn;Sn];
end
%state


%%%%%%%%%%%%%%%%%%%%%%%%%%%%%%%%%%%%%%%%%%%%%%%%%%%%%%%%%%%%%%%%%%%

function [omegan,dynam,state]=natural(r,mu,EI,Ohm,articu,toler)
%
% Finds natural frequency and dynamics matrix using
%
% Myklestad method for beam bending

% Robert L. King
% April 1998

k=0;
nbe=length(r);

if nbe~=length(EI)
   error('The EI vector is not the same size as the r vector.')
elseif nbe~=length(mu)
```

```
   error('The mass/length vector is not the same size as the r
vector.')
end

if articu==1      % first guess at 1st bending freq - use eqn for
uniform beam:
      omega_1=15.4*sqrt(mean(EI)/(mean(mu)*(r(length(r))-r(1))^4));
      % rad/sec
else
      omega_1=3.52*sqrt(mean(EI)/(mean(mu)*(r(length(r))-r(1))^4));
      % rad/sec
end
omega=[0.9 1.1]*omega_1;

%*****************WHILE LOOP*********************
while (abs(omega(1)-omega(2))>toler)
   k=k+1;

      %  Th_tip = 1, all others zero
      tip=[1; 0; 0; 0];
   state=mykll(tip,omega(1),r,mu,EI,Ohm);

      % compute b components of dynamics matrix
   bTh=state(1,1); bX=state(2,1); bM=state(3,1);
      %b=[bTh, bX, bM]
                        % debug
   %plotstate(2,r,state,omega(1)),pause
      % debug

      % X_tip = 1, all others zero
      tip=[0; 1; 0; 0];
      state=mykll(tip,omega(1),r,mu,EI,Ohm);

      % compute a components of dynamics matrix
   aTh=state(1,1); aX=state(2,1); aM=state(3,1);
      %a=[aTh, aX, aM]
                        % debug
   %plotstate(3,r,state,omega(1)),pause
      % debug

      % compute determinant
      if articu==1
      dynam=[bM,aM;bX,aX];                % articulated blade
   else
      dynam=[bTh,aTh;bX,aX];        % cantilevered blade
   end % if statement


      if k==1
      omega=fliplr(omega);
      err=det(dynam);
   else
      err=[det(dynam),err];
      % use linear interpolation for next guess at omega
```

```
            omega=[max(0,omega(1)-err(1)*((omega(2)-omega(1))/(err(2)-
err(1)))), omega];
      %[spline(err,omega,0), omega];            % optional spline
method
   end


end   % while loop
%****************WHILE LOOP*********************

disp([' ',num2str(k),' iterations in natural.m.'])
      % debug
omegan=omega(1);

% debugging
figure(1),plot(omega(2:k+1),err,omega(2:k+1),err,'o')
xlabel('omega'),ylabel('determinant'),grid,title('Convergence Plot')
```

APPENDIX D - MAPLE WORKSHEET FOR COLEMAN MODEL

```
EQUATIONS OF MOTION FOR GROUND RESONANCE CONSIDERING ONLY INPLANE
DEGREES OF FREEDOM
~
```

```
DEFINE COORDINATE TRANSFORMATIONS
~
```

```
Blade undeformed axis -- Hub :
> restart:
> with(linalg):
Warning, new definition for norm
Warning, new definition for trace
> psi:=Omega*t+Phi[k];

                        psi := Omega t + Phi[k]

> T1:=alpha->matrix(3,3,[1,0,0,0,cos(alpha),sin(alpha),0,-
sin(alpha),cos(alpha)]);

T1 := alpha -> matrix(3, 3,

    [1, 0, 0, 0, cos(alpha), sin(alpha), 0, -sin(alpha), cos(alpha)])

> T2:=alpha->matrix(3,3,[cos(alpha),0,-
sin(alpha),0,1,0,sin(alpha),0,cos(alpha)]);

T2 := alpha -> matrix(3, 3,

    [cos(alpha), 0, -sin(alpha), 0, 1, 0, sin(alpha), 0, cos(alpha)])

> T3:=alpha->matrix(3,3,[cos(alpha),sin(alpha),0,-
sin(alpha),cos(alpha),0,0,0,1]);

T3 := alpha -> matrix(3, 3,

    [cos(alpha), sin(alpha), 0, -sin(alpha), cos(alpha), 0, 0, 0, 1])

> diff1:=arg->map(diff,arg,t);

                  diff1 := arg -> map(diff, arg, t)

> M1:=transpose(T3(psi));

                        [cos(%1)     -sin(%1)     0]
                        [                          ]
                   M1 := [sin(%1)     cos(%1)      0]
                        [                          ]
                        [   0           0         1]

                        %1 := Omega t + Phi[k]
```

```
> M2:=transpose(T3(zeta[k](t)));

                [cos(zeta[k](t))    -sin(zeta[k](t))    0]
                [                                       ]
          M2 := [sin(zeta[k](t))    cos(zeta[k](t))     0]
                [                                       ]
                [       0                   0           1]
```

Energy of rotor blades

Kinetic energy of kth rotor blade (TBk)

```
> rhoHI_I:=vector([u[1](t),u[2](t),0]);

                  rhoHI_I := [u[1](t), u[2](t), 0]

> rhoBuH:=vector([e1,0,0]);

                          rhoBuH := [e1, 0, 0]

> rhoBuH_I:=multiply(M1,rhoBuH);

 rhoBuH_I := [cos(Omega t + Phi[k]) e1, sin(Omega t + Phi[k]) e1, 0]

> rhoPBd:=vector([R,0,0]);

                          rhoPBd := [R, 0, 0]

> rhoPBd_I:=multiply(M1,M2,rhoPBd);

rhoPBd_I := [(cos(%1) cos(zeta[k](t)) - sin(%1) sin(zeta[k](t))) R,

    (sin(%1) cos(zeta[k](t)) + cos(%1) sin(zeta[k](t))) R, 0]

%1 := Omega t + Phi[k]

> rho:=map(simplify,matadd(rhoHI_I,matadd(rhoBuH_I,rhoPBd_I)));

rho := [u[1](t) + cos(%1) e1 + R cos(%1) cos(zeta[k](t))

     - R sin(%1) sin(zeta[k](t)), u[2](t) + sin(%1) e1

     + R sin(%1) cos(zeta[k](t)) + R cos(%1) sin(zeta[k](t)), 0]

%1 := Omega t + Phi[k]

> V:=diff1(rho);

     [/d         \
V := [|-- u[1](t)| - sin(%2) Omega e1
     [\dt        /
```

```
     - R sin(%2) Omega cos(zeta[k](t)) - R cos(%2) sin(zeta[k](t)) %1

     - R cos(%2) Omega sin(zeta[k](t)) - R sin(%2) cos(zeta[k](t)) %1

      /d         \
    , |-- u[2](t)| + cos(%2) Omega e1
      \dt        /

     + R cos(%2) Omega cos(zeta[k](t)) - R sin(%2) sin(zeta[k](t)) %1

     - R sin(%2) Omega sin(zeta[k](t)) + R cos(%2) cos(zeta[k](t)) %1

      ]
    , 0]
      ]

      d
%1 := -- zeta[k](t)
      dt

%2 := Omega t + Phi[k]

> TBk:=1/2*mb[k]*(V[1]^2+V[2]^2);

                ///d         \
TBk := 1/2 mb[k] |||-- u[1](t)| - sin(%2) Omega e1
                \\\dt        /

     - R sin(%2) Omega cos(zeta[k](t)) - R cos(%2) sin(zeta[k](t)) %1

     - R cos(%2) Omega sin(zeta[k](t)) - R sin(%2) cos(zeta[k](t)) %1

    \2   //d         \
    |  + ||-- u[2](t)| + cos(%2) Omega e1
    /    \\dt        /

     + R cos(%2) Omega cos(zeta[k](t)) - R sin(%2) sin(zeta[k](t)) %1

     - R sin(%2) Omega sin(zeta[k](t)) + R cos(%2) cos(zeta[k](t)) %1

    \2\
    | |
    / /

      d
%1 := -- zeta[k](t)
      dt

%2 := Omega t + Phi[k]

-------------------------------------
Potential energy for kth blade (UBk)
-------------------------------------
```

```
> UBk1:=1/2*Ke[k]*zeta[k](t)^2; #Linear Elastic Forces

                                                    2
                    UBk1 := 1/2 Ke[k] zeta[k](t)

> UBk2:=1/4*Kd[k]*zeta[k](t)^4; #Duffing Elastic Forces

                                                    4
                    UBk2 := 1/4 Kd[k] zeta[k](t)

> UBk3:=1/4*Ks[k]*signum(zeta[k](t)-z)*(zeta[k](t)^2+z^2-
2*zeta[k](t)*z)+1/4*Ks[k]*signum(zeta[k](t)+z)*(-zeta[k](t)^2-z^2-
2*zeta[k](t)*z)+1/2*Ks[k]*zeta[k](t)^2+1/2*Ks[k]*z^2;

UBk3 :=

    1/4

                                                  2    2
    Ks[k] signum(zeta[k](t) - z) (zeta[k](t)  + z  - 2 zeta[k](t) z)

     + 1/4

                                                 2    2
    Ks[k] signum(zeta[k](t) + z) (-zeta[k](t)  - z  - 2 zeta[k](t) z)

                            2              2
     + 1/2 Ks[k] zeta[k](t)  + 1/2 Ks[k] z

> UBk:=UBk1+UBk2+UBk3;
> UBk:=UBk1+UBk2;

                                     2                          4
         UBk := 1/2 Ke[k] zeta[k](t)  + 1/4 Kd[k] zeta[k](t)

----------------------------------------
Dissapative function for kth blade (DBk)
----------------------------------------
>
DBk:=1/2*Czeta[k]*(diff(zeta[k](t),t))^2+Vzeta[k]*(diff(zeta[k](t),t))^
2*abs(diff(zeta[k](t),t));

                    /d            \2
DBk := 1/2 Czeta[k] |-- zeta[k](t)|
                    \dt           /

                /d            \2 | d             |
     + Vzeta[k] |-- zeta[k](t)|  | -- zeta[k](t) |
                \dt           /  | dt            |
```

Energy of hub

```
Kinetic energy of hub (TH) / Potential energy of hub (UH) / Dissapative
function of hub (DH)
-------------------------------------------------------------------------
-----------------------
> TF:=1/2*M[1]*(diff(u[1](t),t))^2+1/2*M[2]*(diff(u[2](t),t))^2;

                      /d         \2            /d         \2
        TF := 1/2 M[1] |-- u[1](t)|  + 1/2 M[2] |-- u[2](t)|
                      \dt        /             \dt        /

> UF:=1/2*K[1]*u[1](t)^2+1/2*K[2]*u[2](t)^2;

                                    2                   2
             UF := 1/2 K[1] u[1](t)  + 1/2 K[2] u[2](t)

>
DF:=1/2*c[1]*(diff(u[1](t),t))^2+1/2*c[2]*(diff(u[2](t),t))^2+1/2*v[1]*
(diff(u[1](t),t))^2*abs(diff(u[1](t),t))+1/2*v[2]*(diff(u[2](t),t))^2*a
bs(diff(u[2](t),t));

               /d         \2            /d         \2
DF := 1/2 c[1] |-- u[1](t)|  + 1/2 c[2] |-- u[2](t)|
               \dt        /             \dt        /

                /d         \2 | d          |
     + 1/2 v[1] |-- u[1](t)|  | -- u[1](t) |
                \dt        /  | dt         |

                /d         \2 | d          |
     + 1/2 v[2] |-- u[2](t)|  | -- u[2](t) |
                \dt        /  | dt         |
```

```
Generalized forces on generalized displacements
-----------------------------------------------
> F[1]:=0;

                                F[1] := 0

> F[2]:=0;

                                F[2] := 0

> F[3]:=u[1];

                               F[3] := u[1]

> F[4]:=u[2];

                               F[4] := u[2]
```

```
> F[5]:=u[3];
```

$$F[5] := u[3]$$

Derivation of equations of motion using Lagrange's equation

```
> DOFF:=[u[1](t),u[2](t)]:
> DOFB:=[zeta[1](t),zeta[2](t),zeta[3](t)]:
> DOF:=[op(DOFF),op(DOFB)]:
> dDOF:=diff1(DOF):
> ddDOF:=diff1(dDOF):
> setA:={}:setB:={}:setC:={}:
> setD:={}:setE:={}:setF:={}:
> DOFq:=[]:dDOFq:=[]:ddDOFq:=[]:
> for i from 1 to vectdim(DOF) do
>   DOFq:=[op(DOFq),q[i]]:
>   dDOFq:=[op(dDOFq),dq[i]]:
>   ddDOFq:=[op(ddDOFq),ddq[i]]:
>   setA:=setA union {ddDOF[i]=ddDOFq[i]}:
>   setB:=setB union {dDOF[i]=dDOFq[i]}:
>   setC:=setC union {DOF[i]=DOFq[i]}:
>   setD:=setD union {ddDOFq[i]=ddDOF[i]}:
>   setE:=setE union {dDOFq[i]=dDOF[i]}:
>   setF:=setF union {DOFq[i]=DOF[i]}:
> od:
> set1:=setA union setB union setC;
```

$$\begin{aligned}
set1 := \{ & \frac{d^2}{dt^2} u[1](t) = ddq[1], \ \frac{d}{dt} u[1](t) = dq[1], \ u[1](t) = q[1], \\
& \frac{d^2}{dt^2} u[2](t) = ddq[2], \ \frac{d}{dt} u[2](t) = dq[2], \ u[2](t) = q[2], \\
& \frac{d^2}{dt^2} zeta[1](t) = ddq[3], \ \frac{d}{dt} zeta[1](t) = dq[3], \ zeta[1](t) = q[3], \\
& \frac{d^2}{dt^2} zeta[2](t) = ddq[4], \ \frac{d}{dt} zeta[2](t) = dq[4], \ zeta[2](t) = q[4],
\end{aligned}$$

```
     2                          d
    d                           --  zeta[3](t) = dq[5], zeta[3](t) = q[5]
    --- zeta[3](t) = ddq[5],    dt
      2
    dt

    }

> set2:=setD union setE union setF;

                    2
                   d                          d
set2 := {ddq[1] = --- u[1](t), dq[1] = -- u[1](t), q[1] = u[1](t),
                     2                        dt
                   dt

              2
             d                          d
    ddq[2] = --- u[2](t), dq[2] = -- u[2](t), q[2] = u[2](t),
               2                        dt
             dt

              2
             d                            d
    ddq[3] = --- zeta[1](t), dq[3] = -- zeta[1](t), q[3] = zeta[1](t),
               2                          dt
             dt

              2
             d                            d
    ddq[4] = --- zeta[2](t), dq[4] = -- zeta[2](t), q[4] = zeta[2](t),
               2                          dt
             dt

              2
             d                            d
    ddq[5] = --- zeta[3](t), dq[5] = -- zeta[3](t), q[5] = zeta[3](t)
               2                          dt
             dt

    }

> T:=TF:
> U:=UF:
> D1:=DF:
> for i from 1 to vectdim(DOFB) do
>    T:=T+subs(k=i,TBk):
>    U:=U+subs(k=i,UBk):
>    D1:=D1+subs(k=i,DBk):
> od:
> Temp:=subs(set1,T):
> for i from 1 to vectdim(DOF) do
>     temp1:=diff(Temp,dDOFq[i]):
>     temp2:=subs(set2,temp1):
```

```
>     temp3:=diff(temp2,t):
>     L1:=subs(set1,temp3):
>     L2:=diff(Temp,DOFq[i]):
>     L3:=diff(subs(set1,U),DOFq[i]):
>     L4:=diff(subs(set1,D1),dDOFq[i]):
>     EOM[i]:=simplify(L1-L2+L3+L4-F[i]):
> od:
> setS:={signum(1,q[3]-z)=0,signum(1,q[4]-z)=0,signum(1,q[5]-
z)=0,signum(1,q[3]+z)=0,signum(1,q[4]+z)=0,signum(1,q[5]+z)=0,abs(1,dq[
3])=0,abs(1,dq[4])=0,abs(1,dq[5])=0,abs(1,dq[1])=0,abs(1,dq[2])=0}:
> A:=matrix(vectdim(DOF),vectdim(DOF));

                    A := array(1 .. 5, 1 .. 5, [])

> for i from 1 to vectdim(DOF) do
>    for j from 1 to vectdim(DOF) do
>       A[i,j]:=coeff(EOM[i],ddDOFq[j]):
>       A[i,j]:=subs(setS,A[i,j]):
>    od:
> od:
> Ax2dot:=multiply(A,ddDOFq):
> f:=array(1..vectdim(DOF));

                        f := array(1 .. 5, [])

> for i from 1 to vectdim(DOF) do
>    f[i]:=-simplify(EOM[i]-Ax2dot[i]):
>    f[i]:=subs(setS,f[i]):
> od:
> x1dot:=[]:x1:=[]:
> for i from 1 to vectdim(DOF) do x1dot:=[op(x1dot),x[i]] od:
> for i from vectdim(DOF)+1 to 2*vectdim(DOF) do x1:=[op(x1),x[i]] od:
> setX:={}:
> for i from 1 to vectdim(DOF) do
>    setX:=setX union {dDOFq[i]=x1dot[i]}:
>    setX:=setX union {DOFq[i]=x1[i]}:
> od:
> interface(labelling=false);
> A1:=subs(setX ,op(A));

A1 :=

    [M[1] + mb[1] + mb[2] + mb[3] , 0 ,

    -mb[1] R cos(%1) sin(x[8]) - mb[1] R sin(%1) cos(x[8]) ,

    -mb[2] R cos(%2) sin(x[9]) - mb[2] R sin(%2) cos(x[9]) ,

    -mb[3] R cos(%3) sin(x[10]) - mb[3] R sin(%3) cos(x[10])]

    [0 , M[2] + mb[1] + mb[2] + mb[3] ,

    -mb[1] R sin(%1) sin(x[8]) + mb[1] R cos(%1) cos(x[8]) ,
```

```
     -mb[2] R sin(%2) sin(x[9]) + mb[2] R cos(%2) cos(x[9]) ,

     -mb[3] R sin(%3) sin(x[10]) + mb[3] R cos(%3) cos(x[10])]

     [
     [-mb[1] R cos(%1) sin(x[8]) - mb[1] R sin(%1) cos(x[8]) ,

                                                                    2
     -mb[1] R sin(%1) sin(x[8]) + mb[1] R cos(%1) cos(x[8]) , mb[1] R

            ]
     , 0 , 0]

     [
     [-mb[2] R cos(%2) sin(x[9]) - mb[2] R sin(%2) cos(x[9]) ,

     -mb[2] R sin(%2) sin(x[9]) + mb[2] R cos(%2) cos(x[9]) , 0 ,

            2    ]
     mb[2] R  , 0]

     [
     [-mb[3] R cos(%3) sin(x[10]) - mb[3] R sin(%3) cos(x[10]) ,

     -mb[3] R sin(%3) sin(x[10]) + mb[3] R cos(%3) cos(x[10]) , 0 , 0

              2]
     , mb[3] R ]

%1 := Omega t + Phi[1]

%2 := Omega t + Phi[2]

%3 := Omega t + Phi[3]

> f1:=subs(setX ,op(f));

       [
f1 := [-K[1] x[6] - c[1] x[1] - v[1] x[1] | x[1] |

                              2                                2
      + mb[1] cos(%2) Omega  e1 + mb[1] R cos(%2) Omega  cos(x[8])

      - 2 mb[1] R sin(%2) Omega sin(x[8]) x[3]

                                       2
      + mb[1] R cos(%2) cos(x[8]) x[3]

                               2
      - mb[1] R sin(%2) Omega  sin(x[8])

      + 2 mb[1] R cos(%2) Omega cos(x[8]) x[3]

                                       2                       2
```

```
- mb[1] R sin(%2) sin(x[8]) x[3]  + mb[2] cos(%1) Omega  e1

                          2
+ mb[2] R cos(%1) Omega  cos(x[9])

- 2 mb[2] R sin(%1) Omega sin(x[9]) x[4]

                                  2
+ mb[2] R cos(%1) cos(x[9]) x[4]

                          2
- mb[2] R sin(%1) Omega  sin(x[9])

+ 2 mb[2] R cos(%1) Omega cos(x[9]) x[4]

                                  2                         2
- mb[2] R sin(%1) sin(x[9]) x[4]  + mb[3] cos(%3) Omega  e1

                          2
+ mb[3] R cos(%3) Omega  cos(x[10])

- 2 mb[3] R sin(%3) Omega sin(x[10]) x[5]

                                   2
+ mb[3] R cos(%3) cos(x[10]) x[5]

                          2
- mb[3] R sin(%3) Omega  sin(x[10])

+ 2 mb[3] R cos(%3) Omega cos(x[10]) x[5]

                                   2
- mb[3] R sin(%3) sin(x[10]) x[5] , -c[2] x[2] - K[2] x[7]

                                                 2
- v[2] x[2] | x[2] | + mb[2] R cos(%1) Omega  sin(x[9])

+ 2 mb[2] R sin(%1) Omega cos(x[9]) x[4]

                                  2                         2
+ mb[2] R cos(%1) sin(x[9]) x[4]  + mb[3] sin(%3) Omega  e1

                          2
+ mb[3] R sin(%3) Omega  cos(x[10])

+ 2 mb[3] R cos(%3) Omega sin(x[10]) x[5]

                                   2
+ mb[3] R sin(%3) cos(x[10]) x[5]

                          2
+ mb[3] R cos(%3) Omega  sin(x[10])

+ 2 mb[3] R sin(%3) Omega cos(x[10]) x[5]
```

```
                                        2                       2
     + mb[3] R cos(%3) sin(x[10]) x[5]  + mb[1] sin(%2) Omega  e1

                             2
     + mb[1] R sin(%2) Omega  cos(x[8])

     + 2 mb[1] R cos(%2) Omega sin(x[8]) x[3]

                                      2
     + mb[1] R sin(%2) cos(x[8]) x[3]

                             2
     + mb[1] R cos(%2) Omega  sin(x[8])

     + 2 mb[1] R sin(%2) Omega cos(x[8]) x[3]

                                      2                       2
     + mb[1] R cos(%2) sin(x[8]) x[3]  + mb[2] sin(%1) Omega  e1

                             2
     + mb[2] R sin(%1) Omega  cos(x[9])

                                      2
     + mb[2] R sin(%1) cos(x[9]) x[4]

     + 2 mb[2] R cos(%1) Omega sin(x[9]) x[4],

                                          2
    -2 Vzeta[1] x[3] | x[3] | - mb[1] Omega  e1 R sin(x[8]) + u[1]

                               3                          3
     - Ke[1] x[8] - Kd[1] x[8]  - Czeta[1] x[3], -Kd[2] x[9]

     - Czeta[2] x[4] - Ke[2] x[9] - 2 Vzeta[2] x[4] | x[4] | + u[2]

                  2
     - mb[2] Omega  e1 R sin(x[9]), -2 Vzeta[3] x[5] | x[5] | + u[3]

                                3
     - Ke[3] x[10] - Kd[3] x[10]  - Czeta[3] x[5]

                  2                  ]
     - mb[3] Omega  e1 R sin(x[10])]

%1 := Omega t + Phi[2]

%2 := Omega t + Phi[1]

%3 := Omega t + Phi[3]

> realib(fortran):
> B:=augment(A1,f1):
> fortran(B,optimized);
```

```
> fortran(B);
```

APPENDIX E - EQUATIONS OF MOTION FOR COLEMAN MODEL

```
mb[3]*R*sin(Omega*t+Phi[3])*sin(q[5])*dq[5]^2-
mb[3]*R*sin(Omega*t+Phi[3])*cos(q[5])*ddq[5]+mb[2]*R*sin(Omega*t+Phi[2])*Ome
ga^2*sin(q[4])-
2*mb[2]*R*cos(Omega*t+Phi[2])*Omega*cos(q[4])*dq[4]+mb[2]*R*sin(Omega*t+Phi
[2])*sin(q[4])*dq[4]^2-mb[2]*R*sin(Omega*t+Phi[2])*cos(q[4])*ddq[4]-
mb[3]*cos(Omega*t+Phi[3])*Omega^2*e1-
mb[3]*R*cos(Omega*t+Phi[3])*Omega^2*cos(q[5])+2*mb[3]*R*sin(Omega*t+Phi[3])
*Omega*sin(q[5])*dq[5]-mb[3]*R*cos(Omega*t+Phi[3])*cos(q[5])*dq[5]^2-
mb[3]*R*cos(Omega*t+Phi[3])*sin(q[5])*ddq[5]+mb[3]*R*sin(Omega*t+Phi[3])*Ome
ga^2*sin(q[5])-
mb[1]*R*cos(Omega*t+Phi[1])*Omega^2*cos(q[3])+2*mb[1]*R*sin(Omega*t+Phi[1])
*Omega*sin(q[3])*dq[3]-mb[1]*R*cos(Omega*t+Phi[1])*cos(q[3])*dq[3]^2-
mb[1]*R*cos(Omega*t+Phi[1])*sin(q[3])*ddq[3]+mb[1]*R*sin(Omega*t+Phi[1])*Ome
ga^2*sin(q[3])-
2*mb[1]*R*cos(Omega*t+Phi[1])*Omega*cos(q[3])*dq[3]+mb[1]*R*sin(Omega*t+Phi
[1])*sin(q[3])*dq[3]^2-mb[1]*R*sin(Omega*t+Phi[1])*cos(q[3])*ddq[3]-
mb[2]*cos(Omega*t+Phi[2])*Omega^2*e1-
mb[2]*R*cos(Omega*t+Phi[2])*Omega^2*cos(q[4])+2*mb[2]*R*sin(Omega*t+Phi[2])
*Omega*sin(q[4])*dq[4]-mb[2]*R*cos(Omega*t+Phi[2])*cos(q[4])*dq[4]^2-
mb[2]*R*cos(Omega*t+Phi[2])*sin(q[4])*ddq[4]-
mb[1]*cos(Omega*t+Phi[1])*Omega^2*e1-
2*mb[3]*R*cos(Omega*t+Phi[3])*Omega*cos(q[5])*dq[5]+K[1]*q[1]+v[1]*dq[1]*abs(
dq[1])+M[1]*ddq[1]+1/2*v[1]*dq[1]^2*abs(1,dq[1])+c[1]*dq[1]+mb[1]*ddq[1]+mb[2]*
ddq[1]+mb[3]*ddq[1]=0

mb[1]*ddq[2]+mb[3]*ddq[2]-mb[3]*R*cos(Omega*t+Phi[3])*Omega^2*sin(q[5])-
2*mb[3]*R*sin(Omega*t+Phi[3])*Omega*cos(q[5])*dq[5]-
mb[3]*R*cos(Omega*t+Phi[3])*sin(q[5])*dq[5]^2+mb[3]*R*cos(Omega*t+Phi[3])*cos
(q[5])*ddq[5]-mb[3]*R*sin(Omega*t+Phi[3])*Omega^2*cos(q[5])-
2*mb[3]*R*cos(Omega*t+Phi[3])*Omega*sin(q[5])*dq[5]-
mb[3]*R*sin(Omega*t+Phi[3])*sin(q[5])*ddq[5]-
2*mb[2]*R*sin(Omega*t+Phi[2])*Omega*cos(q[4])*dq[4]-
mb[3]*R*sin(Omega*t+Phi[3])*cos(q[5])*dq[5]^2-
mb[1]*sin(Omega*t+Phi[1])*Omega^2*e1-
mb[1]*R*sin(Omega*t+Phi[1])*Omega^2*cos(q[3])-
2*mb[1]*R*cos(Omega*t+Phi[1])*Omega*sin(q[3])*dq[3]-
mb[1]*R*sin(Omega*t+Phi[1])*cos(q[3])*dq[3]^2-
mb[1]*R*sin(Omega*t+Phi[1])*sin(q[3])*ddq[3]-
mb[1]*R*cos(Omega*t+Phi[1])*Omega^2*sin(q[3])-
2*mb[1]*R*sin(Omega*t+Phi[1])*Omega*cos(q[3])*dq[3]-
2*mb[2]*R*cos(Omega*t+Phi[2])*Omega*sin(q[4])*dq[4]-
```

```
mb[2]*R*sin(Omega*t+Phi[2])*cos(q[4])*dq[4]^2-
mb[2]*R*sin(Omega*t+Phi[2])*sin(q[4])*ddq[4]-
mb[2]*R*cos(Omega*t+Phi[2])*Omega^2*sin(q[4])-
mb[1]*R*cos(Omega*t+Phi[1])*sin(q[3])*dq[3]^2+mb[1]*R*cos(Omega*t+Phi[1])*cos
(q[3])*ddq[3]-mb[2]*sin(Omega*t+Phi[2])*Omega^2*e1-
mb[2]*R*sin(Omega*t+Phi[2])*Omega^2*cos(q[4])-
mb[3]*sin(Omega*t+Phi[3])*Omega^2*e1-
mb[2]*R*cos(Omega*t+Phi[2])*sin(q[4])*dq[4]^2+mb[2]*R*cos(Omega*t+Phi[2])*cos
(q[4])*ddq[4]+M[2]*ddq[2]+mb[2]*ddq[2]+1/2*v[2]*dq[2]^2*abs(1,dq[2])+K[2]*q[2]+
c[2]*dq[2]+v[2]*dq[2]*abs(dq[2])=0

2*Vzeta[1]*dq[3]*abs(dq[3])-
u[1]+mb[1]*ddq[2]*R*cos(Omega*t+Phi[1])*cos(q[3])+mb[1]*R^2*ddq[3]-
mb[1]*ddq[1]*R*cos(Omega*t+Phi[1])*sin(q[3])-
mb[1]*ddq[1]*R*sin(Omega*t+Phi[1])*cos(q[3])-
mb[1]*ddq[2]*R*sin(Omega*t+Phi[1])*sin(q[3])+mb[1]*Omega^2*e1*R*sin(q[3])+Vze
ta[1]*dq[3]^2*abs(1,dq[3])+Ke[1]*q[3]+Kd[1]*q[3]^3+Czeta[1]*dq[3]=0

mb[2]*Omega^2*e1*R*sin(q[4])-
mb[2]*ddq[1]*R*sin(Omega*t+Phi[2])*cos(q[4])+mb[2]*ddq[2]*R*cos(Omega*t+Phi[2
])*cos(q[4])+mb[2]*R^2*ddq[4]-
mb[2]*ddq[2]*R*sin(Omega*t+Phi[2])*sin(q[4])+Vzeta[2]*dq[4]^2*abs(1,dq[4])-
u[2]+Ke[2]*q[4]+Kd[2]*q[4]^3+Czeta[2]*dq[4]+2*Vzeta[2]*dq[4]*abs(dq[4])-
mb[2]*ddq[1]*R*cos(Omega*t+Phi[2])*sin(q[4])=0

-u[3]-mb[3]*ddq[1]*R*cos(Omega*t+Phi[3])*sin(q[5])-
mb[3]*ddq[1]*R*sin(Omega*t+Phi[3])*cos(q[5])+mb[3]*Omega^2*e1*R*sin(q[5])+mb
[3]*R^2*ddq[5]-
mb[3]*ddq[2]*R*sin(Omega*t+Phi[3])*sin(q[5])+mb[3]*ddq[2]*R*cos(Omega*t+Phi[3
])*cos(q[5])+2*Vzeta[3]*dq[5]*abs(dq[5])+Vzeta[3]*dq[5]^2*abs(1,dq[5])+Ke[3]*q[5]+
Kd[3]*q[5]^3+Czeta[3]*dq[5]=0
```

APPENDIX F - SIMPLIFIED ROTOR/FUSELAGE EQUATIONS OF MOTION

Equations with viscous and hydraulic damping in the hub degrees of freedom, x and y. [Ref. 19]

$$
\begin{aligned}
&M_x * \ddot{x} + C_x * \dot{x} + V_x * \dot{x} * |\dot{x}| + K_x * x \\
&= mb_1 * R * (\ddot{\zeta}_1 * \sin(\Psi_1 + \zeta_1) + (\Omega + \dot{\zeta}_1)^2 * \cos(\Psi_1 + \zeta_1) \\
&+ mb_2 * R * (\ddot{\zeta}_2 * \sin(\Psi_2 + \zeta_2) + (\Omega + \dot{\zeta}_2)^2 * \cos(\Psi_2 + \zeta_2) \\
&+ mb_3 * R * (\ddot{\zeta}_3 * \sin(\Psi_3 + \zeta_3) + (\Omega + \dot{\zeta}_3)^2 * \cos(\Psi_3 + \zeta_3)
\end{aligned}
$$

$$
\begin{aligned}
&M_y * \ddot{y} + C_y * \dot{y} + V_y * \dot{y} * |\dot{y}| + K_y * y \\
&= mb_1 * R * (\ddot{\zeta}_1 * \sin(\Psi_1 + \zeta_1) - (\Omega + \dot{\zeta}_1)^2 * \sin(\Psi_1 + \zeta_1) \\
&+ mb_2 * R * (\ddot{\zeta}_2 * \sin(\Psi_2 + \zeta_2) - (\Omega + \dot{\zeta}_2)^2 * \sin(\Psi_2 + \zeta_2) \\
&+ mb_3 * R * (\ddot{\zeta}_3 * \sin(\Psi_3 + \zeta_3) - (\Omega + \dot{\zeta}_3)^2 * \sin(\Psi_3 + \zeta_3)
\end{aligned}
$$

$$
\begin{aligned}
&mb_1 * R^2 * \ddot{\zeta}_1 + C_{\zeta_1} * \dot{\zeta}_1 + Ke_1 * \zeta_1 + mb_1 * \Omega^2 * e * R * \sin(\zeta_1) \\
&= mb_1 * \ddot{x} * R * \sin(\Psi_1 + \zeta_1) - mb_1 * \ddot{y} * R * \cos(\Psi_1 + \zeta_1)
\end{aligned}
$$

$$
\begin{aligned}
&mb_2 * R^2 * \ddot{\zeta}_2 + C_{\zeta_2} * \dot{\zeta}_2 + Ke_2 * \zeta_2 + mb_2 * \Omega^2 * e * R * \sin(\zeta_2) \\
&= mb_2 * \ddot{x} * R * \sin(\Psi_2 + \zeta_2) - mb_2 * \ddot{y} * R * \cos(\Psi_2 + \zeta_2)
\end{aligned}
$$

$$
\begin{aligned}
&mb_3 * R^2 * \ddot{\zeta}_3 + C_{\zeta_3} * \dot{\zeta}_3 + Ke_3 * \zeta_3 + mb_3 * \Omega^2 * e * R * \sin(\zeta_3) \\
&= mb_3 * \ddot{x} * R * \sin(\Psi_3 + \zeta_3) - mb_3 * \ddot{y} * R * \cos(\Psi_3 + \zeta_3)
\end{aligned}
$$

APPENDIX G - 5 BLADED EQUATIONS OF MOTION WITH POLYNOMIAL SNUBBER FUNCTIONS

```
                                                    2
mb[4] R sin(Omega t + Phi[4]) Omega  sin(q[6])

     - 2 mb[4] R cos(Omega t + Phi[4]) Omega cos(q[6]) dq[6]

                                                          2
     + mb[4] R sin(Omega t + Phi[4]) sin(q[6]) dq[6]

     - mb[4] R sin(Omega t + Phi[4]) cos(q[6]) ddq[6]

                                          2
     - mb[5] cos(Omega t + Phi[5]) Omega  e1

                                        2
     - mb[5] R cos(Omega t + Phi[5]) Omega  cos(q[7])

     + 2 mb[5] R sin(Omega t + Phi[5]) Omega sin(q[7]) dq[7]

     - 2 mb[5] R cos(Omega t + Phi[5]) Omega cos(q[7]) dq[7]

                                                        2
     - mb[2] R cos(Omega t + Phi[2]) cos(q[4]) dq[4]

     - mb[2] R cos(Omega t + Phi[2]) sin(q[4]) ddq[4]

                                        2
     + mb[2] R sin(Omega t + Phi[2]) Omega  sin(q[4])

     - 2 mb[2] R cos(Omega t + Phi[2]) Omega cos(q[4]) dq[4]

                                                        2
     + mb[2] R sin(Omega t + Phi[2]) sin(q[4]) dq[4]

     - mb[2] R sin(Omega t + Phi[2]) cos(q[4]) ddq[4]

                                        2
     - mb[3] R cos(Omega t + Phi[3]) Omega  cos(q[5])

     + 2 mb[3] R sin(Omega t + Phi[3]) Omega sin(q[5]) dq[5]

                                                        2
     - mb[3] R cos(Omega t + Phi[3]) cos(q[5]) dq[5]

     - mb[3] R cos(Omega t + Phi[3]) sin(q[5]) ddq[5]

                                        2
     + mb[3] R sin(Omega t + Phi[3]) Omega  sin(q[5])

     - 2 mb[3] R cos(Omega t + Phi[3]) Omega cos(q[5]) dq[5]
```

```
                                          2
- mb[1] cos(Omega t + Phi[1]) Omega  e1

                                        2
- mb[1] R cos(Omega t + Phi[1]) Omega  cos(q[3])

+ 2 mb[1] R sin(Omega t + Phi[1]) Omega sin(q[3]) dq[3]

                                                 2
- mb[1] R cos(Omega t + Phi[1]) cos(q[3]) dq[3]

- mb[1] R cos(Omega t + Phi[1]) sin(q[3]) ddq[3]

                                        2
+ mb[1] R sin(Omega t + Phi[1]) Omega  sin(q[3])

- 2 mb[1] R cos(Omega t + Phi[1]) Omega cos(q[3]) dq[3]

                                                 2
+ mb[1] R sin(Omega t + Phi[1]) sin(q[3]) dq[3]

- mb[1] R sin(Omega t + Phi[1]) cos(q[3]) ddq[3]

                                          2
- mb[2] cos(Omega t + Phi[2]) Omega  e1

                                        2
- mb[2] R cos(Omega t + Phi[2]) Omega  cos(q[4])

                                          2
- mb[3] cos(Omega t + Phi[3]) Omega  e1

+ 2 mb[2] R sin(Omega t + Phi[2]) Omega sin(q[4]) dq[4]

                                                 2
+ mb[3] R sin(Omega t + Phi[3]) sin(q[5]) dq[5]

- mb[5] R cos(Omega t + Phi[5]) sin(q[7]) ddq[7]

                                        2
+ mb[5] R sin(Omega t + Phi[5]) Omega  sin(q[7])

                                                 2
+ mb[5] R sin(Omega t + Phi[5]) sin(q[7]) dq[7]

- mb[5] R sin(Omega t + Phi[5]) cos(q[7]) ddq[7]

- mb[3] R sin(Omega t + Phi[3]) cos(q[5]) ddq[5]

                                          2
- mb[4] cos(Omega t + Phi[4]) Omega  e1

                                        2
- mb[4] R cos(Omega t + Phi[4]) Omega  cos(q[6])
```

```
      + 2 mb[4] R sin(Omega t + Phi[4]) Omega sin(q[6]) dq[6]

                                                          2
      - mb[4] R cos(Omega t + Phi[4]) cos(q[6]) dq[6]  - u[1]

      + mb[5] ddq[1] + mb[4] ddq[1]

      + mb[2] ddq[1] + M[1] ddq[1] + mb[1] ddq[1]

      + v[1] dq[1] | dq[1] | + mb[3] ddq[1] + K[1] q[1] + c[1] dq[1]

      - mb[4] R cos(Omega t + Phi[4]) sin(q[6]) ddq[6]

                                                          2
      - mb[5] R cos(Omega t + Phi[5]) cos(q[7]) dq[7]  = 0


v[2] dq[2] | dq[2] |

      - 2 mb[3] R cos(Omega t + Phi[3]) Omega sin(q[5]) dq[5]

                                                          2
      - mb[3] R sin(Omega t + Phi[3]) cos(q[5]) dq[5]

      - mb[3] R sin(Omega t + Phi[3]) sin(q[5]) ddq[5]

                                                2
      - mb[3] R cos(Omega t + Phi[3]) Omega  sin(q[5])

      - 2 mb[5] R cos(Omega t + Phi[5]) Omega sin(q[7]) dq[7]

                                                          2
      - mb[5] R sin(Omega t + Phi[5]) cos(q[7]) dq[7]

      - mb[5] R sin(Omega t + Phi[5]) sin(q[7]) ddq[7]

                                                2
      - mb[5] R cos(Omega t + Phi[5]) Omega  sin(q[7])

      - 2 mb[5] R sin(Omega t + Phi[5]) Omega cos(q[7]) dq[7]

                                                          2
      - mb[5] R cos(Omega t + Phi[5]) sin(q[7]) dq[7]

      + mb[5] R cos(Omega t + Phi[5]) cos(q[7]) ddq[7]

      - 2 mb[3] R sin(Omega t + Phi[3]) Omega cos(q[5]) dq[5]

                                                          2
      - mb[3] R cos(Omega t + Phi[3]) sin(q[5]) dq[5]

      + mb[3] R cos(Omega t + Phi[3]) cos(q[5]) ddq[5]
```

```
                                          2
- mb[4] sin(Omega t + Phi[4]) Omega  e1

                                        2
- mb[4] R sin(Omega t + Phi[4]) Omega  cos(q[6])

- 2 mb[4] R cos(Omega t + Phi[4]) Omega sin(q[6]) dq[6]

                                                  2
- mb[4] R sin(Omega t + Phi[4]) cos(q[6]) dq[6]

- mb[4] R sin(Omega t + Phi[4]) sin(q[6]) ddq[6]

                                        2
- mb[4] R cos(Omega t + Phi[4]) Omega  sin(q[6])

- 2 mb[4] R sin(Omega t + Phi[4]) Omega cos(q[6]) dq[6]

                                                  2
- mb[4] R cos(Omega t + Phi[4]) sin(q[6]) dq[6]

+ mb[4] R cos(Omega t + Phi[4]) cos(q[6]) ddq[6]

                                          2
- mb[5] sin(Omega t + Phi[5]) Omega  e1

                                          2
- mb[1] sin(Omega t + Phi[1]) Omega  e1

                                        2
- mb[1] R sin(Omega t + Phi[1]) Omega  cos(q[3])

- 2 mb[1] R cos(Omega t + Phi[1]) Omega sin(q[3]) dq[3]

                                                  2
- mb[1] R sin(Omega t + Phi[1]) cos(q[3]) dq[3]

- mb[1] R sin(Omega t + Phi[1]) sin(q[3]) ddq[3]

                                        2
- mb[1] R cos(Omega t + Phi[1]) Omega  sin(q[3])

- 2 mb[1] R sin(Omega t + Phi[1]) Omega cos(q[3]) dq[3]

                                                  2
- mb[1] R cos(Omega t + Phi[1]) sin(q[3]) dq[3]

+ mb[1] R cos(Omega t + Phi[1]) cos(q[3]) ddq[3]

                                          2
- mb[2] sin(Omega t + Phi[2]) Omega  e1

                                        2
- mb[2] R sin(Omega t + Phi[2]) Omega  cos(q[4])
```

```
    - 2 mb[2] R cos(Omega t + Phi[2]) Omega sin(q[4]) dq[4]

                                                        2
    - mb[2] R sin(Omega t + Phi[2]) cos(q[4]) dq[4]

    - mb[2] R sin(Omega t + Phi[2]) sin(q[4]) ddq[4]

                                              2
    - mb[2] R cos(Omega t + Phi[2]) Omega  sin(q[4])

    - 2 mb[2] R sin(Omega t + Phi[2]) Omega cos(q[4]) dq[4]

                                                        2
    - mb[2] R cos(Omega t + Phi[2]) sin(q[4]) dq[4]

    + mb[2] R cos(Omega t + Phi[2]) cos(q[4]) ddq[4]

                                          2
    - mb[3] sin(Omega t + Phi[3]) Omega  e1

                                              2
    - mb[5] R sin(Omega t + Phi[5]) Omega  cos(q[7]) + mb[2] ddq[2]

    + M[2] ddq[2] - u[2] + K[2] q[2]

                                                             2
    + c[2] dq[2] - mb[3] R sin(Omega t + Phi[3]) Omega  cos(q[5])

    + mb[1] ddq[2] + mb[5] ddq[2] + mb[3] ddq[2] + mb[4] ddq[2] = 0


- mb[1] ddq[2] R sin(Omega t + Phi[1]) sin(q[3])

    + mb[1] ddq[2] R cos(Omega t + Phi[1]) cos(q[3])

    - mb[1] ddq[1] R cos(Omega t + Phi[1]) sin(q[3])

    - mb[1] ddq[1] R sin(Omega t + Phi[1]) cos(q[3])

                2                                2
    + mb[1] Omega  e1 R sin(q[3]) + mb[1] R  ddq[3] + q[3] Kpoly[5]

    + dq[3] Cpoly[5]

                                  3
    + q[3] Kpoly[2] | q[3] |  + q[3] Kpoly[4] | q[3] |

                                   3
    + dq[3] Cpoly[2] | q[3] |  + dq[3] Cpoly[4] | q[3] |

                          2                          4          5
    + dq[3] Cpoly[3] q[3]  + dq[3] Cpoly[1] q[3]  + 3 q[3]  Kpoly[1]
```

```
                3
      + 2 q[3]  Kpoly[3] - u[3] = 0


             2
mb[2] Omega  e1 R sin(q[4])

      - mb[2] ddq[1] R cos(Omega t + Phi[2]) sin(q[4])

      - mb[2] ddq[1] R sin(Omega t + Phi[2]) cos(q[4])

      - mb[2] ddq[2] R sin(Omega t + Phi[2]) sin(q[4])

      + mb[2] ddq[2] R cos(Omega t + Phi[2]) cos(q[4])

              3                    5
      + 2 q[4]  Kpoly[3] + 3 q[4]  Kpoly[1] + q[4] Kpoly[5]

                                  2                                      4
      + dq[4] Cpoly[5] + mb[2] R  ddq[4] - u[4] + dq[4] Cpoly[1] q[4]

                                3
      + q[4] Kpoly[2] | q[4] |  + q[4] Kpoly[4] | q[4] |

      + dq[4] Cpoly[4] | q[4] |

                                3                       2
      + dq[4] Cpoly[2] | q[4] |  + dq[4] Cpoly[3] q[4]  = 0


       2
mb[3] R  ddq[5]

      - mb[3] ddq[2] R sin(Omega t + Phi[3]) sin(q[5])

      + mb[3] ddq[2] R cos(Omega t + Phi[3]) cos(q[5])

      - mb[3] ddq[1] R cos(Omega t + Phi[3]) sin(q[5])

      - mb[3] ddq[1] R sin(Omega t + Phi[3]) cos(q[5])

                 2
      + mb[3] Omega  e1 R sin(q[5])

                              4                                      3
      + dq[5] Cpoly[1] q[5]  - u[5] + dq[5] Cpoly[2] | q[5] |

      + dq[5] Cpoly[4] | q[5] | + q[5] Kpoly[4] | q[5] |

                                3                       2
      + q[5] Kpoly[2] | q[5] |  + dq[5] Cpoly[3] q[5]

              5                    3
      + 3 q[5]  Kpoly[1] + 2 q[5]  Kpoly[3] + q[5] Kpoly[5]
```

```
     + dq[5] Cpoly[5] = 0

                          3
q[6] Kpoly[2] | q[6] |

                                                          3
     + q[6] Kpoly[4] | q[6] | + dq[6] Cpoly[2] | q[6] |

                                                    2
     + dq[6] Cpoly[4] | q[6] | + dq[6] Cpoly[3] q[6]

                              4
     + dq[6] Cpoly[1] q[6]  + dq[6] Cpoly[5] + q[6] Kpoly[5] - u[6]

             5                    3
     + 3 q[6]  Kpoly[1] + 2 q[6]  Kpoly[3]

     + mb[4] ddq[2] R cos(Omega t + Phi[4]) cos(q[6])

     - mb[4] ddq[2] R sin(Omega t + Phi[4]) sin(q[6])

     - mb[4] ddq[1] R sin(Omega t + Phi[4]) cos(q[6])

     - mb[4] ddq[1] R cos(Omega t + Phi[4]) sin(q[6])

                   2                            2
     + mb[4] Omega  e1 R sin(q[6]) + mb[4] R  ddq[6] = 0

       2                        2
mb[5] R  ddq[7] + mb[5] Omega  e1 R sin(q[7])

     - mb[5] ddq[1] R cos(Omega t + Phi[5]) sin(q[7])

     - mb[5] ddq[1] R sin(Omega t + Phi[5]) cos(q[7])

     - mb[5] ddq[2] R sin(Omega t + Phi[5]) sin(q[7])

     + mb[5] ddq[2] R cos(Omega t + Phi[5]) cos(q[7])

                              2
     + dq[7] Cpoly[3] q[7]  + dq[7] Cpoly[4] | q[7] |

                                   3
     + dq[7] Cpoly[2] | q[7] |

                                                          3
     + q[7] Kpoly[4] | q[7] | + q[7] Kpoly[2] | q[7] |

                              4                    5
     + dq[7] Cpoly[1] q[7]  - u[7] + 3 q[7]  Kpoly[1]
```

```
                                3
+ 2 q[7]   Kpoly[3] + q[7] Kpoly[5] + dq[7] Cpoly[5] = 0
```

APPENDIX H - 5 BLADED POLYNOMIAL S-FUNCTION INPUT FILE

```
function [I1,I2,I3,I4,I5,I6]=poly5in
% This m-file serves as input file for running the simulink
% S-function simple5p.m for the 5 bladed RAH-66 Wind Tunnel Model.
%
%%%%%%%%%%%%%%%%%%%%%%%%%%%%%%%%%%%%%%%%%%%%%%%%%%%%%%%%%%%%%%%%
% Helo Physical and Aerodynamic parameters
%%%%%%%%%%%%%%%%%%%%%%%%%%%%%%%%%%%%%%%%%%%%%%%%%%%%%%%%%%%%%%%%

% Equivalent Length of rotor blade (length).

R=26.5445;                          % inches

% Rotor speed (radians per/sec)

Omega=870*(2*pi/60);    % Run #

% Hinge offset (length).

e1=8.5235;                    % inches (9.804, 7.6898 ??)

% Lead/lag stop position (rad).

z=pi;

% Mass of rotor blades (mass).

mb(1)=0.013074;                     % slugs
mb(2)=0.013074;
mb(3)=0.013074;
mb(4)=0.013074;
mb(5)=0.013074;

% Effective mass of fuselage.

h=0.610;                                    % hub offset in meters
M(1)=3.504/h^2*0.06852; % convert fuselage inertia to equivalent
M(2)=7.495/h^2*0.06852; % mass at hub & convert to slugs

% Blade azimuth phase angles (radians)

Phi(1)=0;
Phi(2)=2*pi/5;
Phi(3)=4*pi/5;
Phi(4)=6*pi/5;
Phi(5)=8*pi/5;

% Blade Parameters

%      Spring stiffness polynomial for lead-lag (moment/radian)
          % snubber stiffness(lb/in) * geogain(in/rad) * (e1-
r_snub)(in)
```

```
      gg=5.1121; % geometric gain of snubber movement from lag, in/rad
%      Kpoly=[0,0,0,0,79.71*gg+660.9141]*(e1-2.5984); % 1inearized 1995
snubber
       Kbeam=[0 0 0 0 660.9141]; % origina1 Myklestad output
%       Ksnub=[38512436.84*gg^5,-4491019.58*gg^4,183336.70*gg^3,-
3147.25*gg^2,...
%         79.71*gg]*(e1-2.5984);
      % 1995 snubber
       Ksnub=[336241084.22*gg^5,-38666827.45*gg^4,1547897.06*gg^3,-
26483.84*gg^2,...
         233.32*gg]*(e1-2.5984);
      % 1992 snubber
%       Kpoly=Kbeam+Ksnub;
       Kpoly=2.5*(Kbeam+Ksnub);

%      Lead-lag stop spring constants (moment/radian)

       Ks(1)=0;
       Ks(2)=0;
       Ks(3)=0;
       Ks(4)=0;
       Ks(5)=0;

%      Linear damping in 1ead-1ag (moment/(rad/sec))
            % snubber damping(lb*s/in) * geogain(in/rad) * (e1-
r_snub)(in)

%      Cpoly=[0,0,0,0,0.59*gg]*(e1-2.5984);                 %
linearized 1995 snubber
%       Cpoly=[116695.68*gg^5,-14022.78*gg^4,609.0*gg^3,-
12.05*gg^2,0.59*gg]...
%            *(e1-2.5984);
      % 1995 snubber
            Cpoly=[-842875.01*gg^5,87576.78*gg^4,-
2847.07*gg^3,25.01*gg^2,0.47*gg]...
         *(e1-2.5984);
      % 1992 snubber
      Cpoly=2*Cpoly;

% Fuse1age Parameters

%      Linear springs in trans1ation (force/1ength)

       K(1)=1416.6/h^2*.2248/39.37*12*1.14;           % convert rotary
spring to latera1
       K(2)=1183.5/h^2*.2248/39.37*12;          % spring at hub p1ane &
convert to 1bf/in


%      Linear damping in trans1ation (force/(1ength/sec))
            % convert rotary damping to lateral
            % damping at hub plane & convert to lbf/in/s
% ?       c(1)=2*0.254/h^2*sqrt(18.43/0.254-(1.15*2*pi)^2)*.06852;
```

```
% ?       c(2)=2*3.75/h^2*sqrt(64.05/3.75-(0.65*2*pi)^2)*.06852;
%           c(1)=6.58*0.22481*39.37/h^2;
%           c(2)=10.21*0.22481*39.37/h^2;
            c=M*2.*[0.0467,0.0542].*sqrt(K./M);

%       Non-linear damping in translation(force/(length/sec)^2)

        v(1)=0;
        v(2)=0;

% Initial conditions


%       Blade lead-lag displacement (radians)

        x1i=0;
        x2i=0;
        x3i=0;
        x4i=0;
        x5i=0;

%       Blade lead-lag rates (radians/sec)

        xr1i=0;
        xr2i=0;
        xr3i=0;
        xr4i=0;
        xr5i=0;

%       Fuselage translational displacements (length)

        xXi=0.1;
        xYi=0.1;

%       Fuselage translational rates (length/sec)

        xrXi=0;
        xrYi=0;

%  Create input arrays:

I1 = [mb, M];

I2 = [R,Omega,e1,z];

I3 = Phi;

I4 = [c, v, Cpoly];

I5 = [Kpoly, Ks, K];

I6 = [xrXi,xrYi,xr1i,xr2i,xr3i,xr4i,xr5i,xXi,xYi,x1i,x2i,x3i,x4i,x5i];
```

APPENDIX I - 5 BLADED POLYNOMIAL S-FUNCTION

```
function [sys, x0] = blade5p(t,x,u,flag,I1,I2,I3,I4,I5,I6)

%
%   S-function arguments:
%   ---------------------
%   t      =  time
%   x      =  state vector
%   u      =  input vector
%   flag   =  switch used by numerical integration (simulation)
%             routine to access certain parts of the s-function
%
%   S-function input parameters:
%   ----------------------------
%
%   I1     =  [mb(1),mb(2),mb(3),mb(4),mb(5),M(1),M(2)]
%
%   I2     =  [R,Omega,e1,z]
%
%   I3     =  [Phi(1),Phi(2),Phi(3),Phi(4),Phi(5)]]
%
%   I4     =  [c(1),c(2),v(1),v(2),
%              Cpoly(1),Cpoly(2),Cpoly(3),Cpoly(4),Cpoly(5)]
%
%   I5     =  [Kpoly(1),Kpoly(2),Kpoly(3),Kpoly(4),Kpoly(5),
%              Ks(1),Ks(2),Ks(3),Ks(4),Ks(5),
%              K(1),K(2)]
%
%   I6     =  [xrXi,xrYi,xr1i,xr2i,xr3i,xr4i,xr5i,
%              xXi,xYi,x1i,x2i,x3i,x4i,x5i]
%
% S-function to represent dynamics of 5 bladed coupled rotor-
% fuselage model which considers only inplane degrees of
% freedom, i.e., x and y translational fuselage degrees of freedom
% and lead-lag rotor blade degrees of freedom.
%
% Explaination of variables:
% --------------------------
%
% mb     ->    mass of blade
% M      ->    effective mass of fuselage
% R      ->    distance from lead-lag hinge to blade center of mass
% e1     ->    blade hinge offset
% Omega  ->    rotor speed
% z      ->    angle at which blade hits stops
% Phi    ->    blade phase angle w.r.t. azimuth postion
% c      ->    fuselage linear damping
% v      ->    fuselage hydraulic damping
% Cpoly  ->    blade damping polynomial coefficients
% K      ->    effective stiffness of fuselage (landing gear stiffness)
% Kpoly  ->    blade elastic spring constant polynomial coefficients
% Ks     ->    blade stop effective spring constant
```

```
% xr_ _i ->    initial rate
% x_ _i  ->    initial displacement
%
%%%%%%%%%%%%%%%%%%%%%%%%%%%%%%%%%%%%%%%%%%%%%%%%%%%%%%%%%%%%%%%%%%%%%%%%%%%%%%%
% Define input parameters
%%%%%%%%%%%%%%%%%%%%%%%%%%%%%%%%%%%%%%%%%%%%%%%%%%%%%%%%%%%%%%%%%%%%%%%%%%%%%%%

mb=I1(1:5);
M=I1(6:7);
R=I2(1);Omega=I2(2);e1=I2(3);z=I2(4);
Phi=I3;
c=I4(1:2);
v=I4(3:4);
Cpoly=I4(5:9);
Kpoly=I5(1:5);
Ks=I5(6:10);
K=I5(11:12);
xrXi=I6(1);xrYi=I6(2);
xr1i=I6(3);xr2i=I6(4);xr3i=I6(5);xr4i=I6(6);xr5i=I6(7);
xXi=I6(8);xYi=I6(9);
x1i=I6(10);x2i=I6(11);x3i=I6(12);x4i=I6(13);x5i=I6(14);

%%%%%%%%%%%%%%%%%%%%%%%%%%%%%%%%%%%%%%%%%%%%%%%%%%%%%%%%%%%%%%%%%%%%%%%%%%%%%%%
% S-function flag conditionals
%%%%%%%%%%%%%%%%%%%%%%%%%%%%%%%%%%%%%%%%%%%%%%%%%%%%%%%%%%%%%%%%%%%%%%%%%%%%%%%
if flag == 0

      sys=[14,0,14,7,0,0];

x0=[xrXi,xrYi,xr1i,xr2i,xr3i,xr4i,xr5i,xXi,xYi,x1i,x2i,x3i,x4i,x5i];

elseif abs(flag) == 1

      t2 = mb(1)*R;
      t3 = Omega*t;
      t4 = t3+Phi(1);
      t5 = cos(t4);
      t6 = sin(x(10));
      t7 = t5*t6;
      t9 = sin(t4);
      t10 = cos(x(10));
      t11 = t9*t10;
      t13 = -t2*t7-t2*t11;
      t14 = mb(2)*R;
      t15 = t3+Phi(2);
      t16 = cos(t15);
      t17 = sin(x(11));
      t18 = t16*t17;
      t20 = sin(t15);
      t21 = cos(x(11));
      t22 = t20*t21;
      t24 = -t14*t18-t14*t22;
      t25 = mb(3)*R;
      t26 = t3+Phi(3);
```

```
      t27 = cos(t26);
      t28 = sin(x(12));
      t29 = t27*t28;
      t31 = sin(t26);
      t32 = cos(x(12));
      t33 = t31*t32;
      t35 = -t25*t29-t25*t33;
      t36 = mb(4)*R;
      t37 = t3+Phi(4);
      t38 = cos(t37);
      t39 = sin(x(13));
      t40 = t38*t39;
      t42 = sin(t37);
      t43 = cos(x(13));
      t44 = t42*t43;
      t46 = -t36*t40-t36*t44;
      t47 = mb(5)*R;
      t48 = t3+Phi(5);
      t49 = cos(t48);
      t50 = sin(x(14));
      t51 = t49*t50;
      t53 = sin(t48);
      t54 = cos(x(14));
      t55 = t53*t54;
      t57 = -t47*t51-t47*t55;
      t62 = Omega^2;
      t63 = t27*t62;
      t66 = t20*t17;
      t67 = x(4)^2;
      t70 = t25*t31;
      t72 = Omega*t28*x(5);
      t74 = t42*t39;
      t75 = x(6)^2;
      t78 = t42*t62;
      t81 = t38*t62;
      t84 = t38*t43;
      t87 = t53*t50;
      t88 = x(7)^2;
      t91 = t36*t38;
      t93 = Omega*t43*x(6);
      t95 = t36*t42;
      t97 = Omega*t39*x(6);
      t99 = t49*t54;
      t102 = t53*t62;
      t105 = t16*t62;
      t108 = t2*t5;
      t110 = Omega*t10*x(3);
      t112 = t9*t6;
      t113 = x(3)^2;
      t116 = t49*t62;
      t120 = t62*e1;
      t122 = -v(1)*x(1)*abs(x(1))-K(1)*x(8)+t25*t63*t32-t14*t66*t67-
2*t70*t72-t36*t74*t75-t36*t78*t39+t36*t81*t43+t36*t84*t75-
t47*t87*t88+2*t91*t93-2*t95*t97+t47*t99*t88-
```

```
t47*t102*t50+t14*t105*t21+2*t108*t110-
t2*t112*t113+t47*t116*t54+mb(4)*t38*t120;
      t131 = t47*t49;
      t133 = Omega*t54*x(7);
      t135 = t20*t62;
      t138 = t47*t53;
      t140 = Omega*t50*x(7);
      t142 = t16*t21;
      t145 = t14*t16;
      t147 = Omega*t21*x(4);
      t149 = t14*t20;
      t151 = Omega*t17*x(4);
      t153 = t9*t62;
      t156 = t5*t62;
      t159 = t31*t28;
      t160 = x(5)^2;
      t163 = t5*t10;
      t166 = t2*t9;
      t168 = Omega*t6*x(3);
      t171 = t27*t32;
      t174 = t31*t62;
      t177 = t25*t27;
      t179 = Omega*t32*x(5);
      t181 =
mb(5)*t49*t120+mb(1)*t5*t120+mb(2)*t16*t120+mb(3)*t27*t120+2*t131*t133-
t14*t135*t17-2*t138*t140+t14*t142*t67+2*t145*t147+u(1)-2*t149*t151-
t2*t153*t6+t2*t156*t10-t25*t159*t160+t2*t163*t113-2*t166*t168-
c(1)*x(1)+t25*t171*t160-t25*t174*t28+2*t177*t179;
      t186 = -t2*t112+t2*t163;
      t189 = t14*t142-t14*t66;
      t192 = -t25*t159+t25*t171;
      t195 = -t36*t74+t36*t84;
      t198 = -t47*t87+t47*t99;
      t230 = u(2)+t14*t18*t67-
v(2)*x(2)*abs(x(2))+2*t91*t97+t36*t81*t39+2*t70*t179+t36*t78*t43+t36*t4
4*t75+2*t177*t72-
c(2)*x(2)+mb(2)*t20*t120+t2*t156*t6+t25*t63*t28+t25*t29*t160+2*t95*t93+
t25*t174*t32+t25*t33*t160+t36*t40*t75+2*t149*t147;
      t265 =
t47*t51*t88+t47*t116*t50+2*t145*t151+t2*t7*t113+2*t138*t133+t47*t55*t88
+2*t131*t140+2*t166*t110+t2*t11*t113+t47*t102*t54+t14*t105*t17+t14*t22*
t67+mb(1)*t9*t120+t14*t135*t21+mb(4)*t42*t120+mb(5)*t53*t120+mb(3)*t31*
t120+2*t108*t168-K(2)*x(9)+t2*t153*t10;
      t267 = R^2;
      t269 = x(10)^2;
      t271 = 0;
      t274 = abs(x(10));
      t275 = t274^2;
      t276 = t275*t274;
      t287 = t269^2;
      t299 = e1*R;
      t302 = -t269*Kpoly(4)*t271/2-x(10)*Kpoly(2)*t276-
x(10)*Kpoly(4)*t274-x(3)*Cpoly(2)*t276-x(3)*Cpoly(4)*t274-
x(3)*Cpoly(3)*t269-x(3)*Cpoly(1)*t287+u(3)-
```

```
3.E0/2.E0*t269*Kpoly(2)*t275*t271-x(10)*Kpoly(5)-x(3)*Cpoly(5)-
3*t287*x(10)*Kpoly(1)-2*t269*x(10)*Kpoly(3)-mb(1)*t62*t299*t6;
      t305 = x(11)^2;
      t306 = t305^2;
      t318 = abs(x(11));
      t319 = t318^2;
      t320 = 0;
      t324 = t319*t318;
      t336 = u(4)-x(4)*Cpoly(1)*t306-3*t306*x(11)*Kpoly(1)-
2*t305*x(11)*Kpoly(3)-x(11)*Kpoly(5)-x(4)*Cpoly(5)-mb(2)*t62*t299*t17-
3.E0/2.E0*t305*Kpoly(2)*t319*t320-x(4)*Cpoly(2)*t324-
x(11)*Kpoly(2)*t324-x(11)*Kpoly(4)*t318-t305*Kpoly(4)*t320/2-
x(4)*Cpoly(3)*t305-x(4)*Cpoly(4)*t318;
      t339 = x(12)^2;
      t340 = t339^2;
      t345 = abs(x(12));
      t348 = t345^2;
      t349 = t348*t345;
      t356 = 0;
      t370 = u(5)-x(5)*Cpoly(1)*t340-x(5)*Cpoly(3)*t339-
x(5)*Cpoly(4)*t345-x(12)*Kpoly(2)*t349-x(12)*Kpoly(4)*t345-
x(5)*Cpoly(2)*t349-t339*Kpoly(4)*t356/2-2*t339*x(12)*Kpoly(3)-
3.E0/2.E0*t339*Kpoly(2)*t348*t356-mb(3)*t62*t299*t28-x(5)*Cpoly(5)-
x(12)*Kpoly(5)-3*t340*x(12)*Kpoly(1);
      t372 = x(13)^2;
      t374 = abs(x(13));
      t375 = t374^2;
      t376 = 0;
      t381 = t372^2;
      t390 = t375*t374;
      t404 = u(6)-3.E0/2.E0*t372*Kpoly(2)*t375*t376-x(13)*Kpoly(5)-
x(6)*Cpoly(5)-3*t381*x(13)*Kpoly(1)-2*t372*x(13)*Kpoly(3)-
mb(4)*t62*t299*t39-x(6)*Cpoly(2)*t390-x(6)*Cpoly(4)*t374-
x(13)*Kpoly(4)*t374-t372*Kpoly(4)*t376/2-x(13)*Kpoly(2)*t390-
x(6)*Cpoly(3)*t372-x(6)*Cpoly(1)*t381;
      t406 = x(14)^2;
      t408 = abs(x(14));
      t409 = t408^2;
      t410 = 0;
      t421 = t409*t408;
      t431 = t406^2;
      t438 = u(7)-3.E0/2.E0*t406*Kpoly(2)*t409*t410-x(7)*Cpoly(4)*t408-
mb(5)*t62*t299*t50-t406*Kpoly(4)*t410/2-x(14)*Kpoly(2)*t421-
x(14)*Kpoly(4)*t408-x(7)*Cpoly(2)*t421-x(7)*Cpoly(3)*t406-
x(7)*Cpoly(5)-x(14)*Kpoly(5)-3*t431*x(14)*Kpoly(1)-
2*t406*x(14)*Kpoly(3)-x(7)*Cpoly(1)*t431;
      B(1,1) = mb(4)+mb(5)+mb(1)+mb(2)+mb(3)+M(1);
      B(1,2) = 0;
      B(1,3) = t13;
      B(1,4) = t24;
      B(1,5) = t35;
      B(1,6) = t46;
      B(1,7) = t57;
      B(1,8) = t122+t181;
```

```
        B(2,1) = 0;
        B(2,2) = mb(1)+mb(2)+mb(3)+mb(4)+mb(5)+M(2);
        B(2,3) = t186;
        B(2,4) = t189;
        B(2,5) = t192;
        B(2,6) = t195;
        B(2,7) = t198;
        B(2,8) = t230+t265;
        B(3,1) = t13;
        B(3,2) = t186;
        B(3,3) = mb(1)*t267;
        B(3,4) = 0;
        B(3,5) = 0;
        B(3,6) = 0;
        B(3,7) = 0;
        B(3,8) = t302;
        B(4,1) = t24;
        B(4,2) = t189;
        B(4,3) = 0;
        B(4,4) = mb(2)*t267;
        B(4,5) = 0;
        B(4,6) = 0;
        B(4,7) = 0;
        B(4,8) = t336;
        B(5,1) = t35;
        B(5,2) = t192;
        B(5,3) = 0;
        B(5,4) = 0;
        B(5,5) = mb(3)*t267;
        B(5,6) = 0;
        B(5,7) = 0;
        B(5,8) = t370;
        B(6,1) = t46;
        B(6,2) = t195;
        B(6,3) = 0;
        B(6,4) = 0;
        B(6,5) = 0;
        B(6,6) = mb(4)*t267;
        B(6,7) = 0;
        B(6,8) = t404;
        B(7,1) = t57;
        B(7,2) = t198;
        B(7,3) = 0;
        B(7,4) = 0;
        B(7,5) = 0;
        B(7,6) = 0;
        B(7,7) = mb(5)*t267;
        B(7,8) = t438;

% Calculate derivatives

        [m,n]=size(B);
        A1=B(:,1:n-1);
        f1=B(:,n);
```

```
      sys=zeros(1,2*m);
      sys(1:7)=A1\f1;
      sys(8:14)=x(1:7);

% Output states

elseif abs(flag) == 3

      sys(1:14)=x;

else

      sys = [];

end
```

INITIAL DISTRIBUTION LIST

1. Defense Technical Information Center.....2
   8725 John J. Kingman Rd., STE 0944
   Ft. Belvoir, Virginia 22060-6218

2. Dudley Knox Library.....2
   Naval Postgraduate School
   411 Dyer Rd.
   Monterey, California 93943-5101

3. Department of Aeronautics and Astronautics.....2
   Naval Postgraduate School
   Code AA
   699 Dyer Road
   Monterey, CA 93943-5106

4. Mr. Robert L. King.....10
   Mississippi State University
   Aerospace/Walker Engineering
   P.O. Box A
   Mississippi State, MS 39762

5. Dr. E. Roberts Wood.....10
   Naval Postgraduate School
   Code AA/Wd
   699 Dyer Road
   Monterey, CA 93943-5106

6. Dr. Russell W. Duren.....1
   Naval Postgraduate School
   Code AA/Dr
   699 Dyer Road
   Monterey, CA 93943-5106

7. Dr. Donald A. Danielson.....1
   Naval Postgraduate School
   Code MA/Dd
   359 Glasgow Hall
   Monterey, CA 93943-5106

8. Dr. Harold A. Titus.....1
   Code EC/Ts
   204 Bullard Hall
   Monterey, CA 93943

9. Dr. Robert Ormiston.....1
   Building: 215, Room: 201C
   NASA Ames Research Center
   MS 215-1
   Moffett Field, CA 94035-1000

10. Dr. Gary Anderson.....1

U. S. Army Research Office
P.O. Box 1211
Research Triangle Park, NC 27709

11. Dr. Jeffrey D. Singleton.....1
Vehicle Structures Directorate
U.S. Army Research Laboratory
Mail Stop 340
NASA Langley Research Center
Hampton, VA 23681-0001

12. Dr. Peretz Friedmann.....1
University of Michigan
Aerospace Engineering
3001 Fxb
Ann Arbor, MI 48109

13. Dr. Earl Dowell.....1
305 Teer Building
Duke University
Durham, NC 27708-0271

14. Dr. Joshua Gordis.....1
Code ME/Go
Mechanical Engineering building
Monterey, CA 93943

15. Dr. D. Banerjee.....1
5000 E. McDowell
Dir Eng/Bld 530, MS B111
Mesa, AZ 85215

16. Dr. Louis V. Schmidt.....1
Code AA/Sc
699 Dyer Road
Monterey, CA 93943-5106

17. Dr. W. Miao.....1
10 Crossbow Lane
Easton, CT 06612-1255

18. Mr. Ajay Sehgal.....1
1204 Wedglea Dr.
Bedford, TX 76021

19. Dr. Jing Yen.....1
1812 Lakemont Dr.
Arlington, TX 76013

20. Dr. Richard L. Bennett.....1
Bell Helicopter Textron, Inc.
P.O. Box 482
Fort Worth, TX 76101

21. Mr. Walter Sonneborn.....1
1936 Loma Linda Ct.
Fort Worth, TX 76112

22. Dr. Andrew Lemnios.....1
Rensselaer Polytechnic Institute
JEC 4010
Troy, NY 12180

23. Dr. Daniel Schrage.....1
250 Drummen Ct.
Atlanta, GA 30328

24. Dr. C. Eugene Hammond.....1
100 Cove Colony Rd.
Maitland, FL 32751

25. Mr. Robert J. Huston.....1
105 Ilex Dr.
Yorktown, VA 23692-3012

26. Dr. Osa Fitch.....1
39378 Sunnyside Rd.
Clements, MD 20624

27. Mr. Henry Kelley.....1
3092 N. Riverside Dr.
Lanexa, VA 23089-9403

28. Dr. William Warmbrodt.....1
MS T12-B
NASA Ames
Moffett Field, CA 94035

29. Dr. Wayne Johnson.....1
MS T12-B
NASA Ames
Moffett Field, CA 94035

30. LCDR Christopher Robinson.....1
1318 Wakefield Drive
Virginia Beach, VA 23455

31. Mr. Andrew W. Kerr.....1
21950 McKean Rd.
San Jose, CA 95120

32. Mr. Robert Tomaine.....1
Attn: SFAE-AV-RAH-TV (Tomaine)
Bldg. 5681
Redstone Arsenal
Huntsville, AL 35898-5000

33. Dr. Richard Carlson.....1
20999 Sarahills Dr.
Saratoga, CA 95070

34. Dr. Robert L Sierakowski.....1
2725 Lymington Rd.
Columbus, OH 43220

35. Dr. G. A. Pierce.....1
Georgia Institute of Technology
Dept. of Aerospace Engineering
Atlanta, GA 30332-0150

36. Mr. William H Weller.....1
11 Pine Rd
W Hartford, CT 06119

37. Dr. Dewey Hodges.....1
Georgia Institute of Technology
Dept. of Aerospace Engineering
Atlanta, GA 30332-0150

38. Mr. Robert Blackwell.....1
103 Old Zoar Rd
Monroe, CT 06468

39. Mr. Euan Hooper.....1
729 Rhodes Dr.
Springfield, PA 19064-1609

40. Mr. Louis Silverthorn.....1
1336 North Pasadena
Mesa, AZ 85201

41. Dr. Friedrich Straub.....1
1760 E. Halifax St.
Mesa, AZ 85203

42. Mr. George Price.....1
Sikorsky Aircraft
PO Box 9729
MS S-330A
Stratford, CT 06497-9129

43. Dr. R. Lowey.....1
Georgia Institute of Technology
Dept. of Aerospace Engineering
Atlanta, GA 30332-0150

44. Dr. Farhan Gandhi.....1
Penn State/Aerospace Eng.
233 Hammond Bldg.

University Park, PA 16802

45. Dr. Inderjit Chopra.....1
Aerospace Engineering
University of Maryland
College Park, MD 20742

46. Dr. Benson Tongue.....1
Department of Mechanical Engineering
6129 Etcheverry Hall
University of California
Berkeley, CA 94720-1740

60 290NPG
TH 2337
6/02 22527-200

DUDLEY KNOX LIBRARY
3 2768 00403129 4